Fall 2001

Seismic response of transformer bushing systems and their rehabilitation using frictional pendulum system

Selahattin Ersoy
New Jersey Institute of Technology

ABSTRACT

SEISMIC RESPONSE OF TRANSFORMER BUSHING SYSTEMS AND THEIR REHABILITATION USING FRICTIONAL PENDULUM SYSTEM

by
Selahattin Ersoy

This thesis is concerned with the performance of electric power transformers and their attachments under earthquake loading. It begins with the description of the transformers, attached bushings, and some typical examples of substation failures in earthquake loading. This is followed by the development of finite element model of three different sizes of transformers. Finite element models consist of several thousand degrees of freedom and they are basic to this thesis. Some of the major findings from these models are utilized to derive a simplified model of a portion of a substation. The frictional pendulum system (a base isolation method) is considered for rehabilitation of existing substations or the mitigation of the seismic requirements for new substations. Results of parametric and experimental study are presented. A simplified model of a transformer with its appendages developed for use in engineering offices is developed and responses of fixed base and isolated transformers are compared. Based on the results of this study, the use of base isolation or anchorage for transformers is suggested. Finally, modifications of the IEEE specifications for qualifications tests for transformers and bushings are proposed.

SEISMIC RESPONSE OF TRANSFORMER BUSHING SYSTEMS AND THEIR REHABILITATION USING FRICTIONAL PENDULUM SYSTEM

by
Selahattin Ersoy

A Dissertation
Submitted to the Faculty of
New Jersey Institute of Technology
in Partial Fulfillment of the Requirements for the Degree of
Doctor of Philosophy in Civil Engineering

Department of Civil And Environmental Engineering

January 2002

APPROVAL PAGE

SEISMIC RESPONSE OF TRANSFORMER BUSHING SYSTEMS AND THEIR REHABILITATION USING FRICTIONAL PENDULUM SYSTEM

Selahattin Ersoy

M. Ala Saadeghvaziri, Dissertation Advisor — Date
Professor of Civil and Environmental Engineering
New Jersey Institute of Technology

Edward G. Dauenheimer, Committee Member — Date
Professor of Civil and Environmental Engineering
New Jersey Institute of Technology

Saeid Rashidi, Committee Member — Date
Research Associate
Stevens Institute of Technology

Pushpendra Singh, Committee Member — Date
Associate Professor of Mechanical Engineering
New Jersey Institute of Technology

William R. Spillers, Committee Member — Date
Distinguished Professor of Civil and Environmental Engineering
New Jersey Institute of Technology

BIOGRAPHICAL SKETCH

Author: Selahattin Ersoy

Degree: Doctor of Philosophy

Date: January 2002

Undergraduate and Graduate Education:

- Doctor of Philosophy in Civil Engineering,
  New Jersey Institute of Technology, Newark, NJ, 2002

- Master of Science in Civil Engineering,
  New Jersey Institute of Technology, Newark, NJ, 1997

- Bachelor of Science in Civil Engineering,
  Middle East Technical University, Ankara, Turkey, 1994

Major: Civil Engineering

Presentations and Publications:

Ersoy, Selahattin, Saadeghvaziri, M. Ala, Liu, K., and Mau, S.T., "Analytical and Experimental Evaluation of Friction Pendulum System for Seismic Isolation of Transformers and Design Aspects", *Earthquake Spectra,* November 2001.

Saadeghvaziri, M. A., Ersoy, Selahattin, "Evaluation of Seismic Response of Transformers and effectiveness of FPS Bearings for Base Isolation," *Proceedings of the 2001 Structures Congress and Exposition*, ASCE, 2001.

Ersoy, Selahattin, Saadeghvaziri, M. Ala, "Experimental Seismic Evaluation of Base-Isolated Transformers", *Proceedings of IMAC-XIX: A Conference on Structural Dynamics*, February 2001.

Saadeghvaziri, M. A., MacBain, K., Ersoy, Selahattin, "Combination Glare Screen Pedestrian Fence Using Recycled Plastics", *Practice Periodical on Structural Design and Construction*, Vol. 5, No. 4 Nov 2000, ASCE 150-156.

Saadeghvaziri, M. A., Ersoy, S., Mau, S. T., "Friction Pendulum System for Seismic Isolation for Transformers," *PVP*, Vol. 402-1, pp 123-134, 2000

To my beloved family

ACKNOWLEDGMENT

I would like to express my gratitude to Dr. M. Ala Saadeghvaziri for his guidance, technical advice and moral support. I also appreciate the guidance and technical support provided by my committee members: Professors Edward G. Dauenheimer, Pushpendra Singh, William R. Spillers, and Saeid Rashidi. Special thanks are given to Dr. Gee-Yu Liu for his experimental work and Dr. David Perel for his instrumental cooperation.

The financial support for this work came from the National Science Foundation under the Multidisciplinary Center for Earthquake Engineering Research (MCEER) program. This support is greatly appreciated. The results, opinions, and conclusions expressed in this report are solely those of the author and do not necessarily reflect those of the sponsor.

TABLE OF CONTENTS

TABLE OF CONTENTS
(Continued)

LIST OF TABLES

LIST OF TABLES
(Continued)

LIST OF FIGURES

LIST OF FIGURES
(Continued)

LIST OF FIGURES
(Continued)

LIST OF FIGURES
(Continued)

LIST OF FIGURES
(Continued)

LIST OF FIGURES
(Continued)

CHAPTER 1
INTRODUCTION

The functionality of electric power systems, especially in the age of information technology, is vital to maintain the welfare of the general public, to sustain the economic activities and to assist in the recovery, restoration, and reconstruction of the seismically damaged environment. This thesis is driven by the desire to improve the reliability of electric power systems during and after an anticipated earthquake.

The performance of transformers and their interaction with bushings, conductors and connecting equipment items has to date not been satisfactory in many earthquakes. Since transformers have a vital function in electric power system substations, they are considered among the most important components of a substation. In order to be able to assess the reliability of power systems under earthquake loading and to provide rehabilitation strategies (base isolation or anchorage), the critical components of the system and their interaction with each other must be identified and their seismic performance must be assessed.

1.1 Power Systems and Power Transformers

Electric power systems can be divided into five major parts: power generating facilities, transmission and distribution lines, transmission and distribution substations, control and data acquisition systems, and ancillary facilities and functions. This study focuses on two substation components, transformer bushing and a connecting equipment item. (See Figure 1). Substations perform many functions including [ASCE, 1999]:

1. Protection of transmission and distribution lines and the equipment within the substation.
2. Triggering other devices to isolate the lines or the equipment in case of abnormal system operating conditions.
3. Providing transfer of power between different voltage levels through the use of power transformers.
4. Reconfiguring of the power network by opening transmission lines or partitioning multi-section busses.

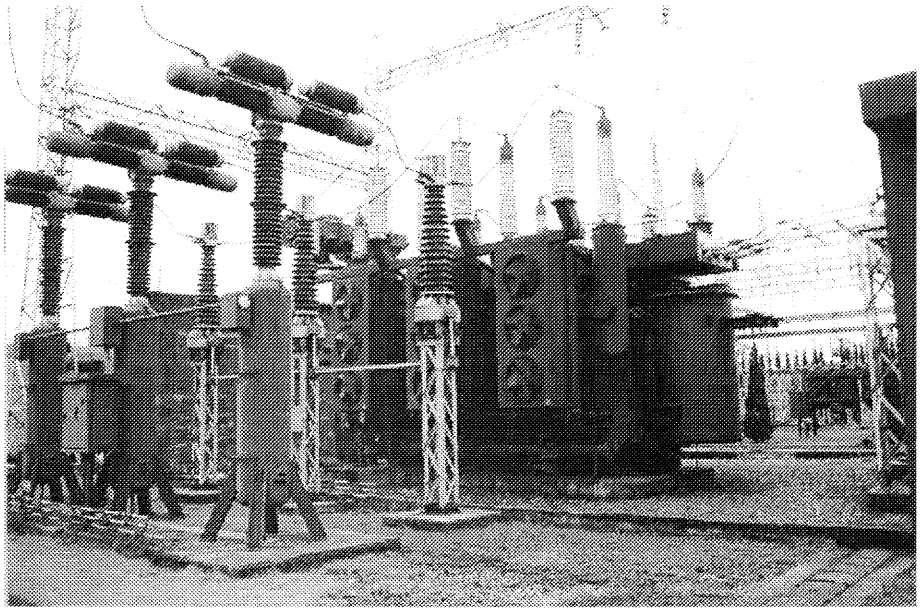

Figure 1 Typical Substation

One of the key components of the substation is the power transformer. Most of the power transformers (and those discussed here) are core type transformers. The size, shape and installation of transformers vary according to the voltage handled. The basic components of a transformer are the coils, core, tank, oil and bushing. The coils and core are usually enclosed in a steel tank to protect them from the elements, vandalism and, for

safety purposes, oil is placed in the tank over the coils and core to provide a means of cooling. Figure 2 shows inner and outer parts of a power transformer. More information on transformers is given in a recent literature [Pansini, 1999]. Bushings are insulated conductors providing electrical connections between high voltage lines and oil-filled transformers. They are typically mounted on the top plate of the transformer tank or a turret attached to a transformer tank. Typical bushing and its components are shown in Figure 3. Bushings take the terminals of the coils through the tank, insulating them from the tank. Typically, they consist of a conductor through an insulating collar, usually porcelain. For higher voltages, the porcelain cylinders may also be filled with oil or contain layers of insulation with metal foil inserted between them to equalize electric stresses among the layers.

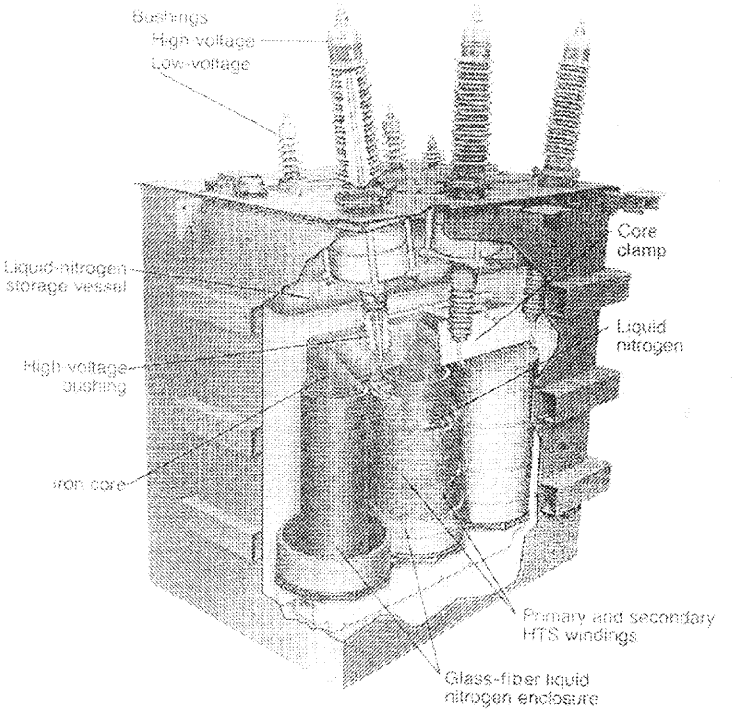

Figure 2 Typical Power Transformer and its Components [Pansini, 1999]

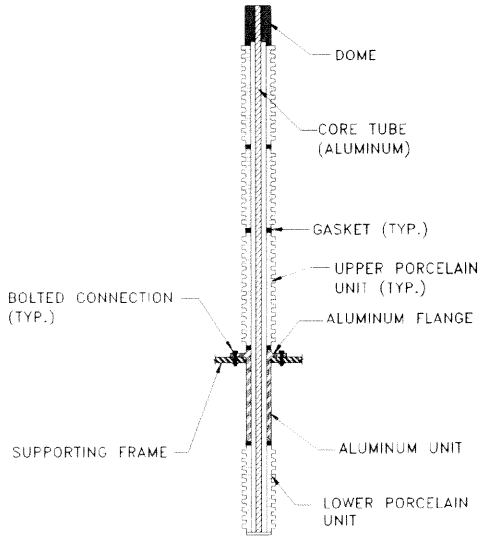

Figure 3 Typical Bushing and its Components

Transformer components include: sudden pressure and protective relays, anchorage, radiators, bushings, conservators, lightning arresters, tertiary bushings, and surge arresters. Some transformer installations also have transfer busses so that a spare transformer can quickly replace a unit that must be taken out of service. The effect of the loss of function of a transformer is generally significant, unless a spare transformer is available or there is a second transformer bank in parallel with the damaged unit. The consequences of transformer damage will depend on system configuration and other system elements that may be damaged or can be out of service. If no damage is observed in an earthquake and earthquake intensity is low to moderate, the transformer will usually be put back into service. If there is any concern regarding an internal fault, a high-potential test of the transformer is performed before it is put back into service.

1.2 Past Earthquake Performance

The failure of electric power systems in the 1994 Northridge earthquake in the United States, the 1999 Izmit earthquake in Turkey, and other recent earthquakes have demonstrated the need for electric power networks during and after an earthquake. Observed failure types of power transformers are categorized as:

1. Failure of unrestrained transformers
2. Anchorage failure of transformers
3. Conservator failure of transformers
4. Foundation failure of transformers
5. Damage to control boxes

The first two are the most common failure types of transformer bodies. Figure 4 and Figure 5 show over-turned transformers from recent earthquakes. The most common power transformer failures are those of unrestrained transformers in earthquake prone regions. It is common practice to fix the transformer base to the foundation either by anchor bolts or welds. However, there are many cases of bolt or weld failure during the past earthquakes [ASCE, 1999]. Designing the anchorage at the supports requires consideration of large forces not only due to gravity and seismic forces but also from overturning moments in both directions. In addition to strength, the anchorage must have adequate stiffness to prevent initiation of impact forces that can damage internal elements or excite higher modes that can damage brittle porcelain members.

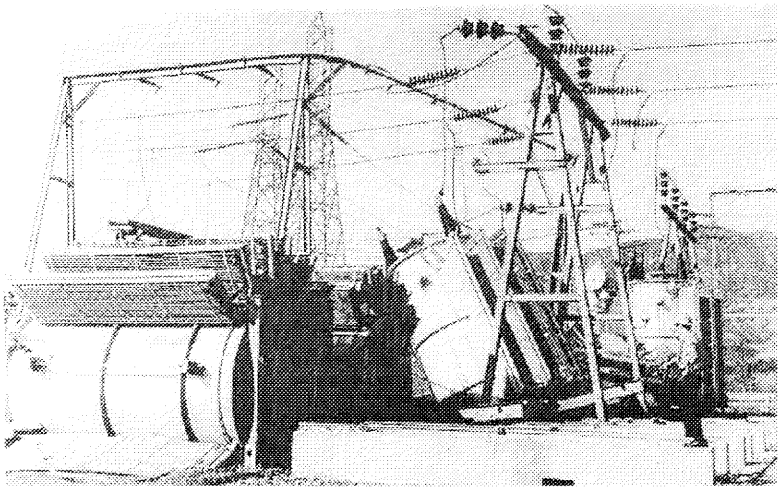

Figure 4 Damage to a Rail-Mounted Transformer [ASCE, 1999]

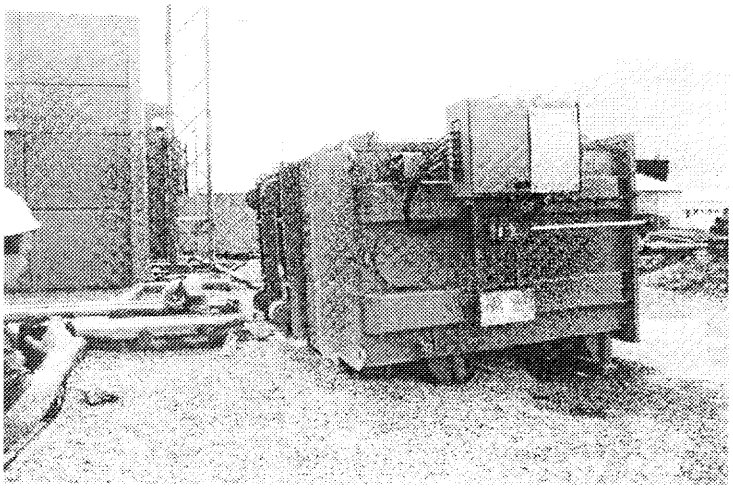

Figure 5 Transformer Turned Over [MCEER, 2000]

Figure 6 shows a foundation failure of a transformer in 1999 Izmit Earthquake. This was an unrestrained transformer placed on top of a foundation pad.

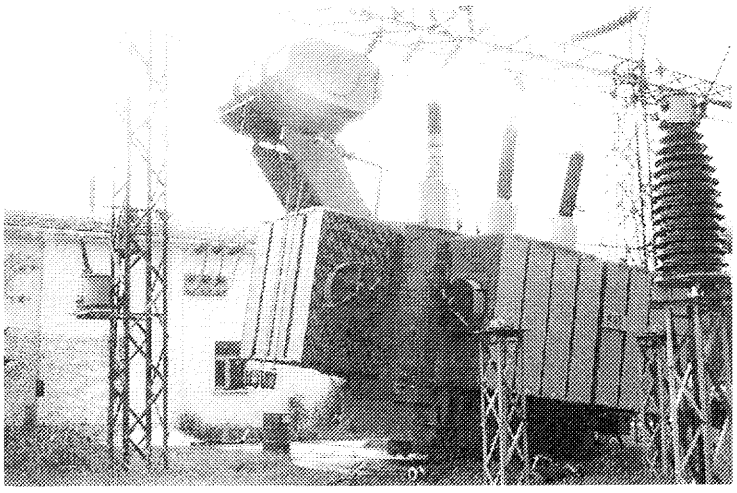

Figure 6 Damage to a Transformer Foundation [EERI, 1999]

Bushing failures are classified in two groups:

1. Oil leaks due to gasket failure

2. Fracture of the porcelain body due to a lack of slack cable between the bushing and the connecting equipment.

Figure 7 shows the failure of a bushing at the gasket level. The most vulnerable gasket is the one closest to the flange connecting the bushing to the transformer.

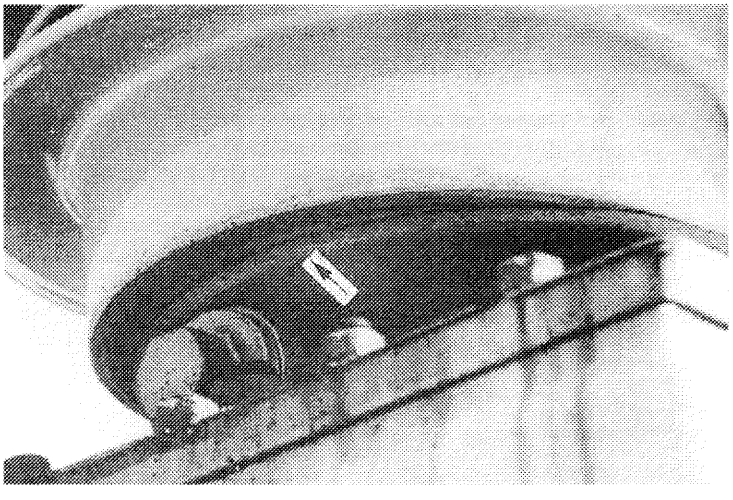

Figure 7 Bushing Failure at the Flange [ASCE, 1999]

There are many more examples of power transformer and bushing failures during recent earthquakes [ASCE, 1998, 1999].

1.3 State-of-the-Art

Amplification of the ground motion by the transformer body itself is one of the most important concerns in transformer and bushing response. (The latter is the classic case of secondary systems in which the motion of connected parts can tear machinery apart.) Based on a study performed at the University of California at Irvine, the dynamic amplification of 500 kV bushings mounted at the top of transformers is handled by the amplification factor given in the IEEE Standard 693. However, a 230 kV bushing mounted on a transformer has been observed to exceed the specifications by a factor of almost two [Villaverde, 1999]. Another study has revealed that the dynamic amplification factor between the ground and bushing flange for 160 MVA, 230/135 kV power transformer is over two [Bellorini, 1998].

Besides these studies, the performance of bushings was analyzed through extensive testing in the Pacific Earthquake Engineering Research Center (PEER). They tested 196 kV, 230 kV and 550 kV bushings mounted on a fixed frame at their flange [Gilani, 1998, 1999]. The experimental setup for this testing is shown in Figure 8. Excellent performance was observed for the 196 kV, 230 kV bushings in spite of their poor performance in the past earthquakes. Even though the tests were conducted for two times the response spectra given in IEEE 693 to account for the dynamic amplification of the transformer tank (an IEEE requirement for the qualification of bushings), bushings performed well. These tests were conducted using a rigid frame to support the bushings

therefore the in-situ effect of the translational motion of transformers is not included. The critical environment for bushings can be either due to the effect of the motion of the transformer body or the interaction of the bushing with the other equipment. Apparently, the fixed frame shown in Figure 8 used for the qualification of the bushings does not take into account the effect of transformer flexibility. It is thus important to revise the qualification procedures for bushings set by IEEE 693-1997.

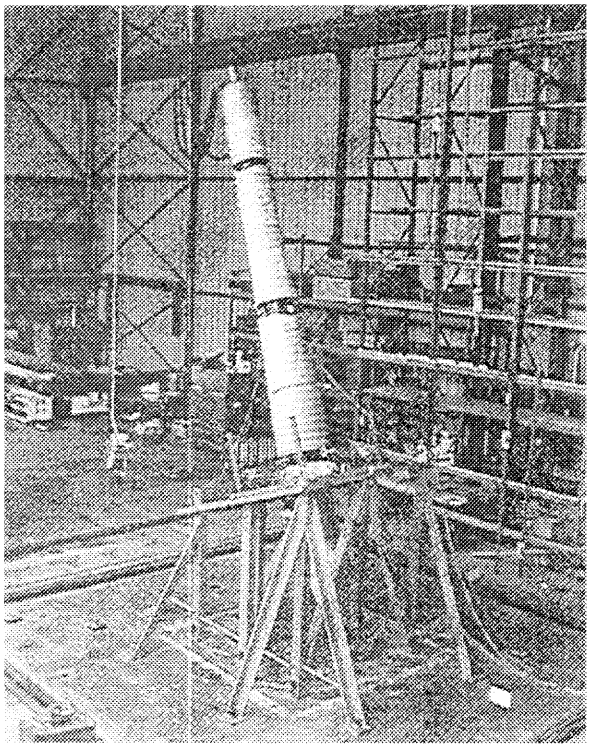

Figure 8 Experimental Setup for Testing 550 kV Bushing at PEER

Even though the previously mentioned tests showed excellent performance of bushings, their poor performance in past earthquakes calls for a suitable remedy. It should be born in mind that one of the reasons of poor performance is interaction of transformer with bushing. Therefore, a suitable remedy for the transformer bushing system can be base isolation. One of the most recent base isolation systems to improve

the earthquake resistance of structures is Frictional Pendulum System (FPS). Since the period of vibration for structures isolated by FPS is independent of mass, it is an ideal device for the isolation of transformers. FPS will reduce the input acceleration into the bushing and will lessen the interaction between the transformer and the bushing.

FPS has been studied by many researchers in an effort to improve the seismic performance of structures [Al-Hussaini, 1994; Almazan, 1998; Mokha, 1990, 1991]. The FPS system is a base isolation system in which the object being isolated is constrained to move on a spherical surface (FPS is described in detail in Chapter 3). Some examples of applications of the FPS system are the San Francisco Airport International Terminal, the U.S. Court of Appeals, and the Hayward City Hall [Mokha, 1996]. There are also industrial applications of FPS in systems like natural gas storage tanks and emergency and fire cooling water tanks. There have also been FPS applications to many bridges throughout USA and Canada [Constantinou, 1993]. More recently, FPS bearings were used to retrofit an international airport terminal building in Turkey [Constantinou, 2001]. This study considers the use of FPS for power transformers for the first time.

There has also been a study of the interaction of interconnected substation components [Kiureghian, 1999]. This was a theoretical study that was conducted for two equipment items. Studies of multiple equipment items with properties closer to real equipment would lead to a better understanding of interaction of electrical equipment.

1.4 Objectives of the Current Study

Methodology to study transformer bushing systems can be given as follows: Finite element analyses of three different sizes of transformer are performed to get the dynamic

response characteristics of the transformer bushing systems. Base isolation and anchorage of transformer is taken as possible retrofit scheme. Analytical and experimental studies are performed on the base isolation system. Based on finite element and base isolation studies, a simplified model of portion of substation is developed.

This thesis begins formally in Chapter 2 with a finite element model of a transformer. This is a detailed model, which includes all relevant components and has several thousand degrees of freedom. Finite element analysis of power transformers and bushings is performed on three different types of transformers in this chapter. Chapter 3 begins the study of seismic rehabilitation with a discussion of the FPS system. It includes extensive analytical studies performed to check the efficiency of the Frictional Pendulum System for power transformer bushing design in an attempt to enhance their seismic performance. In light of the transformer's weight and the mobility requirements for maintenance purposes, base isolation is identified as a practical technology for their seismic rehabilitation and design charts are developed for this base isolation system [Ersoy, 2001; Saadeghvaziri, 2000]. Experimental studies performed in collaboration with National Center for Earthquake and Research (NCEER) in Taiwan are given in Chapter 4.

Chapter 5 develops a simplified transformer model, which is directed at the consulting engineers. Development of a simplified model for portions of substations is driven by reasons of cost. This simplified model also aids the understanding of the interaction of transformer bushing systems with other connecting equipment in the substation in the case of fixed transformer bushing systems and FPS isolated transformer and bushing systems. A simple model for the interaction of the transformer bushing

systems with a connecting equipment item using a flexible cable is studied in Chapter 5. Analytical results and a discussion of the practical aspects of design recommendations and rehabilitation guides are presented therein. The interaction of fixed or isolated transformer bushing systems with connecting equipment has to the best of my knowledge not been studied before. The basic work of Chapter 3 does not take into account transformer and bushing flexibility. In order to include the effect of the flexibility of the transformer on the bushing response, the results of Chapter 2 are utilized in the development of the simplified model.

CHAPTER 2
FINITE ELEMENT STUDY OF TRANSFORMER BUSHING SYSTEM

The reliability of a power systems exposed to earthquake loading is dependent upon the seismic response of its individual components and interaction of these components with each other. Unrestrained or poorly anchored transformers and porcelain transformer bushings have failed in recent earthquakes. Since transformers and their mounted bushings are vital system components which have been damaged in past earthquakes, they are the main focus of the finite element part of this thesis.

Transformers perform the vital function of transferring power between circuits operating at different voltages. The important components of transformers with regard to earthquake performance are anchorage, bushings, and connections to other equipment. Transformers are usually isolated in case of abnormal operating conditions through the opening of the circuit breakers which are usually located next to the transformers. Power transformers typically have several protective relays that monitor performance and provide electrical protection. Some protective relays may be activated by an earthquake and cause the transformer to be taken offline. These relays can prevent damage to the distribution system in an earthquake. Earthquake induced vibrations cause distribution lines to swing and adjacent phases to come in contact. This can cause the lines to wrap around each other, to burn down, or to blow fuses and trip circuit breakers. Therefore special care should be given to the slack configurations of the interconnecting equipment.

The anchorage of transformers is another issue that requires special attention. Transformers are usually placed on top of a concrete pad or on rails without anchorage in seismically safe regions. Another anchorage approach is bolting the transformer to a

concrete foundation where there is seismic risk. There are many transformer configurations and constraints in designing transformer anchorage retrofits. Cost and materials, as well as geometric constraints, may yield less than optimal designs that are nonetheless adequate. The installation of transformers without anchorage should be avoided because of the significant loss associated with the transformer damage. Base isolation can be provided as a rehabilitation scheme for transformers to lessen the earthquake induced accelerations. However, there have been significant problems with existing base isolation designs that use conical shape disked springs (washer) [IEEE, 1998]. Base isolation requires very careful evaluation to assure that the desired effects are achieved. Large displacements resulting from the base isolation causes problems with the amount of slack cable between system components. Generous slack can be provided to accommodate the increased demand for flexible conductor connections as long as the electrical clearances provided are sufficient.

Several researchers have performed experimental and finite element studies on transformers and bushings [Gilani, 1998, 1999; Villaverde, 1999]. Most recent tests were performed at PEER (Pacific Earthquake Engineering Research Center) and Construction Engineering Research Laboratories of US Army Corp of Engineers. Bushings tests were performed using a stiff supporting frame in these cases. Even though the most vulnerable flange to porcelain gasket detail has been used in these tests, the performance of 196 kV, 230 kV and 550 kV bushings was fairly good in terms of the general response based on the qualification of bushings set forth in IEEE 693-1997. However, many bushings of the same type have failed in past earthquakes. This situation points to the need for reassessment of the current IEEE 693-1997 qualification procedures for both transformer

and bushings. Electrical equipment components are typically designed for electrical requirements more than structural performance requirements. Interconnecting substation components can complicate the seismic response. It is likely that significant seismic interaction and equipment damage can occur using either flexible or rigid connectors. Therefore the identification of critical loading environments for bushings using shake table tests alone is not likely. The critical loading of bushings can be either due to shaking of the transformer tank or loads at the terminal end of the bushing due to the shaking of the transformer and its connected equipment. Finite element analysis will help to understand the response characteristics of transformer bushing system. Besides, these analyses will provide input for simplified models of substation.

In this chapter, the seismic qualification procedures of the most recent code for substations are summarized first. Then, modeling and analysis issues of three different types of transformers follow. Finally, the response criteria and the finite element results are given for analyzed transformer bushing systems. One of the main purposes of this chapter is to supply the necessary input for simplified model of a portion of a substation.

2.1 IEEE Seismic Qualification Procedures for Transformers and Bushings

Seismic qualification tests are used to demonstrate through experimentation that a piece of equipment is able to perform its intended function during and after an earthquake. In the United States, electrical equipment is seismically qualified using a standard developed by the Institute of Electrical and Electronic Engineers. The IEEE standard entitled IEEE 693-1997 Recommended Practices for Seismic Design of Substations

details procedures for qualification of electrical substation equipment for different seismic performance levels (high, moderate, and low).

For qualification, the transformer and its appendages, except bushings, are required to satisfy static analysis using 0.5g in two horizontal directions and 0.4g simultaneously in the vertical direction. However, IEEE 693-1997 states that bushings rated at 161 kV and above must be qualified using three-component earthquake-simulator testing. Because it is impractical to test bushings mounted on a transformer, IEEE specifies that bushings must be mounted on a rigid stand for earthquake testing and qualification. IEEE 693-1997 identifies several response spectra of identical shape but different amplitudes for the qualification of a transformer bushing on an earthquake simulator.

Performance Levels (PL) for substation equipment are represented by a response spectrum that is anchored to a peak ground acceleration (PGA) of 0.5g for Moderate Level qualification and 1.0g for High Level qualification. Since it is often impractical to test components to the PL, IEEE 693-1997 permits equipment to be tested using a reduced level of shaking called the Required Response Spectrum (RRS). RRS corresponds to a PGA of 0.25g and PGA of 0.5g, for Moderate Level and High Level qualification respectively. To account for the amplification of earthquake motion due to the flexibility of the transformer and the local flexibility, IEEE 693-1997 states that the input motion measured at the bushing flange shall match a spectrum with ordinates twice that of the RRS, termed as the Test Response Spectra for Mounted Equipment (TRSME). The PGA for the TRSME spectrum is therefore 0.5g for Moderate Level qualification and

1.0g for High Level qualification. For this level of shaking, IEEE recommendations are as follows:

1. The stresses in non-ductile components must be less than one-half the ultimate stress
2. The factor of safety against oil leakage must exceed 2.

Since there are no earthquake simulators capable of subjecting equipment to shaking compatible with the spectrum for High Level qualification, a response amplification factor of 2.0 is applied as bushing input.

Anchorage is stated as one of the most cost effective measure to improve the performance of inadequately anchored equipment. Anchorage must withstand the shear, uplift, and compressive forces resulting from the design earthquake. Conductor length determinations are based on the displacements of the equipment that conductor is attached to at each end. The recommended method in IEEE is summation of the equipment displacements multiplied by a factor of 1.5, straight line distance between connection points, and minimum required slack for conductor configuration under consideration. Three basic configurations are given in the IEEE specifications based on the conductor size, equipment differential movement, vertical and horizontal separation of the termination points and voltage.

2.2 Modeling and Analysis Issues for the Transformer and Bushing

A typical power transformer is composed of six parts: transformer tank, radiators, reservoir, core and coil, mineral oil, and bushings. The transformer tank is the main structural component of power transformers. Lateral bracing of the tank wall is provided usually by plates as channels. It has a core and a coil centrally placed within 2/3 of

transformer height and the tank is completely filled by mineral oil. Radiators and reservoirs are appendages that are externally attached to the transformer tank.

Three different sizes of power transformers were selected for time history analysis. First transformer type is 25 MVA – 650 HV BIL and it is called transformer type 1 (TT1) in this study. This transformer weighs about 179 kips and does not have a reservoir. The dimensions of this transformer are B=85", L=125", H=170" (B, L, and H represents width, length, and height of the transformer tank, respectively). The second transformer type is 33/44/55 MVA 230/133 HV three phase transformer and it is called transformer type 2 (TT2) in this study. It weighs about 300 kips and the radiators (on the side) and reservoir weigh 27 kips and 9 kips, respectively. The dimensions of this transformer are B=100", L=200", H=200". Third transformer type is 250 MVA 230/119.5 kV and it is called transformer type 3 (TT3) hereafter in this study. Its weight is about 512 kips. The dimensions of this transformer are B=100", L=280", H=180".

The finite element package ANSYS is used for development of the finite element model [ANSYS]. The transformer tank is modeled by shell elements. Braces around the transformers are modeled by offset beam elements. The core and coil inside the transformer are modeled as mass elements. The radiators and the reservoir are modeled by 3-D solid elements. The contained oil inside the transformer was modeled with fluid elements in early stage of this study. Later the contained oil is modeled as a solid with modulus of elasticity equal to the bulk modulus of the fluid since the transformer is filled completely with oil and there is no slashing effect under consideration. The results obtained from both methods were the same, but solid modeling of the contained oil is

more computing time efficient. These three types of transformer all support 3-196 kV bushings that are located on top of the transformer tank.

Bushings are composed of several elements like an aluminum support unit, porcelain units, gaskets, aluminum core, and dome. The aluminum support has a built-in flange used to mount the bushing on top of the transformer. The aluminum core runs from the top to the bottom of the bushing and houses the aluminum conductor. Bushings are prestressed through the aluminum core and this prestressing force is distributed evenly to the other components through the dome to hold the units together. There are gaskets located in between the units. Finite element model of one of the transformers with element types and details is shown in Figure 9. Schematic view of a portion of a bushing model is shown in Figure 10. Based on this information, the analytical models for the bushings were created by beam elements with equivalent density and stiffness to represent the porcelain units, the dome, and the aluminum core. Gaskets between these elements are modeled using linear axial and shear springs. The total axial stiffness is introduced as in equation (1)

$$K_a = \frac{AE}{t} \tag{1}$$

and the shear stiffness is obtained by equation (2).

$$K_s = \frac{AG}{t} \tag{2}$$

In these equations, A is the area of the gasket, E is young's modulus, G is the shear modulus and the t is the thickness of the gasket.

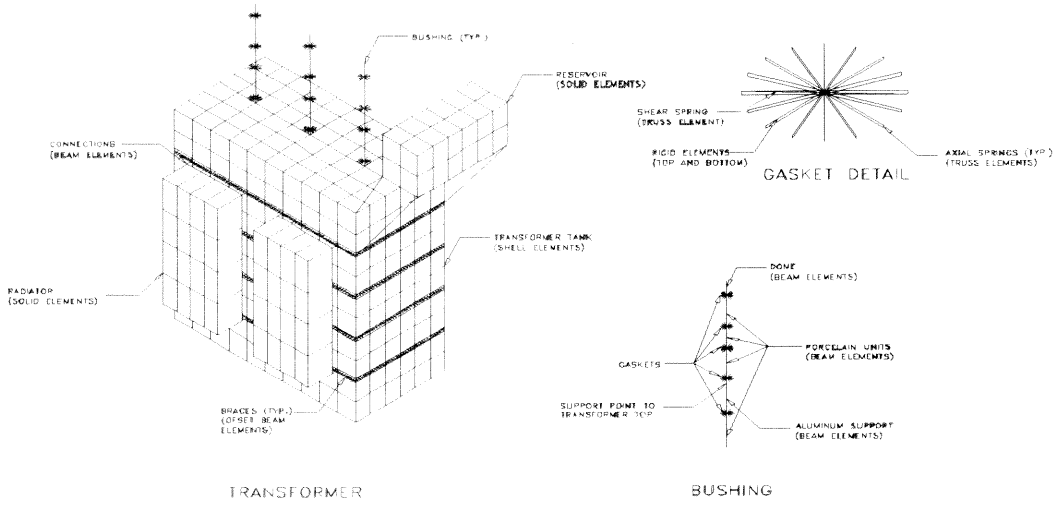

Figure 9 Mesh of Transformer and Element Types

Since anchoring of a transformer at its corners is a common practice, the transformer models are fixed at each corner of the transformer.

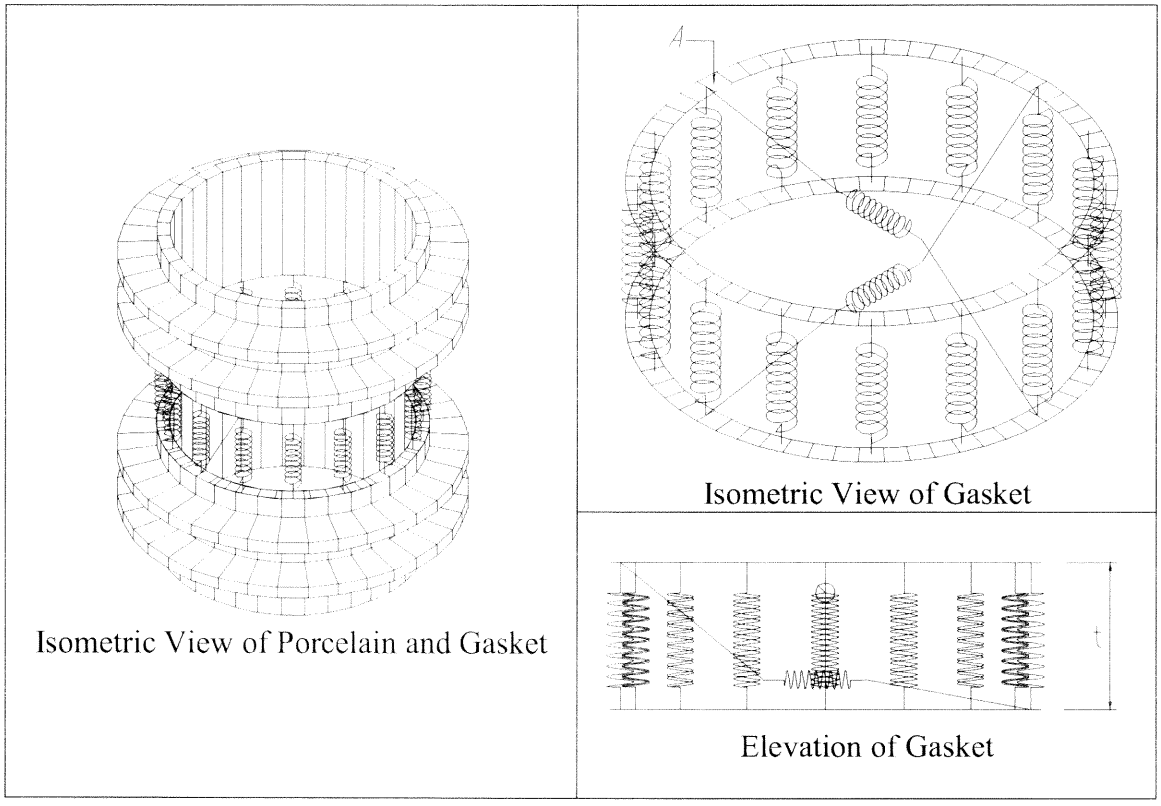

Figure 10 Views of Gasket Model

Full time history analyses are performed for ground input with PGA of 1g in orthogonal horizontal directions and PGA of 0.8 g in the vertical direction as per IEEE recommendation. For each transformer type, 2-soil and 2-rock earthquake records are utilized for 3-D time history analysis. The response spectrum of the earthquake motions (soil records) used for orthogonal horizontal components and vertical component together with the IEEE High Performance level spectra are shown in Figure 11 and Figure 12 for 2 % damping.

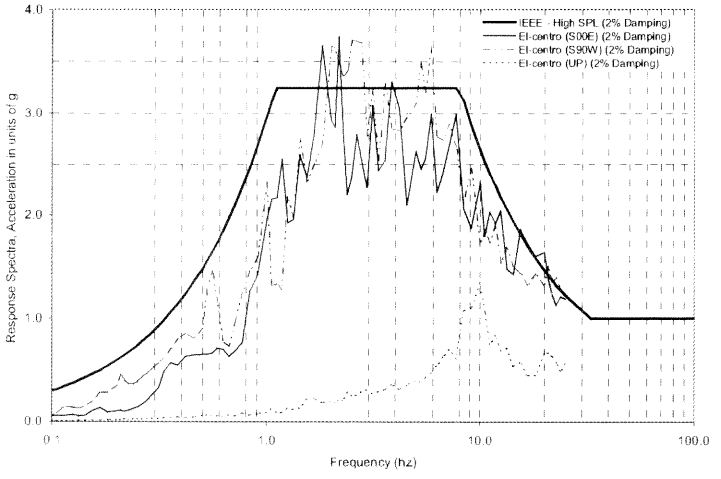

Figure 11 Acceleration Response Spectra for Components of El-Centro Record and IEEE High Performance Level

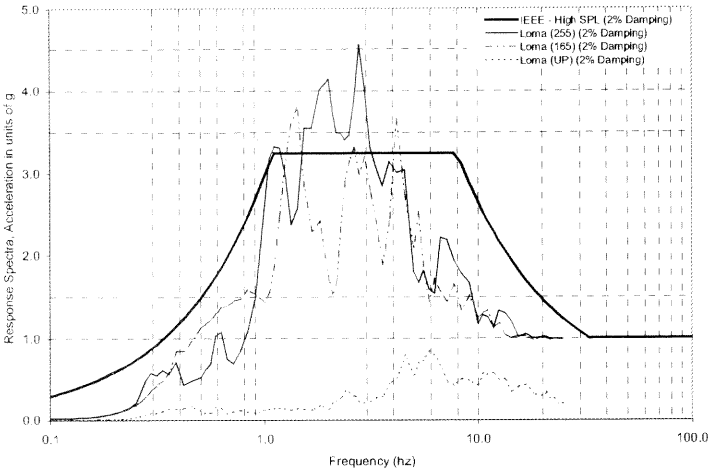

Figure 12 Acceleration Response Spectra for Components of Hollister Airport Record and IEEE High Performance Level

The response spectrum of component of the rock records with IEEE High Performance level spectra are shown in Figure 13 and Figure 14 for 2 % damping.

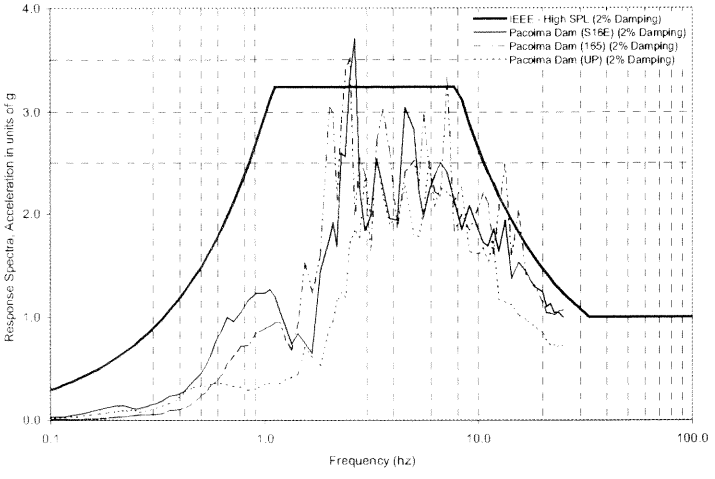

Figure 13 Acceleration Response Spectra for Components of Pacoima Dam Record and IEEE High Performance Level

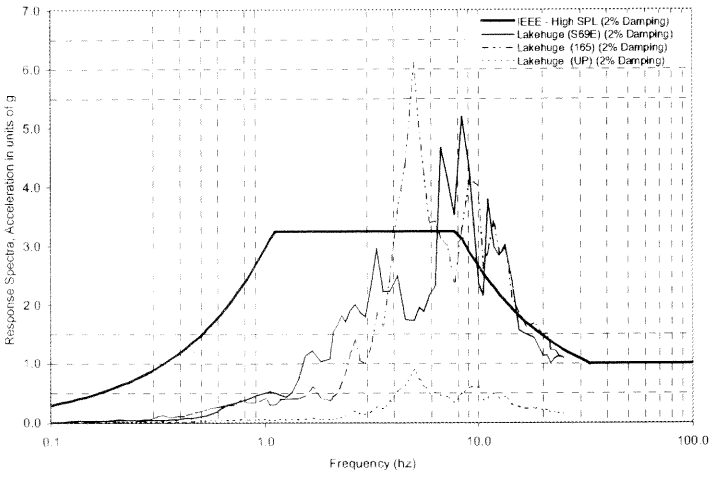

Figure 14 Acceleration Response Spectra for Components of Lake Hughes Array #4 Record and IEEE High Performance Level

Based on the IEEE 693-1997, 2% damping value was employed in the finite element model. Rayleigh damping is used for all the time history analysis and the Rayleigh damping coefficients were obtained by fixing the damping value at 0.02 for frequencies of 8 Hz and 25 Hz (shown in Figure 15). These frequency values were selected based on the response frequencies of the transformer bushing systems. The minimum damping value obtained in this frequency range is 1.71 %.

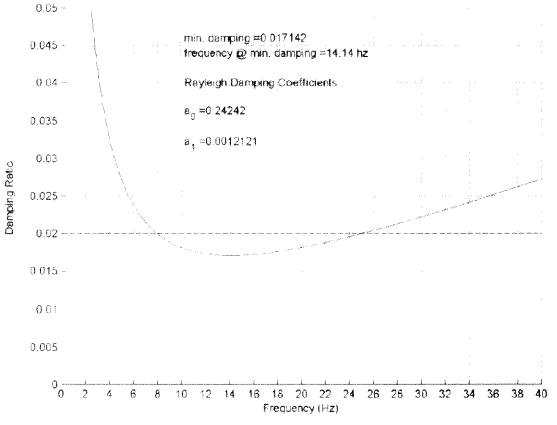

Figure 15 Determination of Rayleigh Damping Coefficients for Analysis

2.3 Response Criteria for Transformer and Bushing

Five fragility criteria for bushings were identified in this study.

1. Gap between the porcelain units and/or aluminum components and the gasket.
2. Stress/Strain levels in the gasket.
3. Stress/Strain levels in porcelain units.
4. Top displacement of bushing based on slack.
5. Loss of pre-stress/relaxation.

The first two of these criteria are related to the gasket. The third and fourth items are associated with the strength of the porcelain units, which may cause failure of bushing such as cracking of the porcelain due to high pressure or insufficient slack provided between bushing and the connecting equipment. There have been examples of failures caused by insufficient slack during past earthquakes.

2.4 Finite Element Analysis Results

In this finite element analysis, weak and strong orthogonal horizontal axes are referred to x and y directions, respectively. The vertical axis is referred to as the z direction. Transformer type 1, transformer type 2, and transformer type 3 are described as TT1, TT2, and TT3, respectively.

Finite Element (FE) responses are monitored at several places throughout the height of the transformer and the bushing. Displacement, velocity and acceleration responses on the transformer tank are obtained for five levels through the height of transformer, at each corner and the center point between the corners. Schematic view of the monitored points is shown in Figure 16. Displacement, velocity and acceleration

responses of 12 points for each of the three bushings are also monitored. Figure 17 shows the monitored points on the bushings. These 12 points are top of bushing, bottom of bushing and a total of 10 points at the top and the bottom of 5 gaskets.

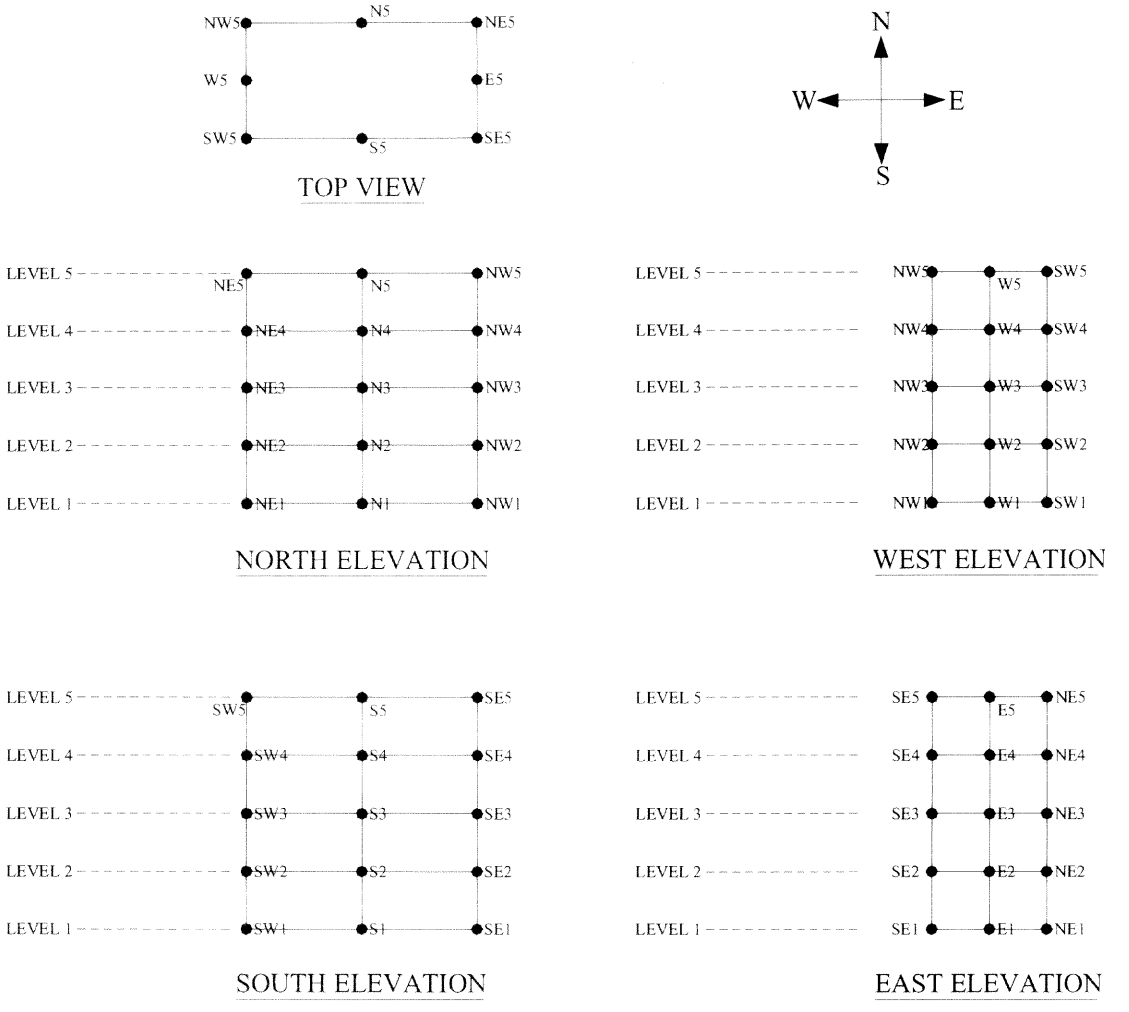

Figure 16 Monitored Nodes on Transformer Model

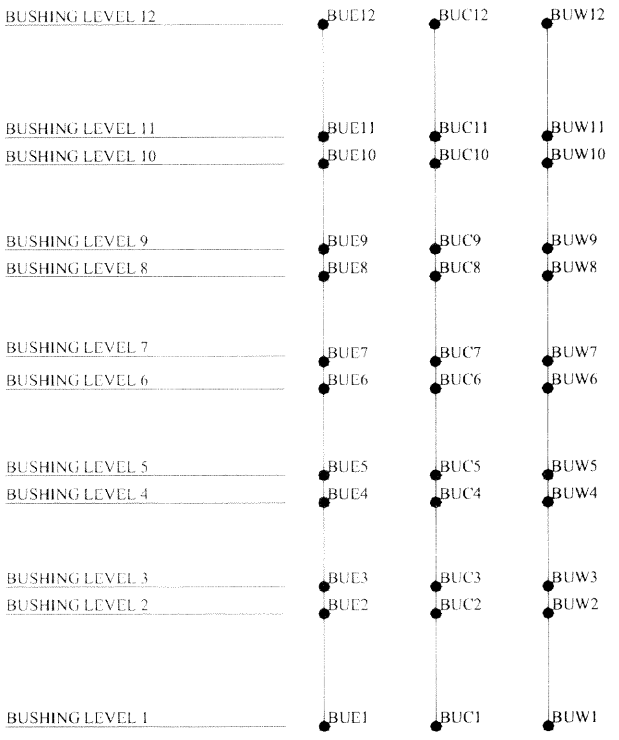

Figure 17 Points Monitored on Bushing Finite Element Model

2.4.1 Dynamic Response of Transformers

Modal analyses show that translational modes of the transformers have the highest participation in their response. Frequency of the translational mode of TT1 in x-direction (weak horizontal axis) is 14.1 Hz. That of TT2 and TT3 is 13.8 Hz. and 11.7 Hz., respectively. Maximum relative displacement and total acceleration responses at mid height of transformer, top of transformer and top of bushing for TT1, TT2, and TT3 are tabulated in, Table 1, Table 2, and Table 3, respectively (the bushings will be discussed later in the next section). The maximum translation at the top of the transformer in x-direction is 0.12 inch for TT1. That of TT2 and TT3 is obtained as 0.14 inch and 0.21 inch, respectively. One can note that the translations in y-direction are always smaller than the ones in the x-direction due to higher stiffness of the transformers in the y-

direction. Comparison of the displacement values at mid-height of the transformer to the top of the transformer show that mid-height displacement values are one half of the top displacements. It can be deduced that there is almost always a linear relationship for the displacement values throughout the height of the transformer.

Table 1 Summary of Maximum Displacement and Acceleration Responses for TT1

Transformer Type	EQ Record	Location	Displacement (in)			Acceleration (g)		
			x	y	z	x	y	z
TT1	El-Centro	Mid level of Transformer	0.045	0.022	0.020	1.011	0.999	0.490
		Top of Transformer	0.091	0.039	0.021	1.383	1.308	0.510
		Top of Bushing	0.550	0.244	0.012	6.179	2.967	0.541
	Hollister Airport	Mid level of Transformer	0.038	0.018	0.017	1.021	1.011	0.185
		Top of Transformer	0.074	0.032	0.018	1.134	1.020	0.193
		Top of Bushing	0.282	0.143	0.011	2.858	1.150	0.419
	Pacoima Dam	Mid level of Transformer	0.046	0.020	0.021	1.092	1.074	0.264
		Top of Transformer	0.093	0.035	0.021	1.532	1.129	0.274
		Top of Bushing	0.600	0.263	0.011	7.975	2.750	0.379
	Lake Hughes Array #4	Mid level of Transformer	0.059	0.022	0.025	1.301	1.116	0.421
		Top of Transformer	0.118	0.038	0.025	2.002	1.293	0.437
		Top of Bushing	0.954	0.372	0.011	10.949	3.962	0.370

The maximum dynamic amplification factor is found to be 2 for TT1. That of TT2 and TT3 is reported as 2.4 and 2.5 respectively. Therefore it can be stated that the dynamic amplification due to the transformer body stated as 2 by IEEE 693-1997 is not

always conservative. The dynamic amplification for smaller transformer, namely TT1 is satisfactory, however it is not suitable for TT2 and TT3.

Table 2 Summary of Maximum Displacement and Acceleration Responses for TT2

Transformer Type	EQ Record	Location	Displacement (in)			Acceleration (g)		
			x	y	z	x	y	z
TT2	El-Centro	Mid level of Transformer	0.059	0.018	0.025	1.056	1.000	0.618
		Top of Transformer	0.120	0.028	0.026	1.495	1.176	0.645
		Top of Bushing	0.597	0.265	0.015	5.449	2.087	0.701
	Hollister Airport	Mid level of Transformer	0.049	0.019	0.022	1.029	1.010	0.235
		Top of Transformer	0.099	0.032	0.023	1.194	1.016	0.245
		Top of Bushing	0.285	0.213	0.014	2.440	1.313	0.485
	Pacoima Dam	Mid level of Transformer	0.054	0.016	0.023	1.154	1.051	0.322
		Top of Transformer	0.105	0.024	0.023	1.724	1.074	0.331
		Top of Bushing	0.577	0.298	0.013	6.737	2.466	0.426
	Lake Hughes Array #4	Mid level of Transformer	0.070	0.019	0.029	1.375	1.083	0.512
		Top of Transformer	0.138	0.030	0.030	2.376	1.195	0.526
		Top of Bushing	0.809	0.433	0.012	8.297	3.722	0.417

Table 3 Summary of Maximum Displacement and Acceleration Responses for TT3

Transformer Type	EQ Record	Location	Displacement (in)			Acceleration (g)		
			x	y	z	x	y	z
TT3	El-Centro	Mid level of Transformer	0.086	0.022	0.025	1.265	1.011	0.501
		Top of Transformer	0.175	0.029	0.045	2.038	1.037	0.709
		Top of Bushing	1.229	0.288	0.036	12.386	2.791	0.730
	Hollister Airport	Mid level of Transformer	0.064	0.020	0.031	1.034	1.012	0.457
		Top of Transformer	0.120	0.026	0.032	1.281	1.015	0.474
		Top of Bushing	0.539	0.188	0.037	5.081	1.368	0.567
	Pacoima Dam	Mid level of Transformer	0.090	0.023	0.036	1.311	1.097	0.410
		Top of Transformer	0.168	0.028	0.037	1.787	1.117	0.428
		Top of Bushing	1.156	0.314	0.028	12.118	2.814	0.403
	Lake Hughes Array #4	Mid level of Transformer	0.111	0.024	0.046	1.624	1.146	0.673
		Top of Transformer	0.212	0.030	0.048	2.515	1.187	0.701
		Top of Bushing	1.563	0.497	0.027	18.385	4.544	0.466

Support reactions are given in Table 4, Table 5, and Table 6 for TT1, TT2, and TT3, respectively, for different earthquake records. Maximum vertical support reaction is 230 kips and corresponding horizontal reaction is 98 kips in x direction (weak axis), for TT1. Maximum vertical support reaction is 256 kips and corresponding horizontal reaction is 103 kips in x direction, for TT2. Similarly, maximum vertical support reaction is 440 kips and corresponding horizontal reaction is 246 kips in x direction, for TT3. The maximum reactions were also computed by the static analysis method specified in IEEE recommendations. The center of gravity of for each transformer type is assumed at center

of the tank. Acceleration of 0.5g in horizontal direction (weak axis) and 0.4g in vertical direction are applied to the center of gravity for each transformer type. Dimensions of the transformer tanks are given earlier in this chapter. Self-weight of transformers are not considered in calculation of overturning moments. The vertical static acceleration (0.4g) is applied in upward direction for critical overturning moment. Static calculations are carried out to get vertical and horizontal reactions. Calculations are given in Appendix A of this thesis. Vertical reaction is 63 kips and horizontal reaction is 22 kips in horizontal weak axis, for TT1. Vertical reaction is 105 kips and horizontal reaction is 38 kips in horizontal weak axis, for TT2. Similarly, vertical reaction is 166 kips and horizontal reaction is 64 kips in horizontal weak axis, for TT3.

In this finite element study, time history analyses are performed for ground input with PGA of 1g in orthogonal horizontal directions and PGA of 0.8 g in the vertical direction. However, static analysis recommended for transformer tanks utilizes 0.5g in horizontal directions and 0.4g in vertical direction, applied to the center of the transformer tank. It is seen that the vertical reaction obtained from the IEEE recommendations is 73% less than the finite element analysis result for TT1. Similarly, the vertical reactions are 59% and 62% less than the finite element analysis results for TT2 and TT3, respectively. It is also noted that the horizontal reaction obtained from the recommendations is 78% less than the finite element analysis result for TT1. Similarly, the horizontal reactions are 63% and 74% less than the finite element analysis results for TT2 and TT3, respectively.

Table 4 Summary of Maximum Support Reactions for TT1

Transformer Type	EQ Record	Location	Force (kips)		
			x	y	z
TT1	El-Centro	Support 1	60.6	70.8	132.1
		Support 2	76.4	79.9	159.3
		Support 3	72.6	83.3	173.2
		Support 4	60.4	70.7	130.1
	Hollister Airport	Support 1	77.9	75.3	140.8
		Support 2	71.6	82.7	137.3
		Support 3	73.2	84.7	149.3
		Support 4	73.3	71.5	134.8
	Pacoima Dam	Support 1	88.4	103.8	186.7
		Support 2	70.2	74.3	138.7
		Support 3	56.0	63.4	111.2
		Support 4	98.0	125.9	230.1
	Lake Hughes Array #4	Support 1	79.4	97.0	188.6
		Support 2	90.0	91.6	200.8
		Support 3	89.4	107.5	204.6
		Support 4	85.2	99.1	183.1

Table 5 Summary of Maximum Support Reactions for TT2

Transformer Type	EQ Record	Location	Force (kips)		
			x	y	z
TT2	El-Centro	Support 1	87.8	105.1	198.8
		Support 2	90.8	97.5	180.8
		Support 3	90.0	96.0	181.8
		Support 4	74.4	95.6	192.3
	Hollister Airport	Support 1	93.5	94.1	175.7
		Support 2	79.4	103.9	189.6
		Support 3	107.2	107.8	204.9
		Support 4	85.5	78.9	156.3
	Pacoima Dam	Support 1	96.5	114.3	186.3
		Support 2	81.8	89.1	173.2
		Support 3	75.3	64.7	139.0
		Support 4	117.6	134.9	221.5
	Lake Hughes Array #4	Support 1	104.2	112.6	232.9
		Support 2	103.4	109.5	256.3
		Support 3	115.7	111.6	242.5
		Support 4	109.6	113.0	234.0

Table 6 Summary of Maximum Support Reactions for TT3

Transformer Type	EQ Record	Location	Force (kips)		
			x	y	z
TT3	El-Centro	Support 1	152.7	182.4	346.5
		Support 2	181.3	199.0	368.9
		Support 3	191.7	203.9	358.0
		Support 4	160.3	161.1	318.5
	Hollister Airport	Support 1	160.8	168.9	241.5
		Support 2	145.3	182.2	224.6
		Support 3	162.7	183.1	257.2
		Support 4	151.3	151.8	235.8
	Pacoima Dam	Support 1	196.9	180.0	339.0
		Support 2	191.7	176.7	339.6
		Support 3	164.9	135.9	262.6
		Support 4	174.7	207.3	282.2
	Lake Hughes Array #4	Support 1	245.5	280.6	440.2
		Support 2	220.0	233.0	375.0
		Support 3	223.5	259.6	383.6
		Support 4	226.2	230.3	387.5

Figure 18 through Figure 20 show relative displacement, acceleration responses, and the normalized power spectrum of the acceleration responses at top of transformer at one of the top corners (SW5) for TT2. As an example, Figure 18 contains 2-time history graphs and 1-normalized power spectrum graph. The upper plot shows the relative displacement time history and the second graph in this figure shows the acceleration time history. Normalized power spectra graphs help us better understand the frequency response of the components. Normalized power spectra are obtained by taking advantage of the Fast Fourier Transformation (FFT). As it is seen in this figure, the response

frequency of SW5 point in this graph gives us the value 13.85 Hz and this value is very close to that of mode 7 of TT2 (14.1 Hz). It can be pointed out that the translational modes of transformers have the highest participation in the response at the top of transformers.

Failure of transformer and its components other than bushing was not found in the finite element analysis performed in this study. The stress responses of the transformer tank are below the allowable material stresses. Failure of the transformer bushing system is introduced at the gap between the bushing units. For the fixed case, since the base forces are so high, providing proper anchorage is problem. A base isolation system (FPS) is introduced as a retrofitting scheme in the next chapter of this thesis. Base isolation of the transformer reduces the base forces of the transformer; therefore it can be a possible solution for eliminating high anchorage forces.

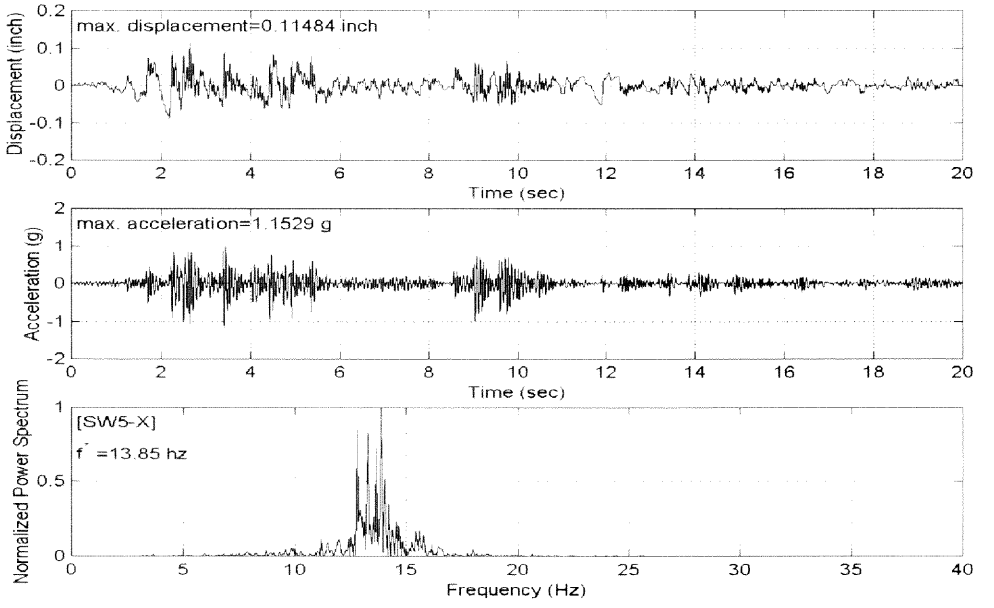

Figure 18 Displacement, Acceleration Responses and Normalized Power Spectrum at SW5 of TT2 for El-Centro Record in X-direction

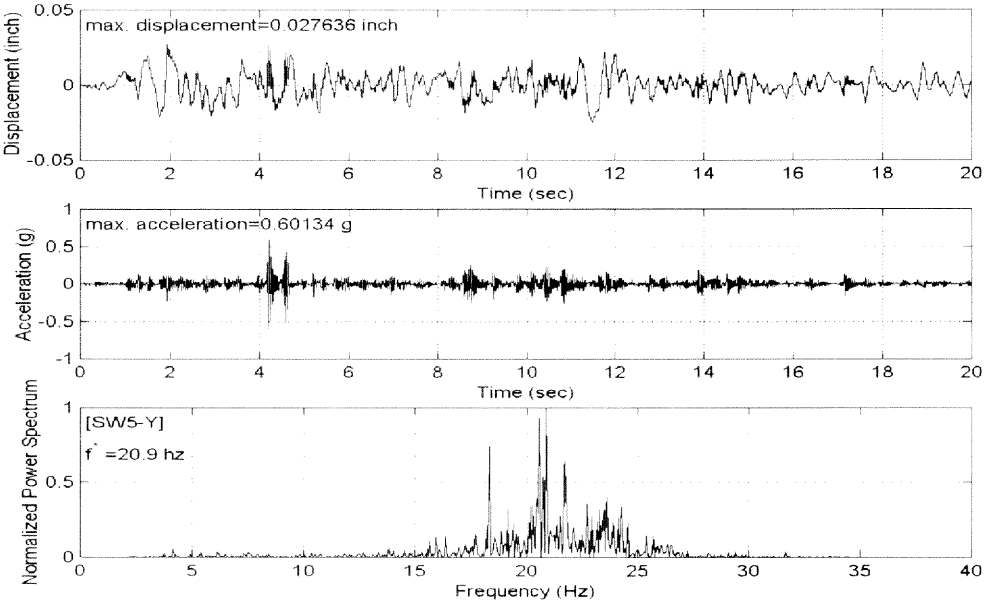

Figure 19 Displacement, Acceleration Responses and Normalized Power Spectrum at SW5 of TT2 for El-Centro Record in Y-direction

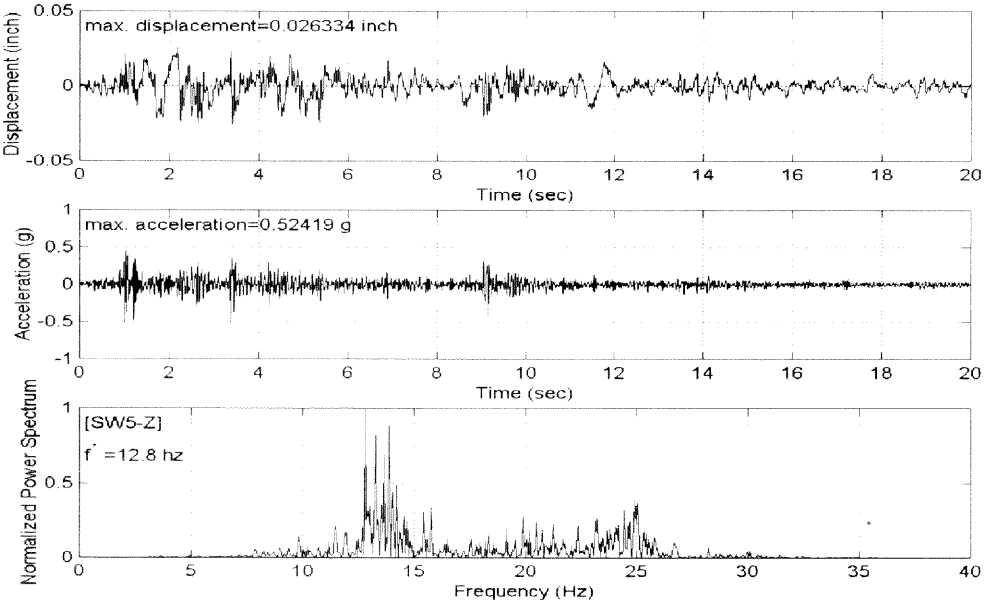

Figure 20 Displacement, Acceleration Responses and Normalized Power Spectrum at SW5 of TT2 for El-Centro Record in Z-direction

2.4.2 Dynamic Response of Bushing

Maximum responses at top of bushing mounted on top of transformers TT1, TT2, and TT3 are tabulated in Table 1, Table 2, and Table 3, respectively, for four different earthquake records. Figure 21 through Figure 23 show relative displacement, acceleration response, and the normalized power spectrum of the acceleration responses at the top of the east bushing (BUE12), center bushing (BUC12), and west bushing (BUW12) mounted on TT2.

As an illustrative example, Figure 21 contains two time history graphs and one normalized power spectrum graph. The upper plot shows the relative displacement time history and the second graph in this figure shows the acceleration time history. Bushing frequency is obtained as 9.9 Hz from normalized power spectrum. The fundamental frequency of the bushing was obtained as 14.4 Hz from the modal analysis of bushing itself fixed at flange of the bushing. The transformer top plate has an effect on the dynamic characteristics of the bushing. As a general tendency, the translation mode of the transformer effects the input into the bushing by filtering the motion and causing higher mode to be excited. For the bushing mounted on TT1, frequency is reduced to 11 Hz. For the bushing mounted on TT2, frequency is reduced to 10 Hz. And the response frequency of bushing mounted on TT3 is reduced to 10.5 Hz.

The maximum displacement response at the top of the bushing in x-direction (weak horizontal axis) for four earthquake inputs throughout the time history analysis is 0.95 inch for bushing mounted on TT1. That of the bushing mounted on TT2 and TT3 is obtained as 0.81 inch and 1.56 inch, respectively. The maximum total acceleration

response at the top of the bushing in x-direction (weak horizontal axis) for four earthquake inputs throughout the time history analysis is 10.9g for bushings mounted on TT1. That of bushings mounted on TT2 and TT3 is obtained as 8.3g and 18.4g, respectively.

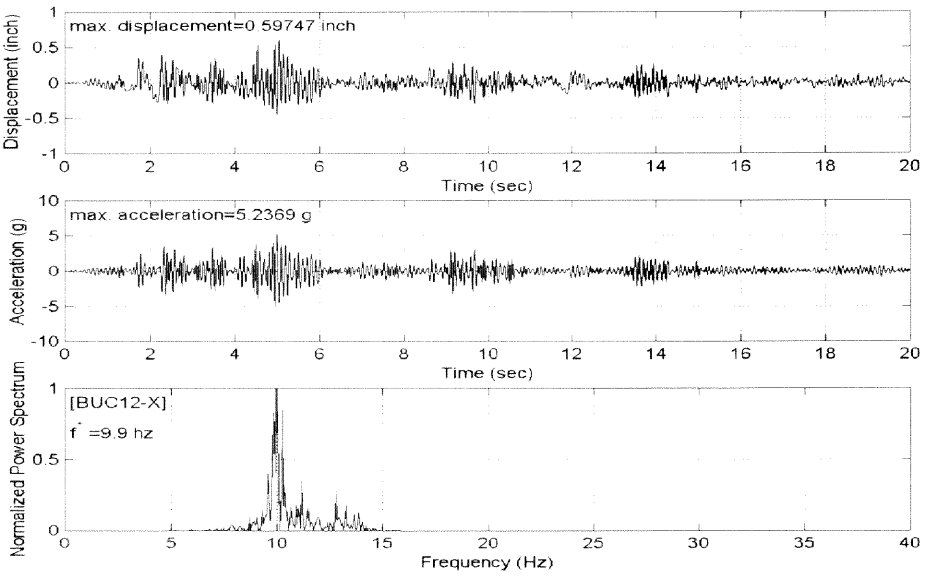

Figure 21 Displacement, Acceleration Responses and Normalized Power Spectrum at BUC12 of TT2 for El-Centro Record in X-direction

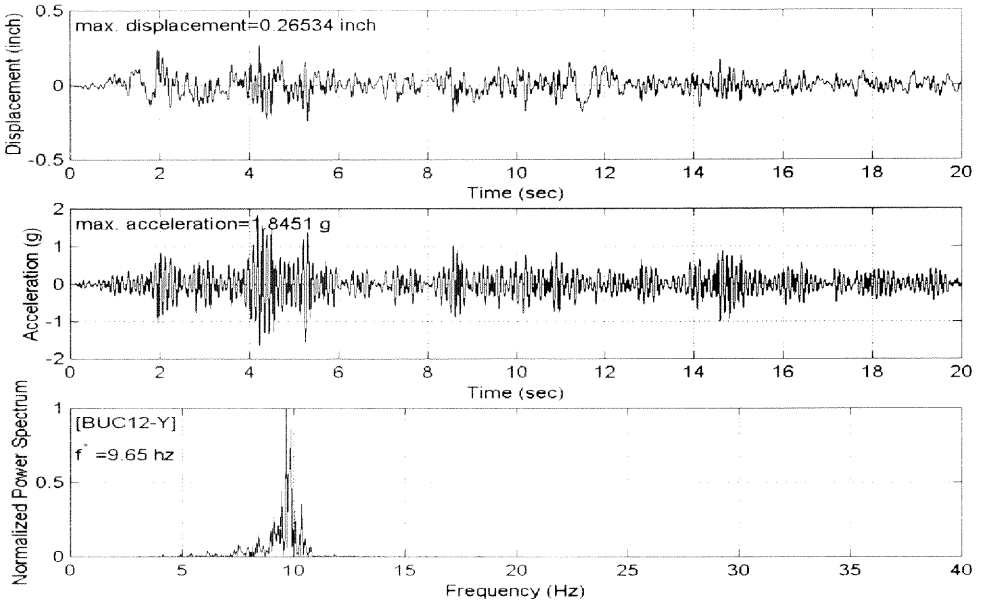

Figure 22 Displacement, Acceleration Responses and Normalized Power Spectrum at BUC12 of TT2 for El-Centro Record in Y-direction

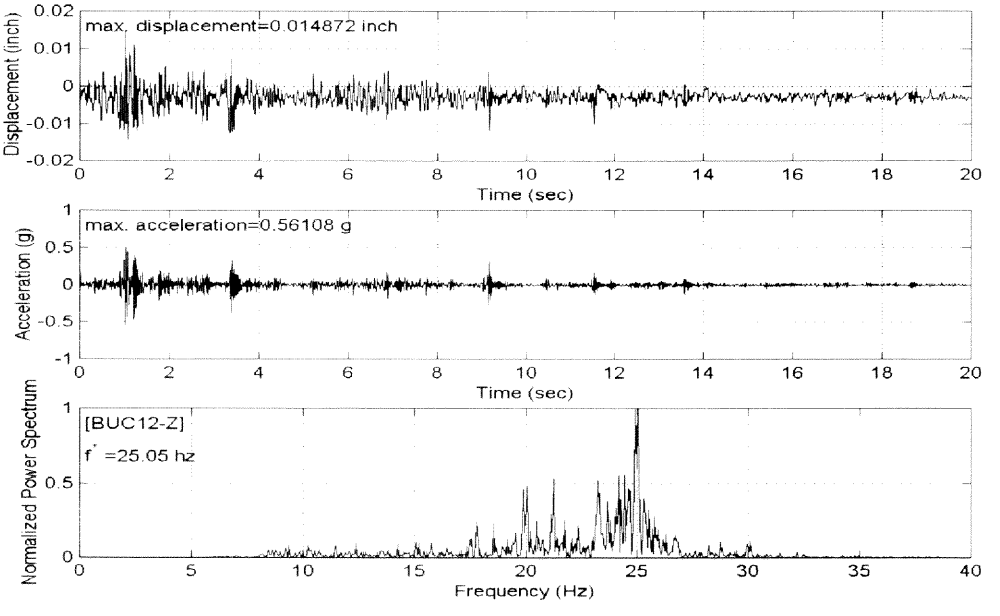

Figure 23 Displacement, Acceleration Responses and Normalized Power Spectrum at BUC12 of TT2 for El-Centro Record in Z-direction

Axial responses of bushing gaskets are also analyzed in this section. The seismic response of the bushings is dominated by the behavior of the gaskets between the porcelain units. One of the common failure modes involves movement of the upper porcelain unit relative to its support flange, causing oil leakage. In the following figure two gaskets located right above the flange are referred to as gasket 2 and the first gasket from the top of bushing is referred to as gasket 5. The vertical axis in the graph shows the gap between the gasket and the porcelain components. Since the bushing is prestressed, the gap initially starts from some value showing the initial displacement of the gasket under prestress force. The positive gap amount illustrates that there is a gap during the time history loading between the gasket edge and porcelain unit. The positive gap causes oil leakage from the bushing. As one can note from Figure 24 the gap near the aluminum flange of the bushing, called gasket 2 in this study, is always more serious for bushing. The gap forms due to the relative vertical displacements of the units right above and below the gaskets and the rotation of these units. No formation of a positive gap is observed in time history analyses performed for TT1. However, a gap forms during the analysis for TT2 and TT3. Figure 24 shows the most critical condition, which occurs for TT3 with Lake Hughes Array #4 record. Since failure is likely some preventive measures are needed.

The porcelain units are fragile components so that stress and strain levels in them have also been investigated in this study. Based on the previous studies performed on the porcelain units, their ultimate axial strain capacity is 4000E-6 in/in [Gilani, 1998]. It is observed that stress/strain levels in the porcelain units are well below the capacity.

The bushing has an aluminum core housing the copper cables between equipment items and the coils, throughout its length. The bushing is post-tensioned through its aluminum core and the springs in the metallic dome ensure the uniform distribution of this prestress force. The relaxation effect of the axial dynamic force is examined also. It is found that the effect of axial vibration of the bushing on the prestressing is insignificant, indicating that there has not been any prestress loss.

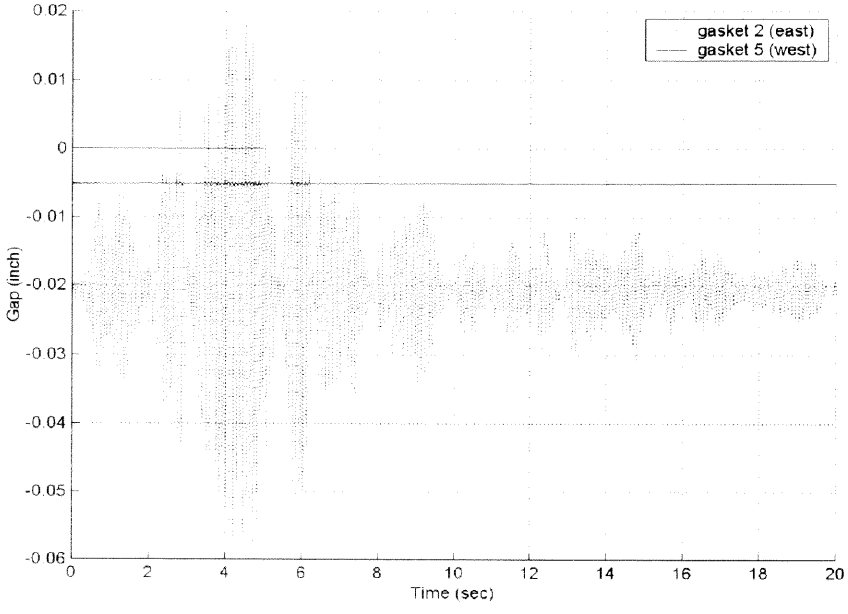

Figure 24 Gap in the Bushing Gasket Mounted on TT3 for Lake Hughes Array # 4 Record

As was stated previously in this chapter, the transformer models used in these finite element analyses were fixed at each corner of bottom transformer plate. The finite element analysis results show that anchoring of transformer to its base does not prevent the interaction between transformer and bushing and causes bushing failure for some of the cases. For this reason, the implementation of well-designed anchorage for retrofit of existing transformers can be difficult and costly. Furthermore, in many situations, for

both new and existing transformers, a well-designed anchorage may only change the mode of failure to the foundation. Boundary gaps due to back and forth motion of transformers and rocking of transformers and their footings due to soil-structure interaction have been observed during past earthquakes [ASCE, 1999]. Therefore, in many cases the use of base-isolation for transformers may be the only suitable remedy to alleviate these problems, especially for existing transformers in high seismic regions. Base-isolation will also reduce the input acceleration into the bushing and will lessen the interaction between the transformer and the bushing, which has been the cause of many bushing failures during past earthquakes. Furthermore, by reducing the inertia forces, base-isolation can also prevent the possibility of internal damage. The after effect of an earthquake on reliability and longevity of a transformer is directly related to the level of shaking of internal elements. High level of uncontrolled shaking may very well reduce the life expectancy and reliability of internal elements. Therefore, Chapter 3 is devoted to further detailed analytical investigation of Frictional Pendulum System (FPS) as a base isolation remedy to transformer bushing system. Furthermore, in collaboration with the National Center for Research on Earthquake Engineering (NCREE) in Taiwan, a series of tests were conducted on a transformer model supporting a bushing. Chapter 4 presents the results of these tests.

CHAPTER 3
STUDY OF THE FRICTIONAL PENDULUM SYSTEM

Base isolation is a simple structural design approach to mitigate or reduce potential earthquake damage. Base isolation reduces the seismic force transmitted to the structure by supporting it with flexible element at the base to elongate the natural period of the structure and decouple it from ground. The first patent regarding base isolation was proposed in early 1900 and the first research paper on the base isolation was published in 1891. Most early publications were limited to the description of the concept. In the last 30 years, however, the base isolation technology has been developed to the point of practical applications with the aid of new materials and computer analysis. Recent earthquakes in USA and Japan verified the effectiveness of base isolation for many structures. Through this experience, base isolation technology has been widely accepted and gained popularity.

Basically, base isolation systems provide both a restoring force and energy dissipation. The rubber bearings which are made up with layers of alternating rubber and steel plates are the most popular for providing restoring force and energy dissipation. The plates and rubber layers are bonded to each other by strong special adhesive materials and the plates act as confinement for the rubber layers to support vertical load with low horizontal stiffness.

Some of the effective base isolation systems which are being utilized today are listed below. Their system performance characteristics are given in a recent study [Naeim, 1999].

1. Elastomeric-based system
2. Low damping natural and synthetic rubber bearings
3. Lead plug bearings
4. High damping natural rubber bearings
5. Resilient friction natural rubber bearing
6. Friction pendulum system
7. Resilient-friction based isolation system
8. EERC combined system

Among these base isolation methods, the frictional pendulum system is selected for this study to retrofit the power transformer. The frictional pendulum is one of the most effective base isolation methods since it can accommodate larger displacements compared to others systems, and is easy to design. The most important design parameter of this system is the radius of curvature of the bearing.

3.1 Friction Pendulum System

The Friction Pendulum System (FPS) is an effective and practical base isolation technology for reducing the damaging effects on a structure of an earthquake. This base isolation device, which was originally developed by MCEER (Multidisciplinary Center for Earthquake Engineering and Research) researchers, is based on the effective concept of pendulum motion combined with velocity dependent damping characteristics. Typical FPS is shown in Figure 25 and Figure 26. This isolation system combines sliding action and restoring force. The FPS isolator shown in Figure 26 has an articulated slider that moves on a stainless steel spherical surface. The side of the articulated slider in contact

with the spherical surface is coated with a low friction composite material. As the slider moves over spherical surface, it causes the supported mass to rise and provides the gravity induced restoring force for the system. Friction between the articulated slider and the spherical surface provides damping in the isolator. The radius of curvature of the concave surface controls the effective stiffness of the isolator. Geometry and gravity of the FPS achieve the desired seismic-isolation. In light of transformer's weight and the mobility requirements for maintenance purposes, FPS has been identified as a practical technology for their seismic rehabilitation. A parametric study of FPS for transformers is performed in this chapter.

3.1.1 Geometric Description and Technical Characteristics

Dynamic periods from one to five seconds and displacement capacities up to 48" can be provided. The dynamic coefficient of friction ranges from 3% to 20%. Effective damping ranges from 10 to 50%. Individual capacities up to 12 million pounds can be provided. Bearings can be fitted with enclosing tension restraint plates that carry tension loads. The pendulum properties of FPS make the FPS system particularly effective at minimizing adverse torsional motions that result from accidental mass eccentricities. The bearing's dynamic stiffness is directly proportional to the supported weight; hence the center of lateral stiffness of the bearings always coincides with the center of mass of the structure. Therefore, the stiffness and friction forces automatically adjust for accidental mass eccentricities. The materials used in the FPS bearings can maintain their performance properties for temperatures as low as -100°F. The total assembly height eases the installation of the bearings and the bearing can be installed with the concave surface facing up or down.

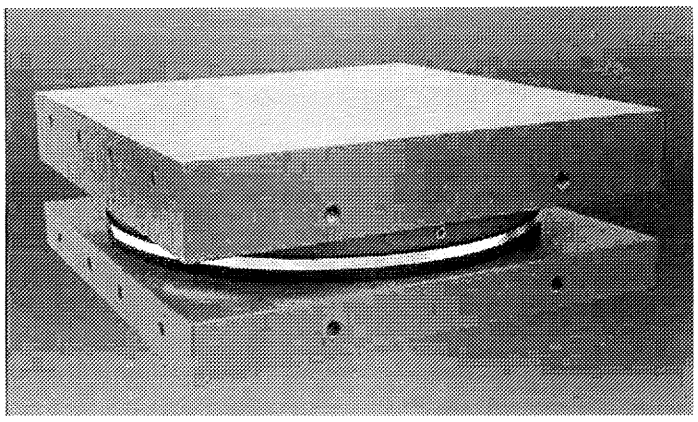

Figure 25 Photograph of a FPS Isolator [EPS]

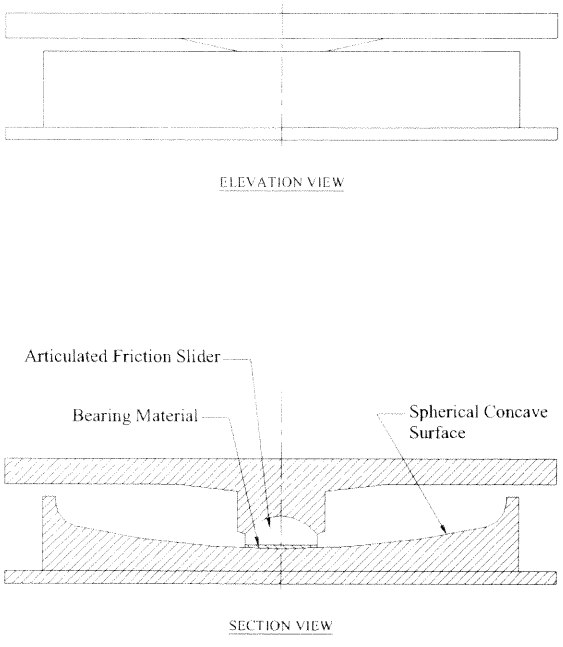

Figure 26 Typical Elevation and Section of FPS

3.2 Formulation of the Equation of Motion for the Friction Pendulum System

The formulation discussed in this section is based on the assumption of small displacements. As it can be seen in Figure 27, there are three forces acting on the free

body diagram of the FPS bearing. Having θ as angle between initial and displaced positions, the geometric relations imply that

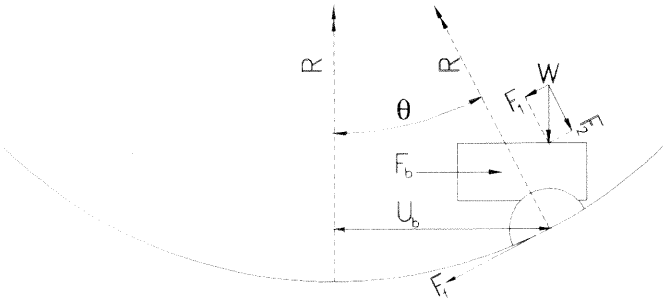

Figure 27 Force Diagram of FPS

$$\sin\theta = \frac{F_I}{W} \tag{3}$$

$$\sin\theta = \frac{U_b}{R} \tag{4}$$

where

W= supported weight

R= the radius of curvature of the bearing

F_I = restoring force

U_b = bearing displacement.

Restoring force is expressed as,

$$F_I = W\sin\theta = \frac{W}{R}U_b \tag{5}$$

Friction force acts opposite to the motion,

$$F_f = F_2\mu_s = \mu_s W\cos\theta \tag{6}$$

Having $\cos\theta = 1$ for small displacement assumption, and introducing $\text{sgn}(\dot{U}_b)$ for direction of friction force, equation (6) can be rewritten as follows:

$$F_f = \mu_s W\,\text{sgn}(\dot{U}_b) \tag{7}$$

μ_s = the coefficient of friction mobilized during sliding

$\dot{U}_b$ = bearing sliding velocity

F_f = friction force

The model of friction for teflon-steel interface used in this study is based on principles of theory of viscoplasticity and is referred to as a modified viscoplasticity model [Constantinou, 1990]. This model is based on equation (8).

$$Y\dot{Z} + \gamma|\dot{U}_b|Z|Z|^{\eta-1} + \beta\dot{U}_b|Z|^{\eta} - A\dot{U}_b = 0 \tag{8}$$

In this equation, β, r, A, η are dimensionless constants, and Y represents a small elastic displacement for teflon-steel interfaces before sliding. The frictional force is given by equation (9)

$$F_f = \mu_s WZ \tag{9}$$

This equation is essentially identical to equation (7). It should be noted that during sliding (yielding), Z takes values of ± 1. A time history graph of Z, for one of the parametric studies performed in this chapter is shown in Figure 28. During sticking (elastic behavior) the absolute value of Z is less than unity. The conditions of separation and reattachment are accounted by equation (8). In this respect Z may be regarded as a continuous

approximation to the function of $\mathrm{sgn}(\dot{U}_b)$ in equation (7). Teflon-steel interfaces undergo some very small elastic displacements before sliding. Experimental observation suggests a value of Y of about 0.005 to 0.02 inch [Constantinou, 1990]. The value of η =2, with A =1 and $\beta+\gamma=1$ (β=0.1, γ=0.9) produces loops of frictional force versus sliding displacement that are in good agreement with experimental results. The lateral force at the isolation level, F_b, is equal to the sum of the restoring force and the friction force and it is given in equation (10).

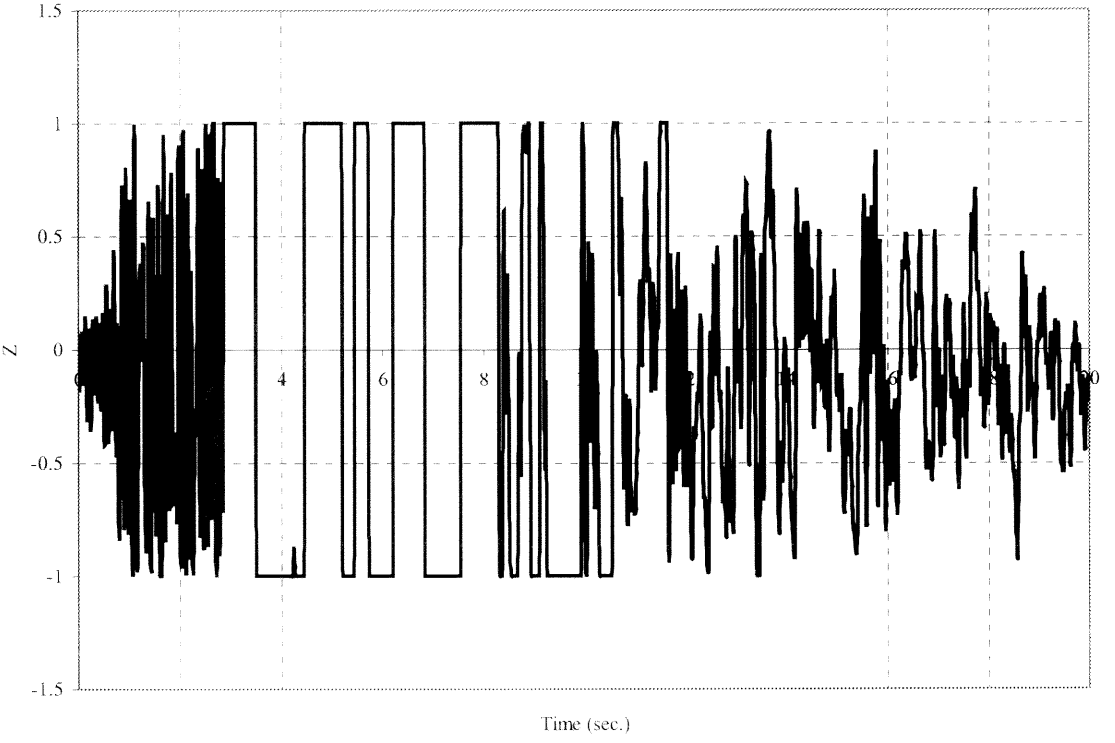

Figure 28 A Time History for Variable Z

$$F_b = U_b \frac{W}{R} + \mu_s WZ \qquad (10)$$

The period of vibration of the structure in its rigid body condition is,

$$T = 2\pi\sqrt{\frac{R}{g}} \tag{11}$$

g is the gravitational acceleration. This is the natural period of a pendulum of length R, which shows that the natural period of vibration of a FPS isolated structure is independent of the structure weight. Assuming that the system behaves as a rigid body, dynamic equilibrium in horizontal direction can be expressed as follows:

$$M_b(\ddot{U}_b + \ddot{U}_g) + F_b = 0 \tag{12}$$

$$M_b\ddot{U}_b + F_b = -M_b\ddot{U}_g \tag{13}$$

$$M_b\ddot{U}_b + \mu_s WZ + \frac{W}{R}U_b = -M_b\ddot{U}_g \tag{14}$$

where

$\ddot{U}_b$ = bearing base acceleration

$\ddot{U}_g$ = ground acceleration

M_b = mass of the block

R= the radius of curvature of the bearing

3.2.1 Numerical Solution of the Equation of Motion for FPS

The analysis was performed by employing a Fortran code, which uses an IMSL routine IVPAG. This routine solves an initial-value problem for ordinary differential equations using the Adams-Moulton's method. This Fortran code is provided in Appendix B of this thesis. The formulation for the 1-D case is as follows. Let

$$\dot{U}_b = V \tag{15}$$

where

V = bearing sliding velocity

Equations (8) and (14) can be reduced to a system of first-order differential equations,

$$\dot{V} = -\frac{W}{M_b R} U_b - \mu_s \frac{W}{M_b} Z - \ddot{U}_g \tag{16}$$

$$\dot{Z} = -\frac{\gamma}{Y}|V|Z|Z|^{\eta-1} - \frac{\beta}{Y} V|Z|^{\eta} + \frac{A}{Y} V \tag{17}$$

Equations (15), (16), and (17) are solved for the 1-D analysis. For 2-D analysis, let

$$\dot{U}_{bx} = V_x \tag{18}$$

and

$$\dot{U}_{by} = V_y \tag{19}$$

where

V_x = bearing sliding velocity in x-direction

V_y = bearing sliding velocity in y-direction, then

$$\dot{V}_x = -\frac{W}{M_b R} U_{bx} - \mu_s \frac{W}{M_b} Z_x - \ddot{U}_{gx} \tag{20}$$

$$\dot{V}_y = -\frac{W}{M_b R} U_{by} - \mu_s \frac{W}{M_b} Z_y - \ddot{U}_{gy} \tag{21}$$

The 2-D model is based on the following system of coupled equations [Constantinou, 1990],

$$Y\dot{Z}_x + \gamma\left|\dot{U}_{bx}Z_x\right|Z_x + \beta\dot{U}_{bx}Z_x^2 + \gamma\left|\dot{U}_{by}Z_y\right|Z_x + \beta\dot{U}_{by}Z_xZ_y - A\dot{U}_{bx} = 0 \tag{22}$$

$$Y\dot{Z}_y + \gamma\left|\dot{U}_{by}Z_y\right|Z_y + \beta\dot{U}_{by}Z_y^2 + \gamma\left|\dot{U}_{bx}Z_x\right|Z_y + \beta\dot{U}_{bx}Z_xZ_y - A\dot{U}_{by} = 0 \tag{23}$$

Equations (22) and (23) are extensions of equation (8) for η=2.0 then,

$$\dot{Z}_x = -\frac{\gamma}{Y}\left|\dot{U}_{bx}Z_x\right|Z_x - \frac{\beta}{Y}\dot{U}_{bx}Z_x^2 - \frac{\gamma}{Y}\left|\dot{U}_{by}Z_y\right|Z_x - \frac{\beta}{Y}\dot{U}_{by}Z_xZ_y + \frac{A}{Y}\dot{U}_{bx} \tag{24}$$

$$\dot{Z}_y = -\frac{\gamma}{Y}\left|\dot{U}_{by}Z_y\right|Z_y - \frac{\beta}{Y}\dot{U}_{by}Z_y^2 - \frac{\gamma}{Y}\left|\dot{U}_{bx}Z_x\right|Z_y - \frac{\beta}{Y}\dot{U}_{bx}Z_xZ_y + \frac{A}{Y}\dot{U}_{by} \tag{25}$$

Equations (18), (19), (20), (21), (24), and (25) then are solved for 2-D case.

3.2.2 Input Parameters for Numerical Solution

A representative graph of the coefficient of sliding friction is shown in Figure 29 for a pressure value of 2.5 ksi. As it is observed from Figure 29, the coefficient of sliding friction at low velocity is smaller than the maximum friction value. As the sliding velocity increases, the amount of friction reaches the maximum. The coefficient of friction used for this parametric study is 0.10, which is a good approximation for bearing pressures of transformer used in this thesis. The values of the constants used for solution of equation (8) are given in Table 7.

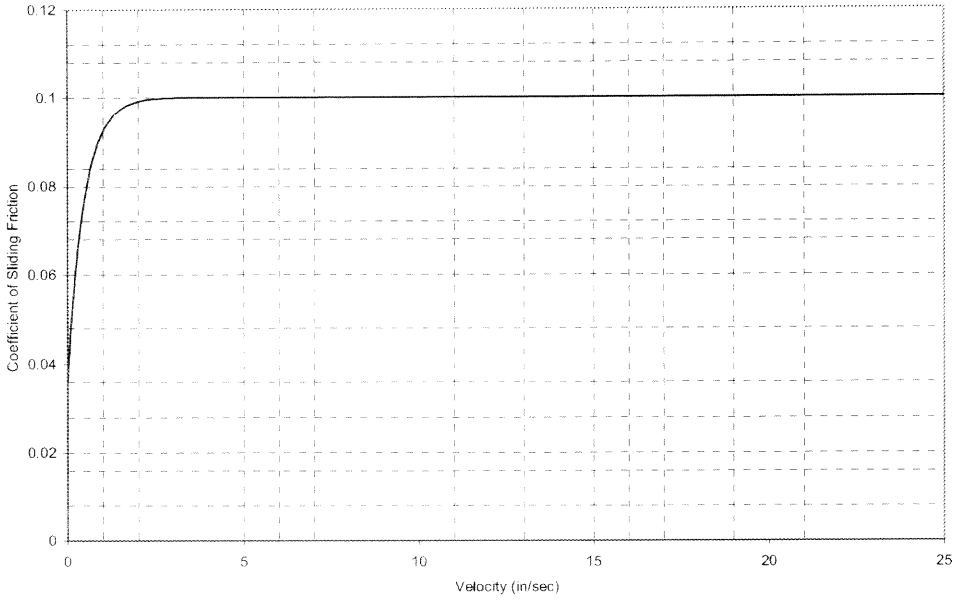

Figure 29 Variation of Coefficient of Sliding Friction

Table 7 Values of Equation (8) Constants

β	0.1
γ	0.9
A	1.0
η	2.0
Y	0.005

3.2.3 Ground Motion Input

Earthquake ground motions are random and irregular. Therefore, earthquake-resistant design is based on the general characteristics of an ensemble of earthquakes. Earthquakes can be classified into four categories [Newmark, 1971]:

1. Single shocks: Motions of this type occur at short distances from the epicenter, on firm ground, and only for shallow earthquakes.

2. Moderately long, extremely irregular motions: Motions of this type occur at moderate distances from the epicenter, on firm ground. They have the characteristics of white noise and have almost equal severity in all directions.

3. Long ground motions exhibiting pronounced prevailing periods of vibration: Motions of this type result from the filtering of earthquakes of the preceding type through layers of soft soils.

4. Ground motions involving larger-scale permanent deformations of the ground: Motions of this type are representative of near-source ground motions.

Earthquakes belonging to the second and third groups cause the seismic hazard in most locations. Therefore, 20 records belonging to these two classes are selected for a parametric study. They are tabulated in Table 8. These records were scaled based on peak ground acceleration (PGA) throughout this study. For design purposes the average of all records is presented and discussed. In addition, results based on rock and soil records are individually presented in the subsection on ground motion effects in this chapter.

Table 8 Ground Motion Records Employed

Type of Motion	Earthquake Name	Station Component	Station Name	PGA (g)
ROCK	San Fernando	S16E	Pacoima Dam	1.170
	San Fernando	S74W	Pacoima Dam	1.075
	San Fernando	S69E	Lake Hughes Array #4	0.172
	San Fernando	S21W	Lake Hughes Array #4	0.146
	Loma Prieta	227	Apeel Array #9	0.108
	Loma Prieta	137	Apeel Array #9	0.117
	Loma Prieta	360	Calaveras Array	0.079
	Loma Prieta	270	Calaveras Array	0.076
	Kern County	S69E	Taft	0.179
	Kern County	N21E	Taft	0.156
SOIL	Northridge	N21E	Sylmar	0.826
	Northridge	N79W	Sylmar	0.492
	Kern County	S00W	Hollywood Storage	0.059
	Kern County	N90E	Hollywood Storage	0.042
	Imperial Valley	S00E	El Centro	0.348
	Imperial Valley	N90W	El Centro	0.214
	Loma Prieta	255	Hollister Airport	0.287
	Loma Prieta	165	Hollister Airport	0.282
	Northridge	90	Norwalk	0.141
	Northridge	360	Norwalk	0.141

3.3 Parametric Study Results

Three different types of parametric studies were conducted: Unidirectional (1-D) analysis, bi-directional (2-D) analysis where two orthogonal horizontal motions were considered, and tri-directional (3-D) analysis to investigate the effect of the vertical component of ground motion on the horizontal responses. These results are discussed in the following sections.

The 1-D analyses were performed for 400 different cases. This consisted of five different bearing radii (R = 30", 60", 90", 120", and 150"), and four different PGAs (0.25g, 0.5g, 0.75g and 1.0g). The 2-D analyses included 200 cases. Similar to the 1-D

case, radius and PGA were the parameters. It consisted of five different bearing radii (R = 30", 60", 90", 120" and 150") and four different PGAs (0.25g in x and 0.25 in y, 0.50g in x and 0.50g in y, 0.75g in x and 0.75g in y, 1.0 g in x and 1.0g in y). Using the same parameters another 200 cases were analyzed to investigate the effect of vertical motion.

In the following sections, the criteria used for performance evaluation are the maximum displacement and the inertia reduction. Inertia reduction refers to the decrease in the force at the isolation level, $-M_b(\ddot{U}_b + \ddot{U}_g)$, compared to $-M_b\ddot{U}_g$. It should be noted that the inertia reduction compared to a fixed base situation (i.e., if FPS was not used) is generally much higher than these numbers. However, under a SDOF idealization such comparison is not possible.

3.3.1 Results of 1-D Analyses

The acceleration time history for one of the case studies is shown in Figure 30. The parameters used for this particular case are as follows: radius of bearing is 30", and PGA is 1.0g. The maximum response acceleration, as seen from Figure 30, is equal to 0.41g and the maximum displacement is 10 inches for this example case. Thus, there is about a 60% reduction in system acceleration compared to ground PGA for this particular case.

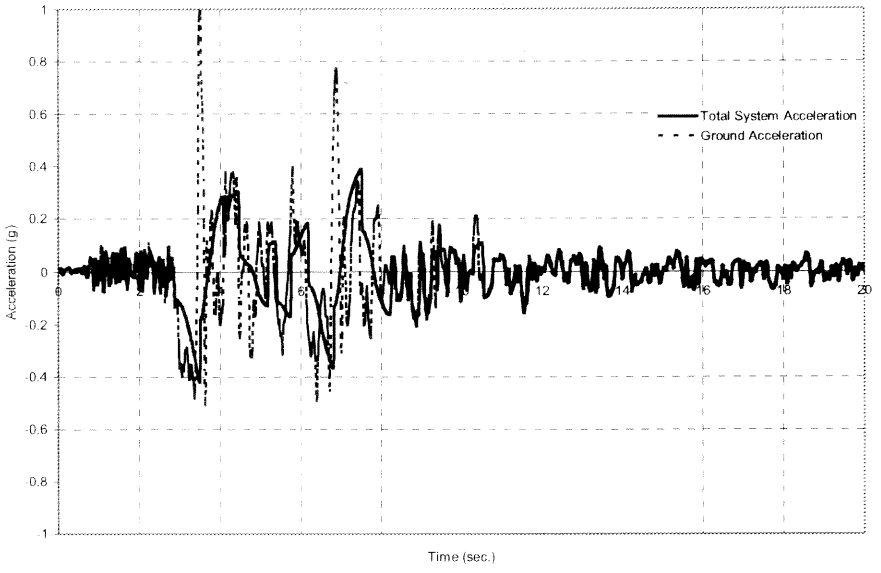

Figure 30 Acceleration Time Histories for an Example Case

Considering the parameters used, the period of vibration for this example, using equation (11), is equal to 1.75 second. It is instructive to compare the results of this case to that of an equivalent single-degree-of-freedom model. Assuming unit mass, the equivalent stiffness, K = W/R will be 12.88 lb/in. Using these system parameters and the same input motion, several analyses with various damping ratios were performed. The maximum displacement for the equivalent SDOF with 5% damping is equal to 18.3 inches. To get the equivalent damping for the isolated system, other cases of damping were analyzed and it was determined that the equivalent damping for this particular case is 40% of the critical damping. However, the manufacturer's data indicates that the equivalent damping for FPS bearings can be as high as 50%.

Based on the 1-D analyses using all 20 records, the average inertia reduction varies from 40% to 75%. The maximum displacements range from 1" to 22" for different cases. The average maximum displacement and inertia reduction are shown in Figure 31

through Figure 33 for a PGA of 0.25g, 0.50g, and 1.0g. Note that the wide difference between the inertia reductions of smaller PGA compared to higher PGA is due to the fact that for lower PGAs the static friction is not exceeded at all times. Therefore, the isolator is more effective for higher PGAs. The charts in Figure 31 through Figure 33 can be used in the seismic design of transformers.

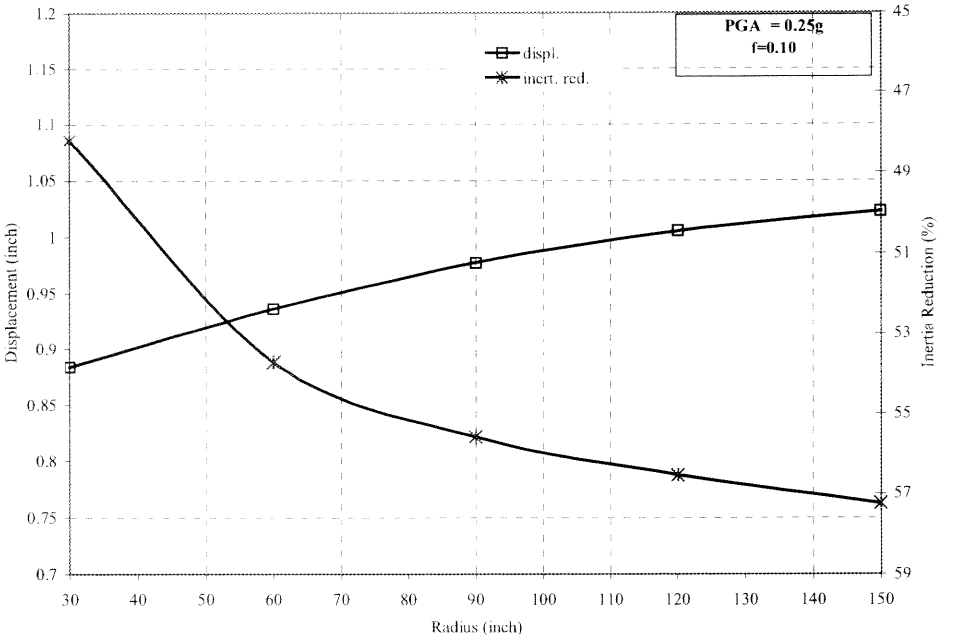

Figure 31 Displacement-Inertia Reduction Chart for PGA of 0.25g

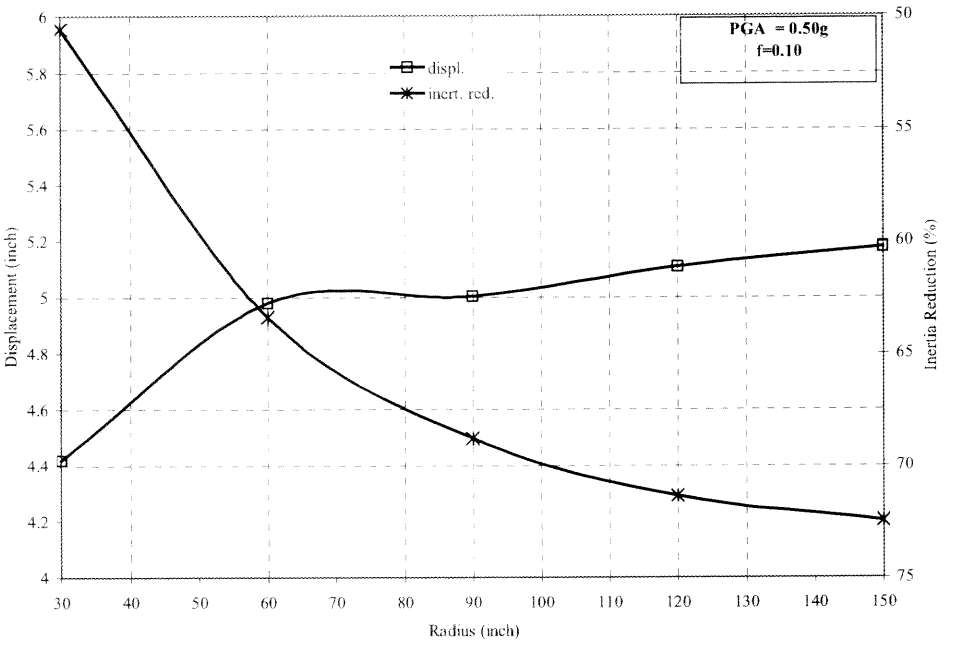

Figure 32 Displacement-Inertia Reduction Chart for PGA of 0.50g

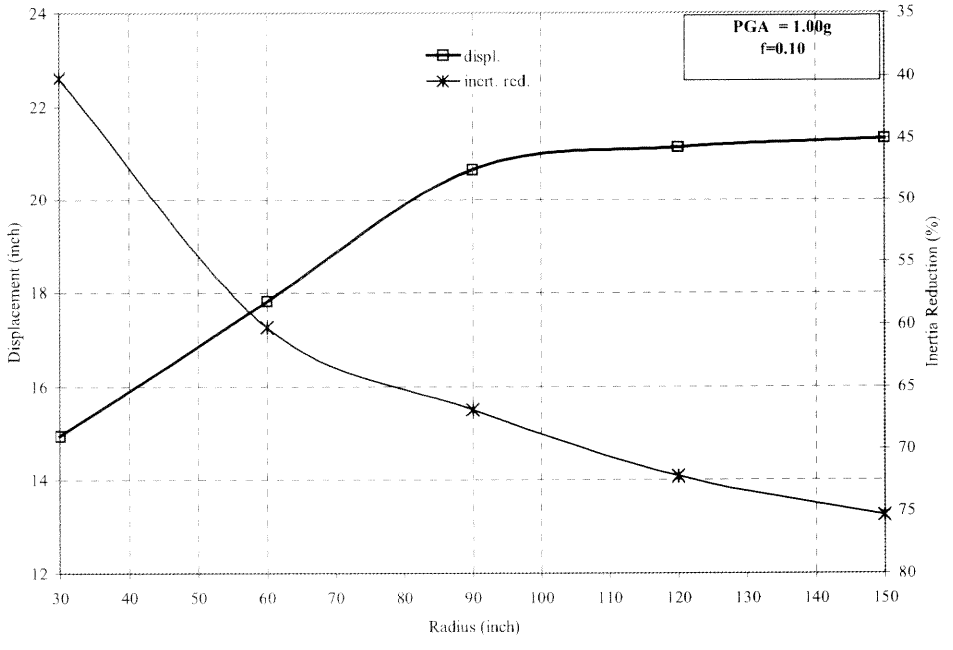

Figure 33 Displacement-Inertia Reduction Chart for PGA of 1.00g

The challenge in design will be the selection of radius of curvature of the bearing such that there is a balance between the desired inertia reduction and the displacement limitations.

3.3.2 Results of 2-D Analyses and Response Combinations

A total of 200 cases were analyzed under two orthogonal horizontal earthquake ground motions. The objectives of the 2-D analyses were to investigate the possibility of coupling between responses in the horizontal directions and to determine a suitable combination rule to be used in design. Due to dependency of friction force on total velocity, it is expected that there is coupling between responses in two horizontal directions that needs to be quantified.

Figure 34 through Figure 36 show comparisons of one-dimensional results with the corresponding component of two-dimensional analyses for PGAs of 0.25g, 0.50g, and 1.0g respectively. It can be seen from these figures, both inertia reduction and displacement are affected, however, the effect on displacement is much more pronounced. Furthermore, the effect of coupling is more significant for lower ground accelerations. As mentioned before, this is due to the effect of total velocity on frictional parameters. Consequently, the individual components of a 2-D response are always larger than the responses of two 1-D cases.

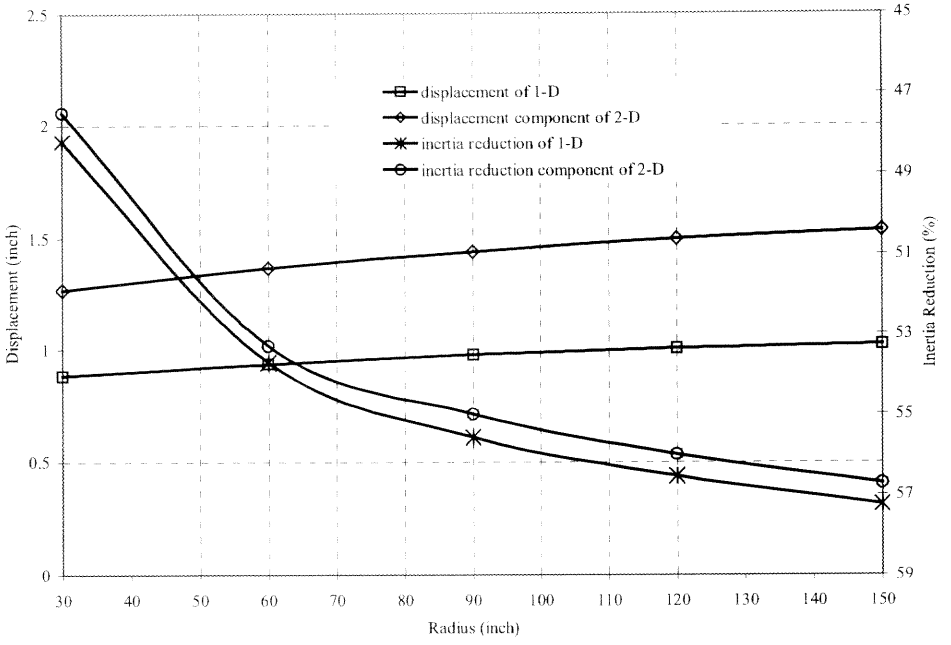

Figure 34 Comparison of 1-D and Corresponding Component of a 2-D Case for PGA of 0.25g

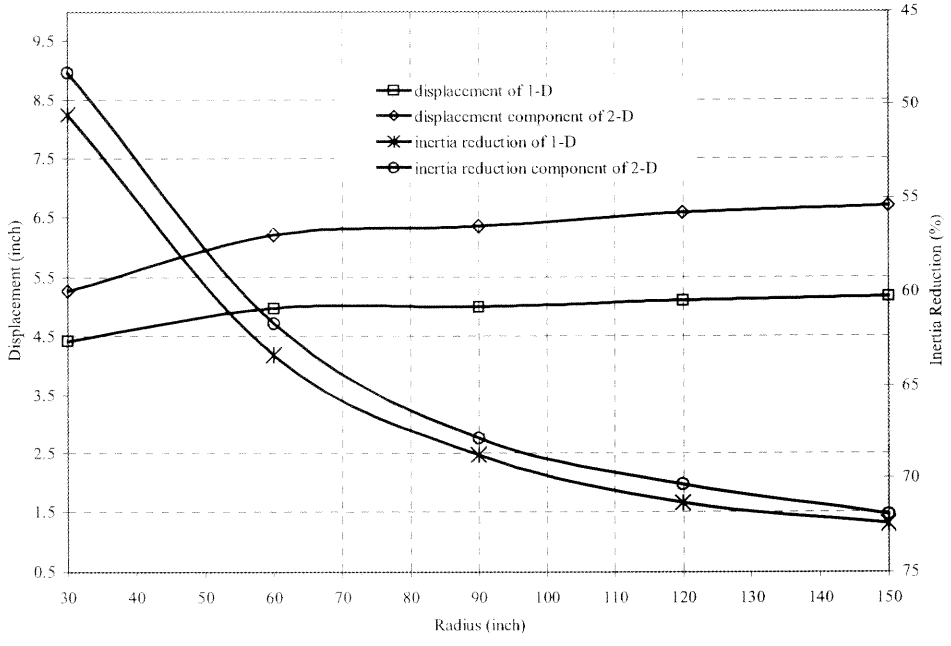

Figure 35 Comparison of 1-D and Corresponding Component of a 2-D Case for PGA of 0.50g

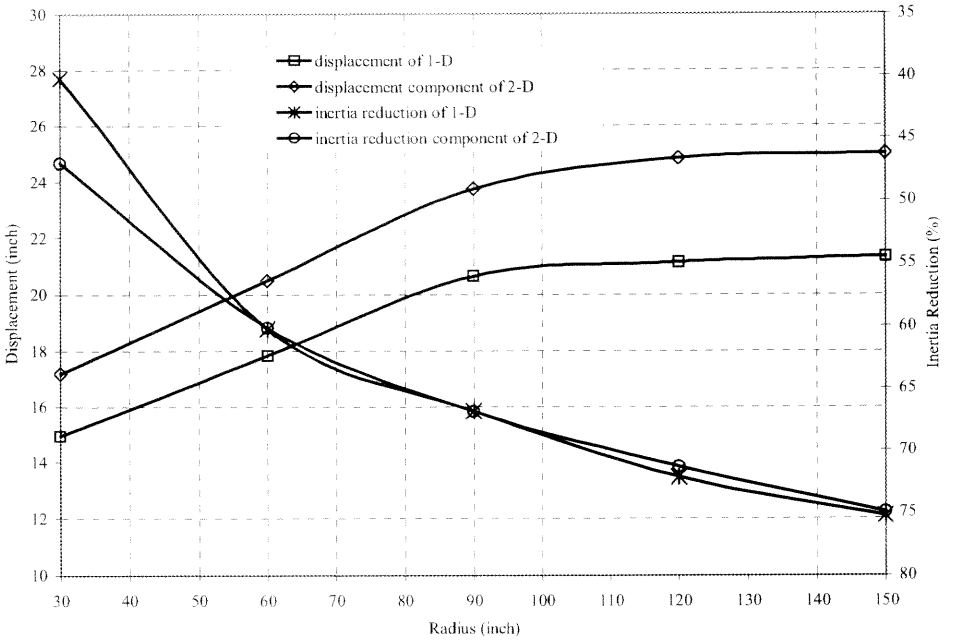

Figure 36 Comparison of 1-D and Corresponding Component of a 2-D Case for PGA of 1.00g

The comparison of total displacement responses using the SRSS (square-root-of-sum-of-squares) and CQC (complete quadratic combination) methods of 1-D analysis with 2-D analysis are shown in Figure 37 through Figure 39 for PGA of 0.25g, 0.50g, and 1.0g.

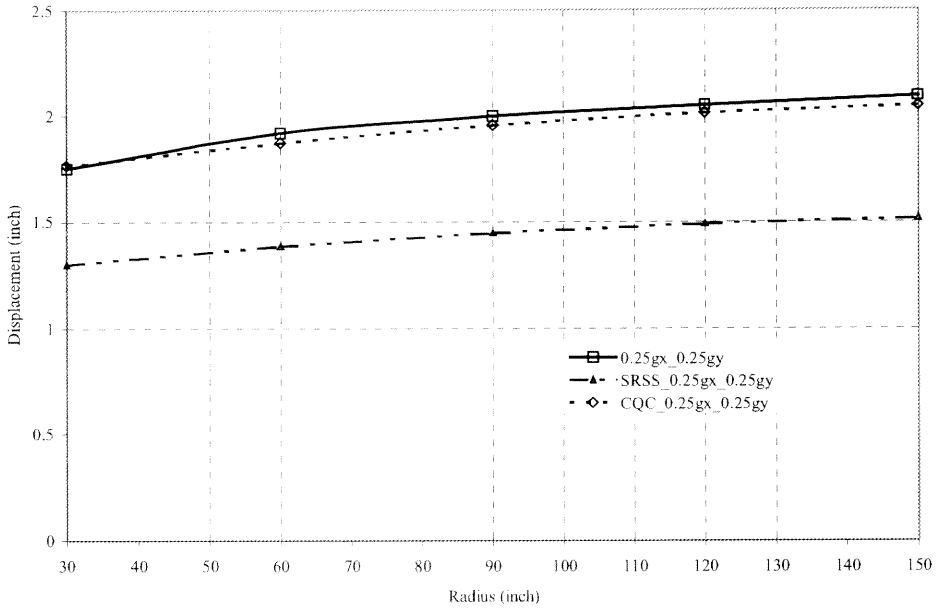

Figure 37 Comparison of Displacement Responses for Combination Methods with 2-D Case for PGA of 0.25g

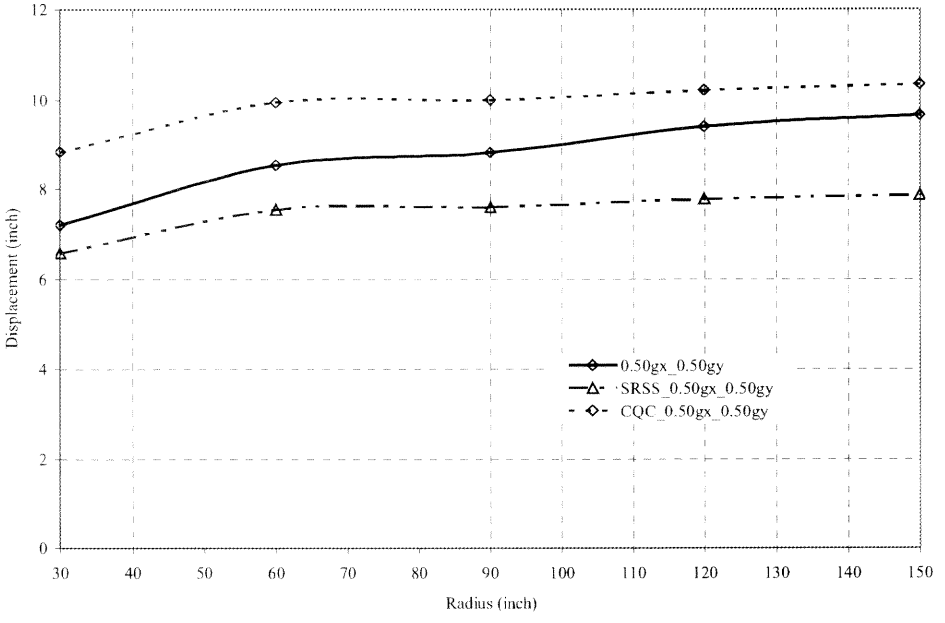

Figure 38 Comparison of Displacement Responses for Combination Methods with 2-D Case for PGA of 0.50g

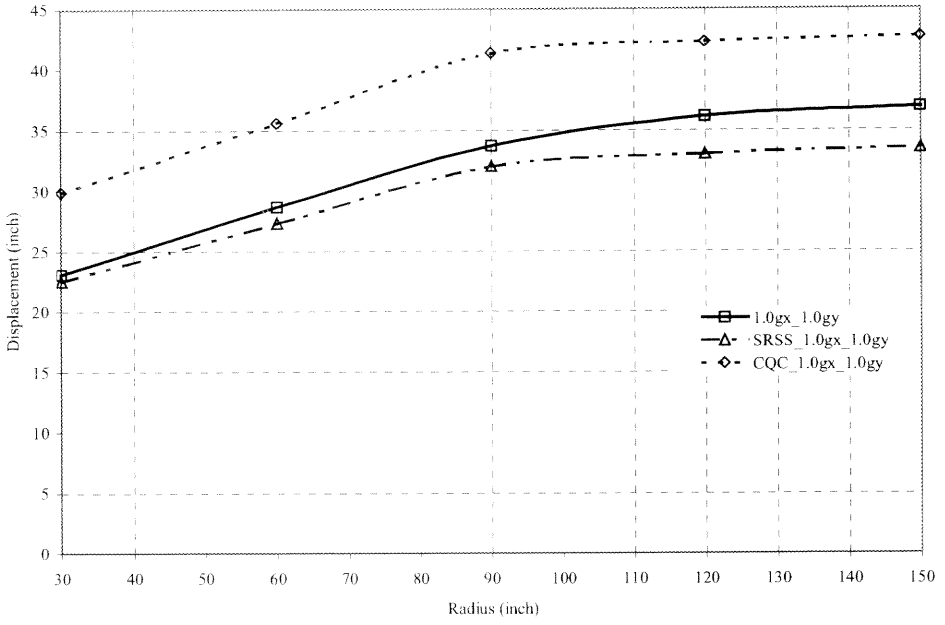

Figure 39 Comparison of Displacement Responses for Combination Methods with 2-D Case for PGA of 1.0g

The comparison of inertia reduction responses using the SRSS and CQC methods of 1-D analysis with 2-D analysis are shown in Figure 40 through Figure 42 for PGAs of 0.25g, 0.50g, and 1.0g respectively.

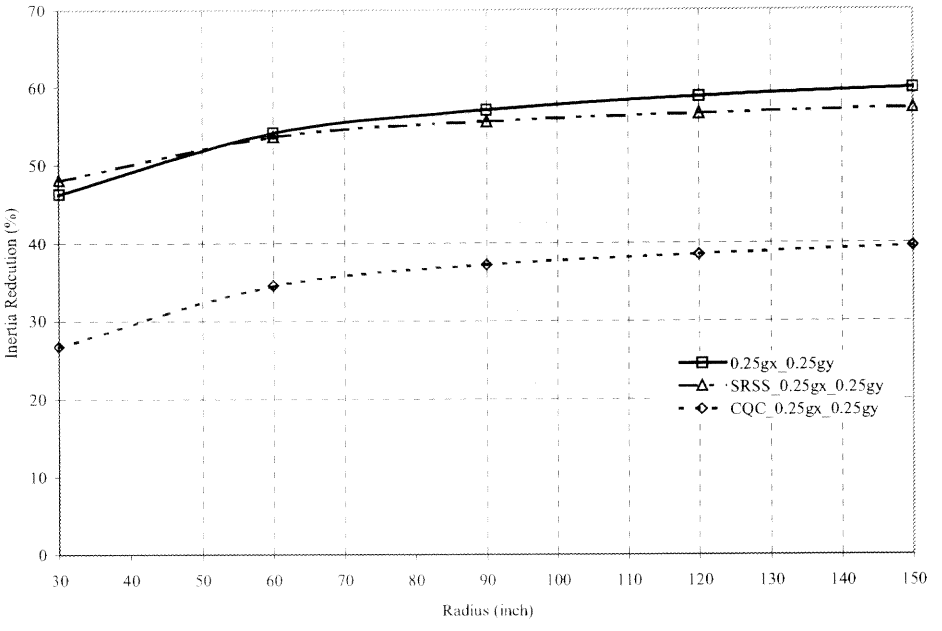

Figure 40 Comparison of Inertia Reduction Responses for Combination Methods with 2-D Case for PGA of 0.25g

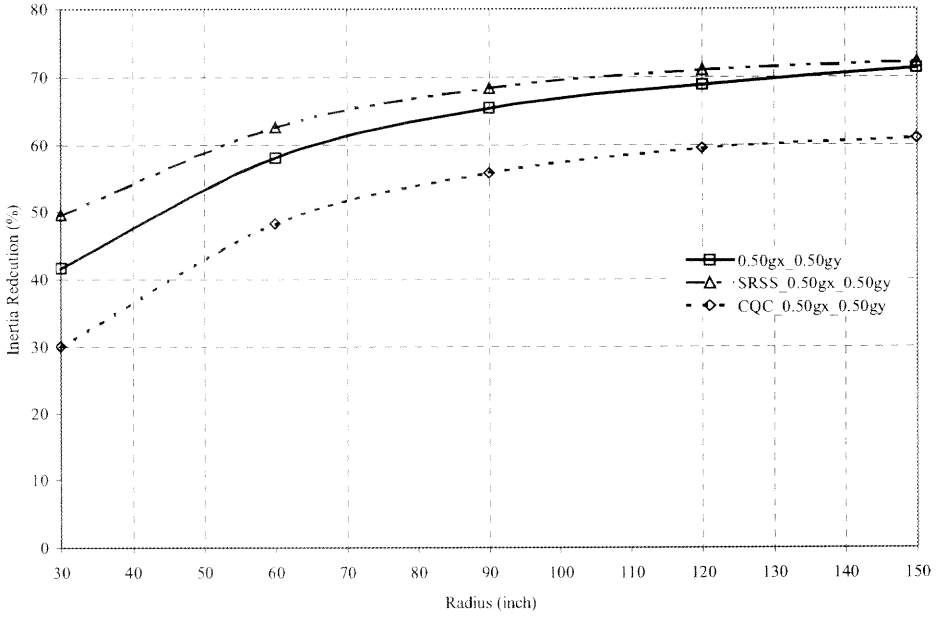

Figure 41 Comparison of Inertia Reduction Responses for Combination Methods with 2-D Case for PGA of 0.50g

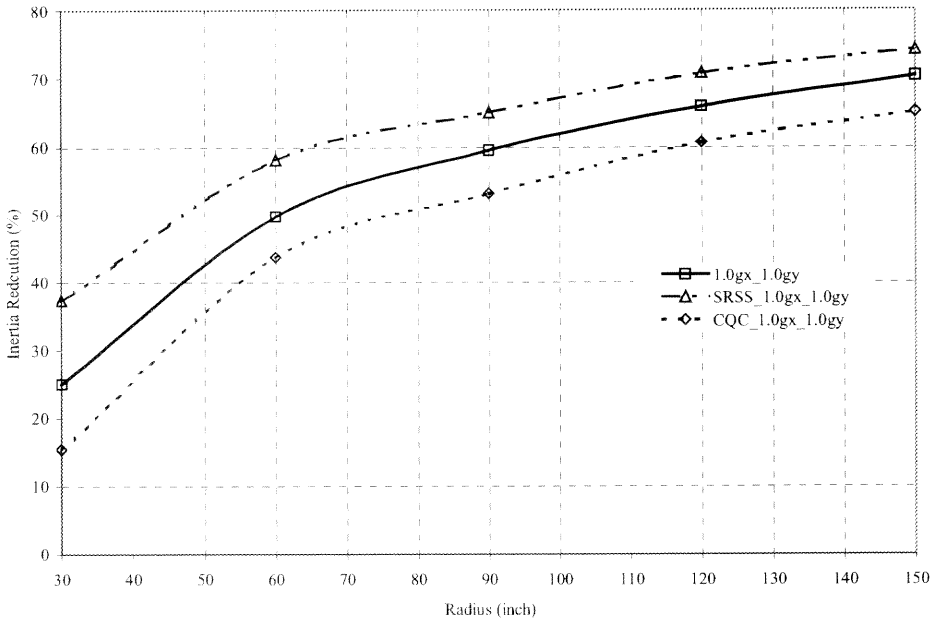

Figure 42 Comparison of Inertia Reduction Responses for Combination Methods with 2-D Case for PGA of 1.00g

In these figures, the SRSS and the CQC response values are obtained by combining responses of two orthogonal 1-D cases. The SRSS method is basically the square root of the sum of the squares of the maximum responses in both horizontal directions. The CQC method turns out to be the absolute sum of the responses since FPS is symmetric. The equation for the CQC method is given in equation (23) [Chopra, 1995].

$$d_0 \cong \left(\sum_{i=1}^{N}\sum_{i=1}^{N} \rho_{in} d_{i0} d_{n0}\right)^{\frac{1}{2}} \tag{23}$$

For $N=2$ modes with equal frequencies (FPS is symmetric), $\rho_{in}=1.0$ and the equation reduces to equation (24).

$$d_0 \cong d_{10} + d_{20} \tag{24}$$

As it is seen from Figure 40 through Figure 42, one can say that the CQC method is always conservative in estimating both displacements and inertia reductions. That is, it overestimates the maximum total displacement and it underestimates the total inertia reduction. However, the SRSS method is almost always unconservative by underestimating the displacements and overestimating the inertia reductions. Based on these results, which include 40 records (20 sites, 2 orthogonal horizontal component site) and many analysis cases, the use of CQC method is recommended for estimating the total displacement for PGAs less than 0.5g. For higher PGAs, the average of the two methods could be used for displacements in order to reduce the conservatism of the CQC method, which can be as high as 30%. For inertia reductions, the average of the two methods is recommended for all PGAs.

3.3.3 Effect of Vertical Motion

Horizontal responses could be affected by vertical motion since the period of the isolated system which depends on the gravitational and vertical motions also affects the normal contact force. To consider vertical effects, the same Fortran code, written for the 2-D case was employed. The weight of the transformer was revised to include the effect of vertical motion for every time step, i.e. $W = M_b * (g \pm \ddot{U}_{g,up})$. To study the former factor, 200 cases were analyzed using earthquake records. Note that for all sites the actual vertical acceleration record was used. With regard to the latter factor, the frictional characteristics of the isolator are affected as a result of the changes in pressure. However, for typical transformer weights the change in pressure is not large enough to have noticeable effect on the response. Results for displacement with and without the vertical motion are shown

in Figure 43 and Figure 44 for different PGAs. For lower PGA values, effect of vertical is negligible. For higher PGA values, however, the effect of vertical on the response of FPS is more pronounced. On the average, the displacement responses are affected by about ±10%.

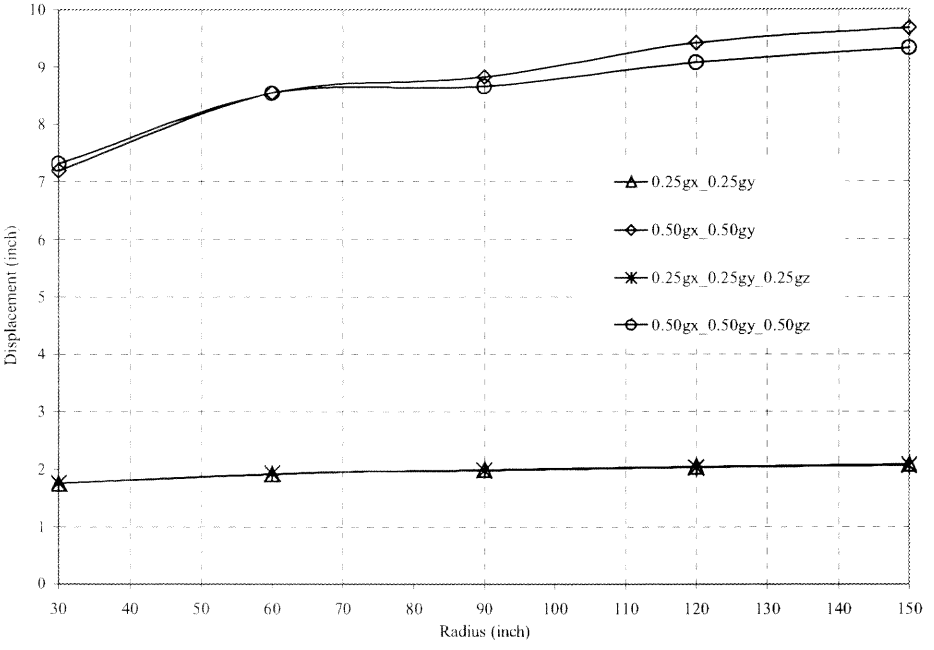

Figure 43 Effect of Vertical Motion on Displacements for PGA of 0.25g and 0.5g (3-D Analyses)

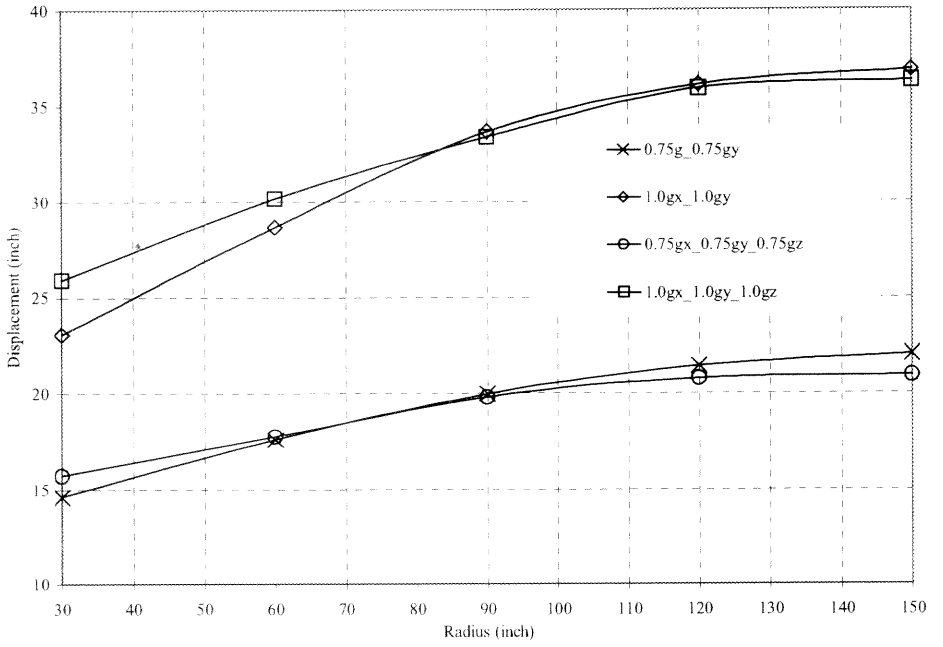

Figure 44 Effect of Vertical Motion on Displacements for PGA of 0.75g and 1.0g (3-D Analyses)

Results for inertia reduction with and without the vertical motion are shown in Figure 45 and Figure 46 for different PGAs. It can be seen from these figures that this effect of vertical motion changes from marginal to significant, depending on response parameter under consideration. It is noted that the vertical ground acceleration has a considerable adverse effect on system performance in reducing the inertia forces. The inertia reductions attained without consideration to vertical motion were higher, in some cases by as much as 40%. This adverse effect of vertical motion becomes more pronounced for higher PGAs.

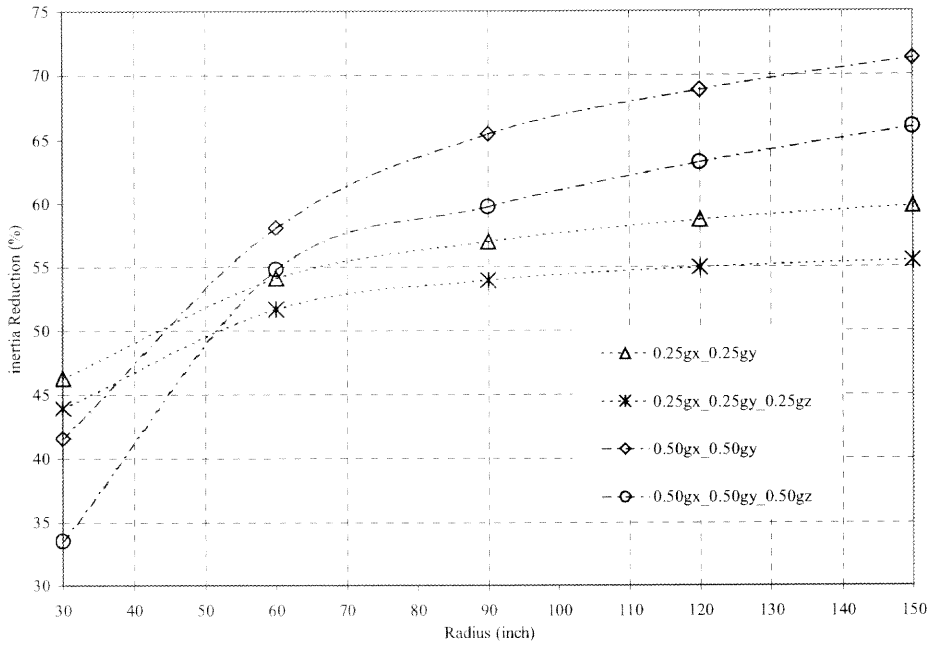

Figure 45 Effect of Vertical Motion on Inertia Reduction for PGA of 0.25g and 0.5g (3-D Analyses)

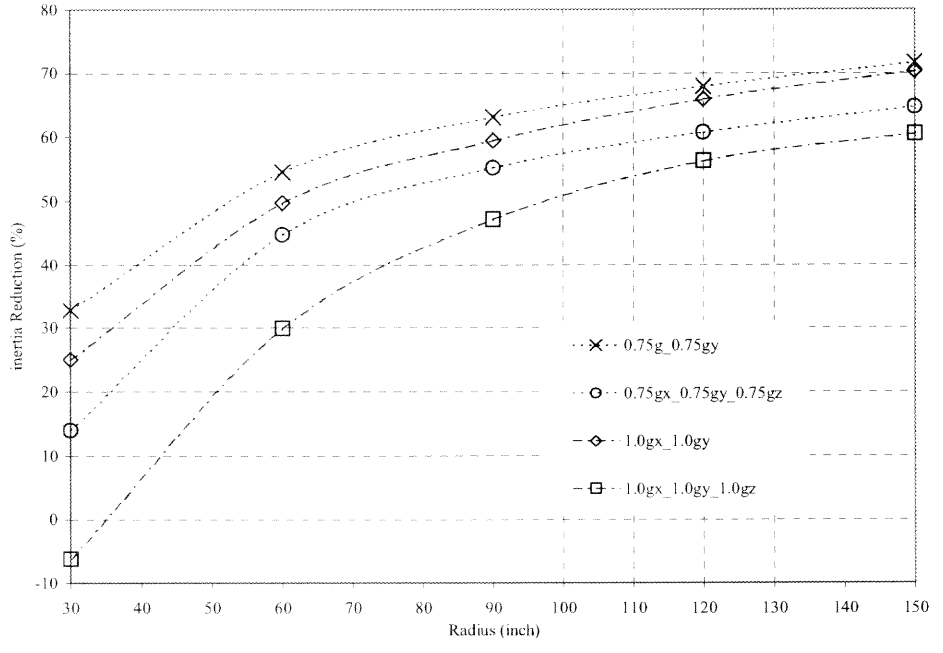

Figure 46 Effect of Vertical Motion on Inertia Reduction for PGA of 0.75g and 1.0g (3-D Analyses)

Furthermore, for vertical acceleration records of higher periods (i.e., lower frequency content) the effect of this component of ground motion becomes more evident. This is because vertical motion of a higher period has enough time to significantly alter the system period. To elaborate on this point one of the previous cases is analyzed with sinusoidal vertical acceleration. The period of the sinusoidal vertical motion is assumed to be equal to $2T_{bearing}$ and $5T_{bearing}$, with PGA of 1g. As can be seen from Figure 47, vertical motions of higher period significantly affect the horizontal responses by influencing both amplitude and frequency content. It should be noted that vertical records are generally rich in frequency and normally of higher frequency content than the horizontal ones. This example is provided only to more clearly demonstrate the effect of vertical motion. Nevertheless, it is recommended that for sites where the motion can be filtered through layers of soft soils, the effect of vertical motion be explicitly considered in design.

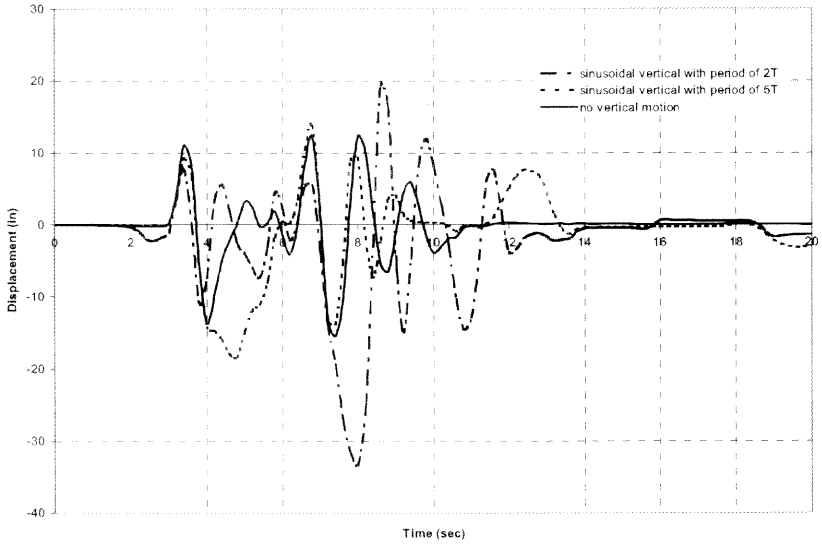

Figure 47 Displacements Time Histories with (Sinusoidal) and without Vertical Motion

3.3.4 Ground Motion Characteristics

The effect of ground motion characteristics on the response of FPS has been investigated for 10 soil and 10 rock earthquake records. Displacement results for soil and rock sites are given in Figure 48 and Figure 49 respectively. It is noted that the soil records on the average cause more displacement than the rock records for every PGA employed. This is due to lower frequency content of soil records in general.

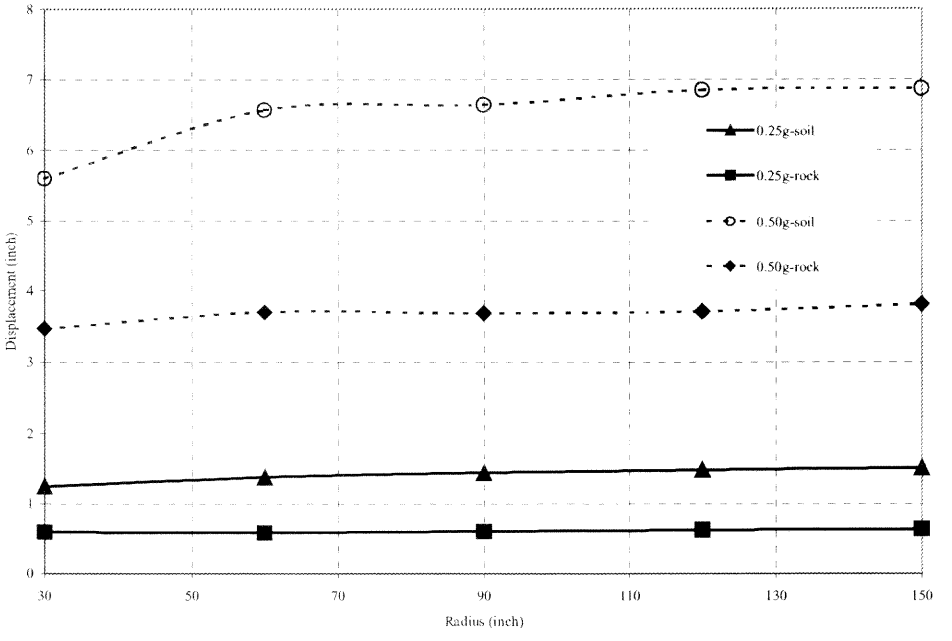

Figure 48 Comparison of Rock and Soil Displacements for PGA of 0.25g and 0.50g

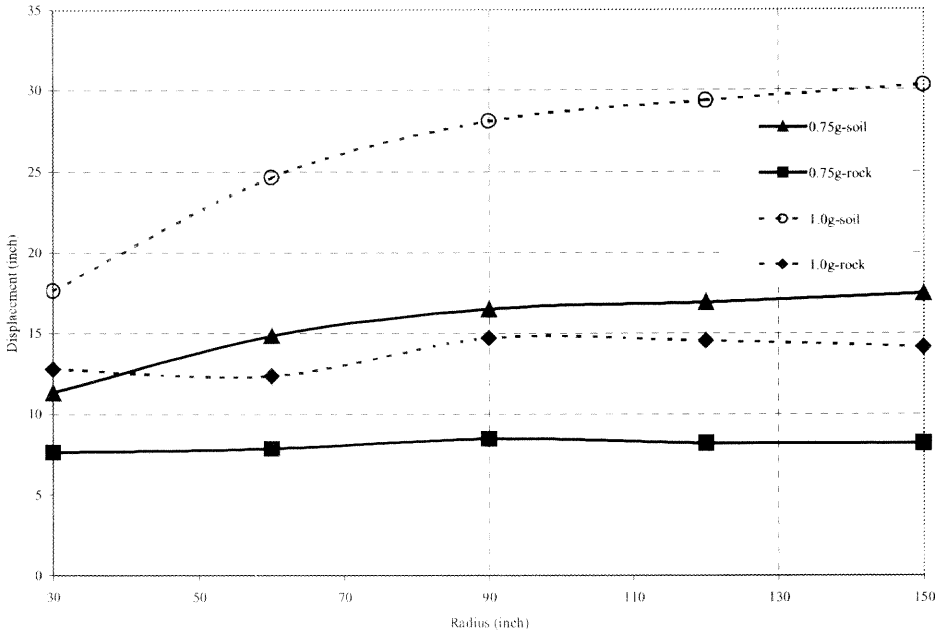

Figure 49 Comparison of Rock and Soil Displacements for PGA of 0.75g and 1.0g

Figure 50 and Figure 51 show the variation between the inertia reduction responses of soil and rock records. Rock records attained more inertia reduction, i.e., the acceleration values for all PGA input are less than the soil acceleration levels.

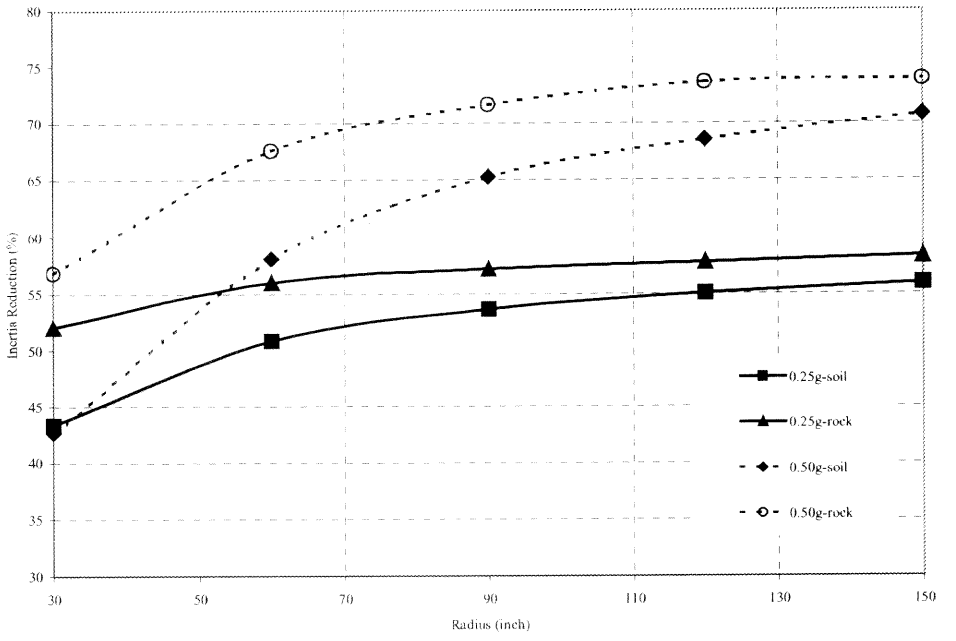

Figure 50 Comparison of Rock and Soil Inertia Reduction for PGA of 0.25g and 0.50g

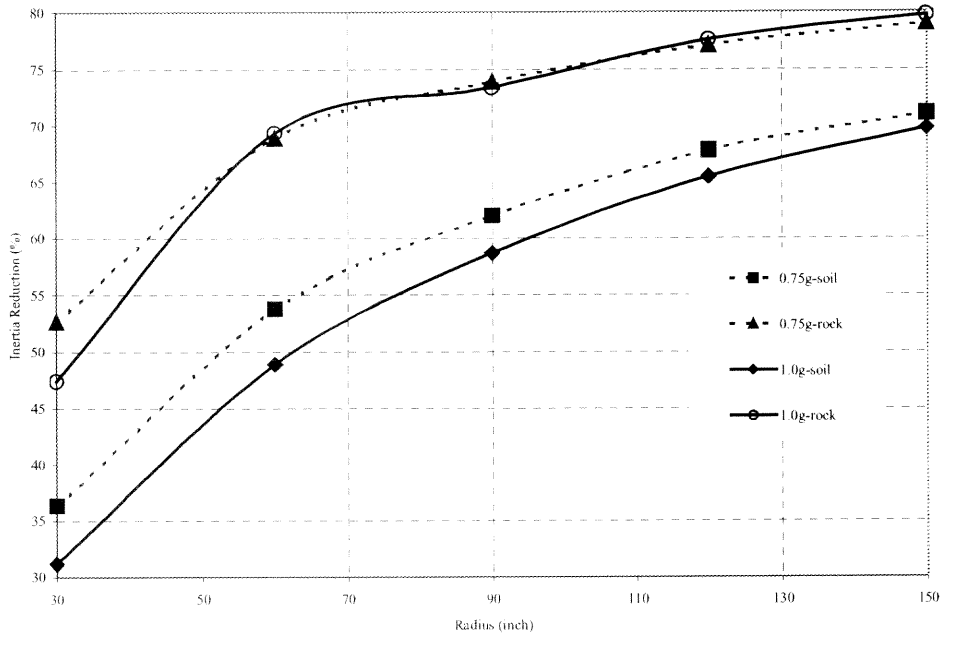

Figure 51 Comparison of Rock and Soil Inertia Reduction for PGA of 0.75g and 1.0g

3.4 FPS System for Large Displacement Assumption and Results

Based on the large displacement assumption, the normalized force N is perpendicular at the contact point of the articulated slider. The equilibrium equation in tangential direction becomes (see Figure 27),

$$-F_f - W\sin\theta - M\ddot{U}_{gx}\cos\theta - M\ddot{U}_{gz}\sin\theta = MR\ddot{\theta} \tag{26}$$

where

F_f = friction force

W = weight of system

$\ddot{U}_{gx}$ = ground motion in horizontal direction

$\ddot{U}_{gz}$ = ground motion in vertical direction

R = radius of curvature of bearing

The equilibrium equation in radial direction becomes,

$$N - W\cos\theta + M\ddot{U}_{gx}\sin\theta - M\ddot{U}_{gz}\cos\theta = MR\dot{\theta}^2 \tag{27}$$

From equation (25) the normal force N is obtained as,

$$N = W\cos\theta - M\ddot{U}_{gx}\sin\theta + M\ddot{U}_{gz}\cos\theta + MR\dot{\theta}^2 \tag{28}$$

The friction force can be given as follows,

$$F_f = \mu_s NZ \tag{29}$$

Substituting equation (28) and equation (29) into equation (26) leads to equation (30),

$$\ddot{\theta} = \frac{-\mu_s Z}{R}(g\cos\theta - \ddot{U}_{gx}\sin\theta - \ddot{U}_{gz}\cos\theta + R\dot{\theta}^2) - \frac{1}{R}(g\sin\theta + \ddot{U}_{gx}\cos\theta + \ddot{U}_{gz}\sin\theta) \tag{30}$$

Since the tangential velocity at the steel-teflon interface of bearing becomes $R\dot{\theta}$, equation (6) (for parameter Z) becomes

$$Y\dot{Z} + r\left|R\dot{\theta}\right|Z\left|Z\right|^{\eta-1} + \beta R\dot{\theta}\left|Z\right|^{\eta} - AR\dot{\theta} = 0 \tag{31}$$

Equation (30) and equation (31) are solved simultaneously by employing a Fortran code using the IVPAG routine in IMSL.

Figure 52 through Figure 54 compare the average displacement response of FPS based on large and small displacement assumptions. The response deviation of ±5% from large displacement assumption values is also shown for each radius of curvature on the graphs. It is noted that the displacement values from both methods for smaller PGA values (0.25g, 0.5g) are in good agreement. For larger PGA values (1.0g) with small radius of curvature there is a larger deviation from the small displacement values.

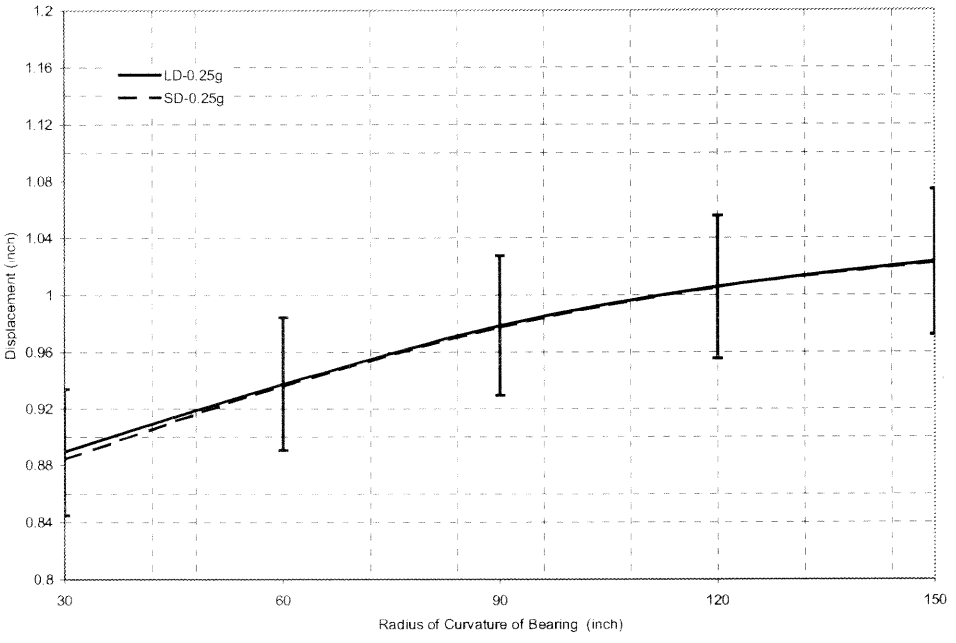

Figure 52 Comparison of Displacements Based on Small and Large Displacement Assumptions for PGA of 0.25g

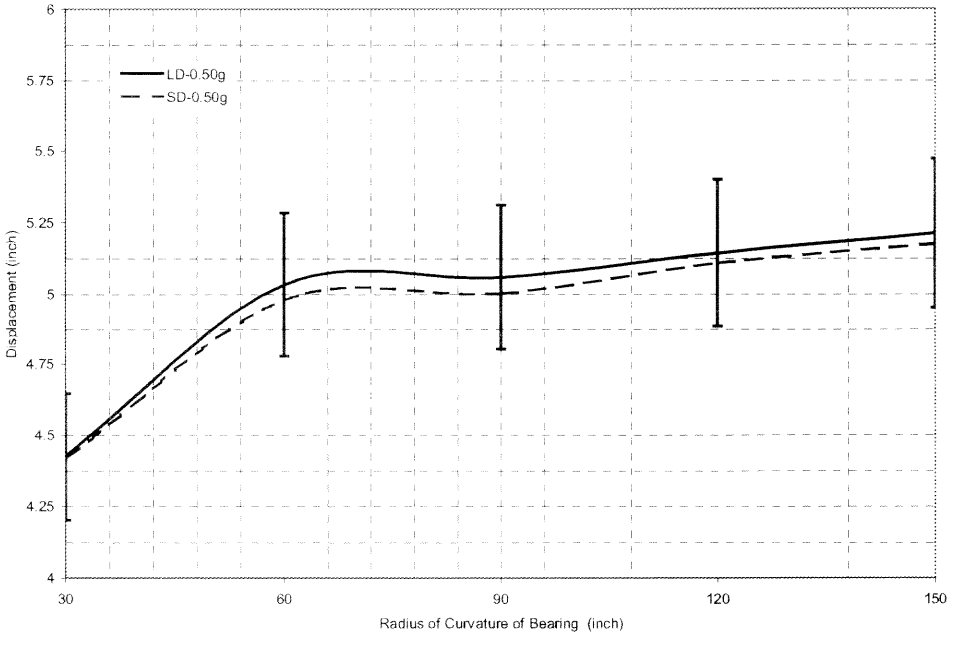

Figure 53 Comparison of Displacements Based on Small and Large Displacement Assumptions for PGA of 0.50g

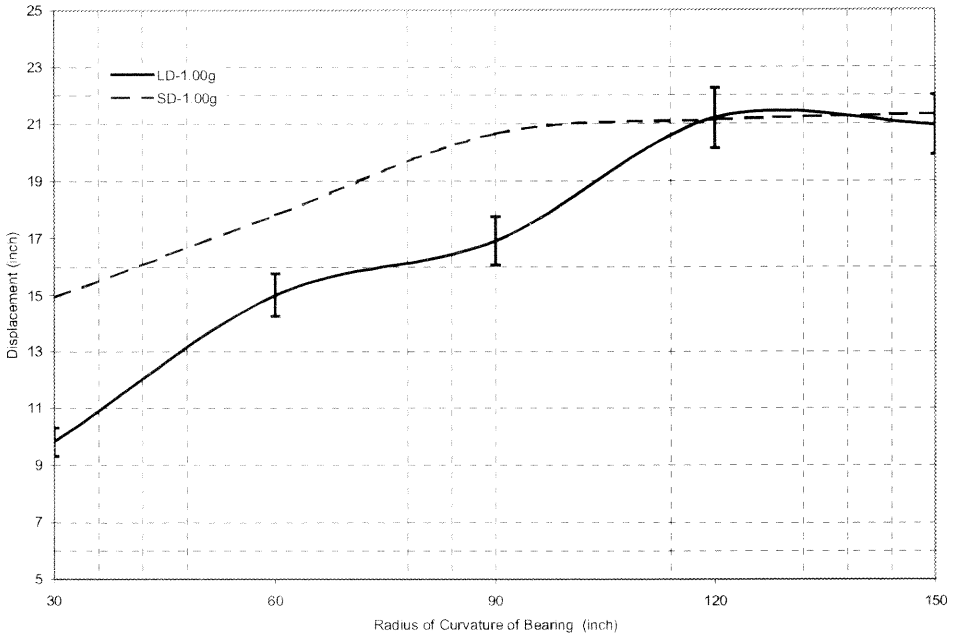

Figure 54 Comparison of Displacements Based on Small and Large Displacement Assumptions for PGA of 1.0g

Figure 55 through Figure 57 compare the average inertia reduction response of FPS based on large and small displacement assumptions. Also shown for each radius of curvature is ±5% deviation from large displacement assumption values. Inertia reduction responses for smaller PGA values (0.25g, 0.5g) are in good agreement using both assumptions. For larger PGA values (1.0g) with a small radius of curvature there is a larger deviation, however the small displacement assumption is almost always conservative. It can be stated that using the small displacement assumption is in fairly good agreement with the large displacement assumption up to the PGA of 1.0g, which is stated as high performance level in IEEE 697.

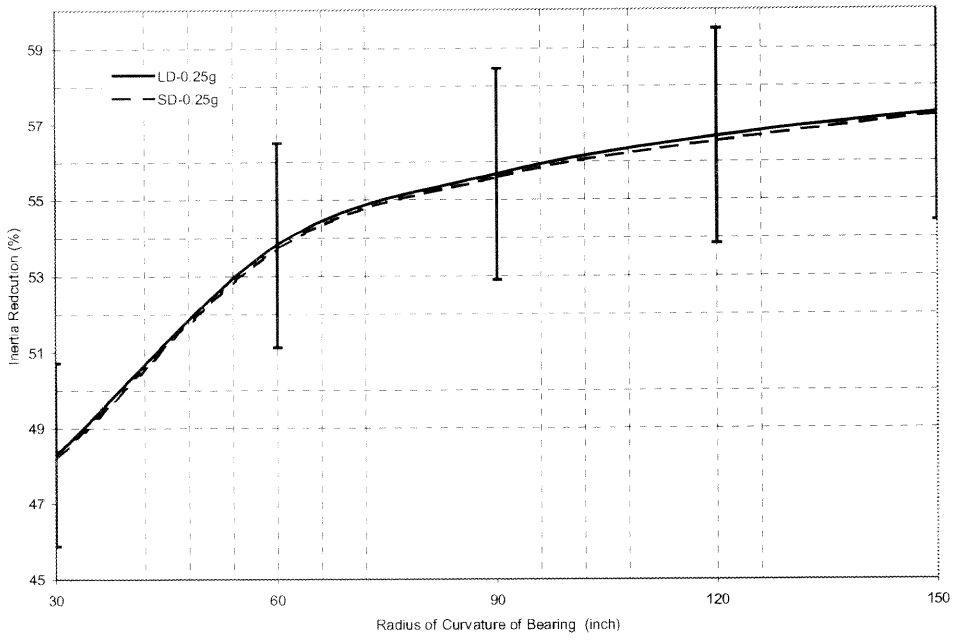

Figure 55 Comparison of Inertia Reductions Based on Small and Large Displacement Assumptions for PGA of 0.25g

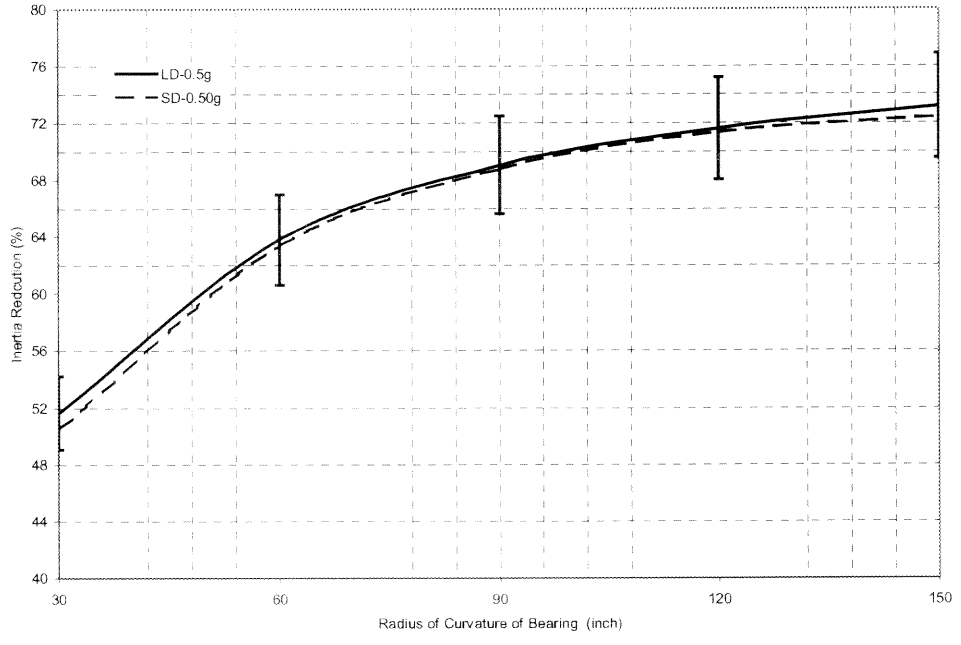

Figure 56 Comparison of Inertia Reductions Based on Small and Large Displacement Assumptions for PGA of 0.50g

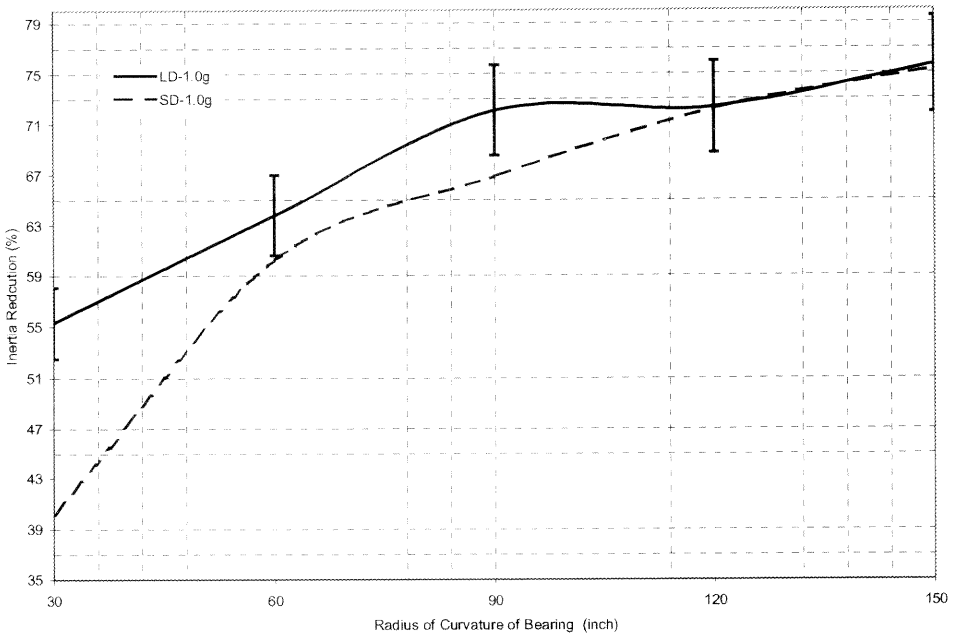

Figure 57 Comparison of Inertia Reductions Based on Small and Large Displacement Assumptions for PGA of 1.00g

3.5 Force Displacement Response of FPS Model

As discussed before, the design of FPS bearings combines the concepts of sliding and pendulum response. Therefore, for a horizontal load lower than the static friction force, the force-displacement response of a FPS bearing is rigid (sticking mode). The slope of this part of the curve is equal to stiffness of non-isolated structure. For higher loads, "yielding" or more exactly, sliding takes place and the stiffness of the structure is controlled by the isolation system stiffness. For a SDOF system, the post-yield stiffness is equal to the equivalent stiffness (or W/R). A typical load-displacement response for FPS bearings is shown in Figure 58. This graph shows the overall energy dissipation behavior, which is very stable and can be represented with an ideal bi-linear response relationship.

These characteristics have been verified through experimental work [Zayas, 1990]. The area enclosed by the hysteresis loops represents the energy dissipation capacity of the isolation device and is related to its frictional characteristics. Under the small displacement assumption, the loops take on a parallelogram shape. The vertical height of the parallelogram is twice the "yield" force or the force required to cause sliding (i.e., μW). Thus, using the length parameter D as defined in Figure 58, the effective friction coefficient is equal to the enclosed area divided by 2DW.

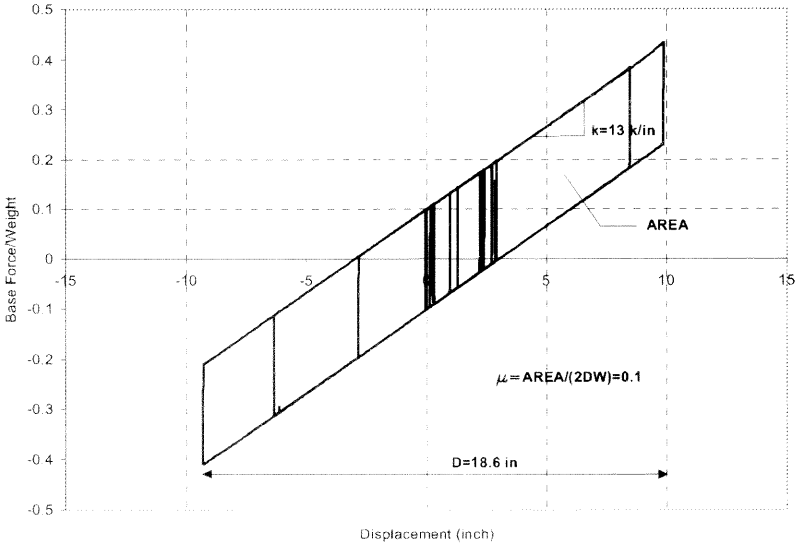

Figure 58 Typical Load-Displacement Hysteresis Loop for FPS Isolator

In Chapter 3, detailed analytical investigation of FPS as a base isolation remedy to transformer bushing system is presented. In addition to these analytical studies, a series of test were conducted at National Center for Research on Earthquake Engineering (NCREE) in Taiwan, through a collaborative effort. This was the first effort to test FPS isolated transformer model, using an earthquake simulator. Chapter 4 presents the results of these tests.

CHAPTER 4
EXPERIMENTAL STUDY OF FRICTIONAL PENDULUM SYSTEM

As a part of this research project, in the summer of 1999, about 100 tests were conducted at the National Center for Research on Earthquake Engineering (NCREE) in Taiwan through a collaboration effort. The objective was to compare the response of fixed base transformer model supporting a bushing to those when the systems are isolated using FPS bearings. It represents the first effort in testing base isolated large-scale transformer bushing systems using an earthquake simulator. The testing schedule also included white noise tests to identify dynamic characteristics of the bushings and the transformer model. 1-D, 2-D and 3-D excitations were conducted employing several earthquake records with PGAs in the range of 0.125g to 0.375g. One type of bushing, namely 161 kV was used in the experimentation. Consistent with the practice employed by TaiPower, the bushing was attached perpendicular to the top of transformer model. The following sections discuss the test set-up and experimental results. Furthermore, comparisons between the analytical and experimental results are presented.

4.1 Earthquake Simulator

The earthquake simulator at the National Center for Research on Earthquake Engineering (NCREE) in Taiwan was used for the experiments described in this section. The NCREE earthquake simulator, also known as a shaking table, possesses 6 degrees of freedom to simulate earthquake motion in 3 axes. The size of the shaking table of the seismic simulator is 16' x 16' and its mass is 29.8 tons. Structural models with a maximum

payload of 55.1 tons can be accommodated on the table. The table is driven by 12 hydraulic actuators (4 actuators for each axis). The reaction forces of the actuators are provided by the reaction mass of about 4400 tons. To further improve the quality of the testing environment, the reaction mass is isolated from the fixed foundation by 96 air springs and 80 dampers.

The total number of earthquake tests performed on the transformer model including both isolated and fixed conditions was 77. To this should be added many tests to identify the system's dynamic characteristics. These were the first experimental tests on base isolated transformer models. Parallel to these tests, several hundred more tests were conducted to investigate the performance of other isolation devices. It is not within the scope of this thesis to present the results of those latter tests.

4.2 Instrumentation

The transformer model was equipped with LVDTs and accelerometers at three different levels; the load cells were placed at the bottom corners of the transformer model: Level 1, Level 2 and Level 3. The top of the bearing is referred to as Level 1. That of the load cell or bottom of the transformer is referenced as Level 2 and the top of the transformer is labeled as Level 3. The relative displacement of the bearing is obtained by subtracting the LVDT records at Level 2 from the shake table displacements.

The response of the 161 kV bushing was measured at four locations, namely bottom of the bushing, transformer level (or flange), middle of the bushing and at the top of the bushing.

A total of 70 channels were used to record response parameters. Accelerations were recorded on 34 of these channels. Load cell readings were taken on 12 channels and 18 channels were used for LVDT records. Six channels were used for shake table displacement and acceleration records.

4.3 Transformer Model and Bushing

Photographs of the transformer model and its instrumentation are shown in Figure 59 and Figure 60. The dimensions of the transformer model are 7'-10 ½" x 7'-2 10/16" in plan. The height of the transformer is 8'-10 5/16". Four 18.64" radius FPS bearings were used to support the model for the isolated case.

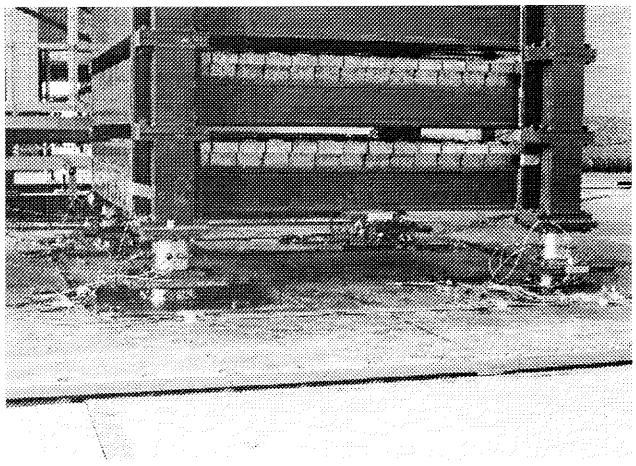

Figure 59 A View of the Transformer Model and Instrumentation

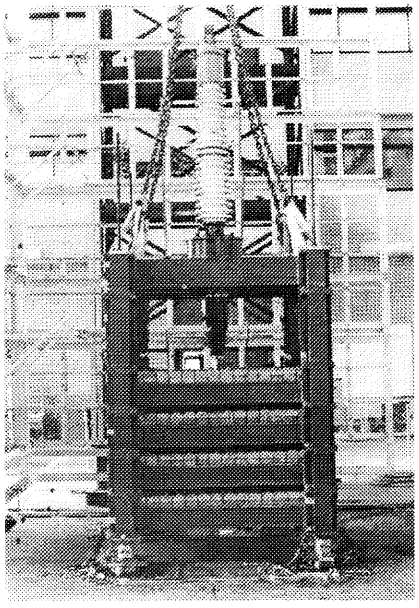

Figure 60 Transformer Model with the Bushing Mounted on the Top

The characteristics of the bushing (161 kV) are summarized in Table 9. Those of the isolation system are shown in 0.

Table 9 Characteristics of 161 kV Bushing

Type Form	VEU-140ZT
Insulation Class	161 kV
Rated Current	1200 A
BIL	750 kV
Approximated Weight	772 lbs
Total Length	11'-5 10/16"

Table 10 Characteristics of the Isolation System

Characteristics	Designed Value
Radius of Bearing	18.64 inch
Effective Stiffness	3.016 kips/inch
Equivalent Damping Ratio	0.14
Effective Period	1.38 s

4.4 Modal Analysis of Transformer Model and Bushing

The dynamic characteristics of the transformer model and the bushing were computed from the response of the model to random noise. They are presented in Table 11.

Table 11 Dynamic Characteristics of the Transformer Model and the Bushing

	Frequency		
	x-direction	y-direction	Yaw-direction
Transformer Model	12.5	12.5	22.5
161 kV Bushing	12.0-12.5	12.0-12.5	24.0

The dynamic characteristics of the transformer model and the bushing were also obtained by FFT of the response of the testing frame and the bushing. Figure 61 shows the FFT of the testing frame. FFT of the bushing response and the bushing response with respect to the testing frame are shown in Figure 62 and Figure 63 respectively. As it can be seen, the same frequency responses are obtained from FFT analysis. The random noise analysis given in Table 11 also shows the same values.

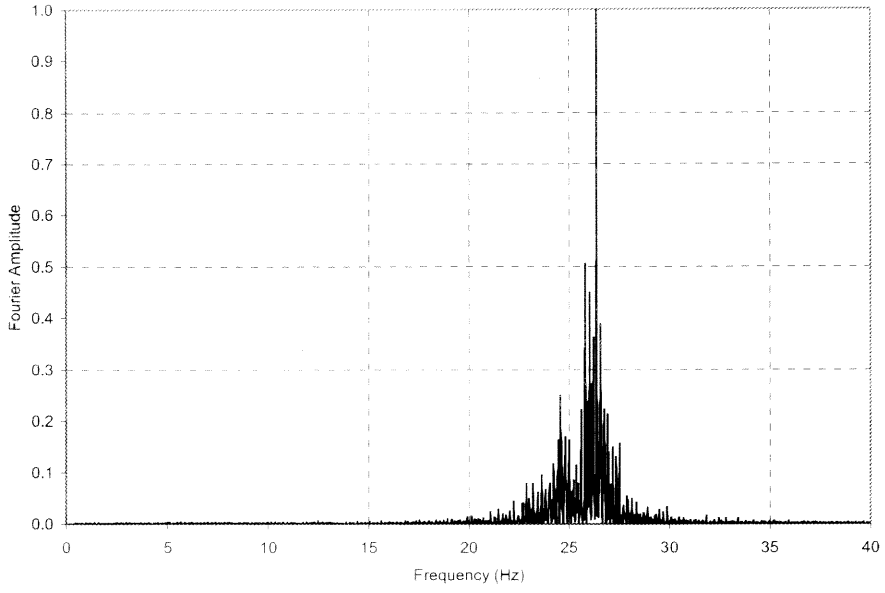

Figure 61 FFT of Testing Frame Response for 1-D Case of Sylmar Record with 0.375g in X direction

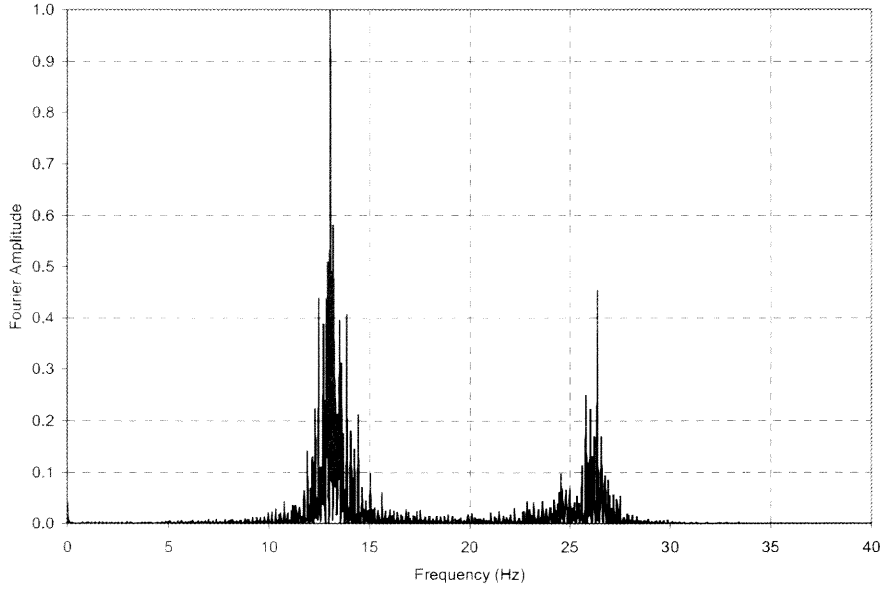

Figure 62 FFT of Bushing Response for 1-D Case of Sylmar Record with 0.375g in X Direction

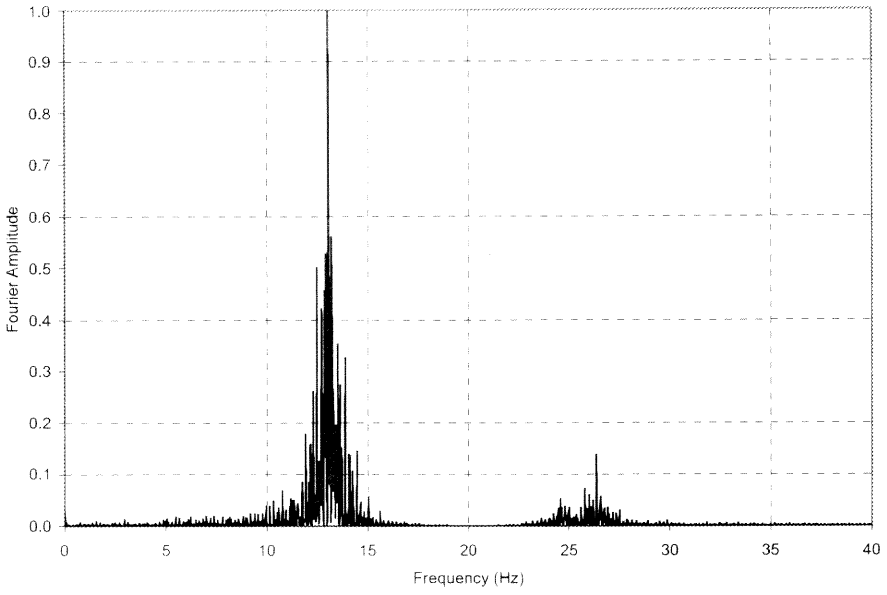

Figure 63 FFT of Bushing Response with Respect to Testing Frame for 1-D case of Sylmar Record with 0.375g in X Direction

4.5 Results

Several earthquake records were used in the tests, namely: CKS (Chiang Kai-Shek), Chi-I Ray-Li, El-Centro, Kobe-Takotori and Northridge-Sylmar. The test results for 1-D cases of the Sylmar record are tabulated in Table 12 for isolated and non-isolated cases. And the results of the 2-D and 3-D cases of same record are tabulated in Table 13. In these tables, A_2 and A_3 show the acceleration values (in g) at the bottom and the top of the transformer model, respectively. A_{b1}, A_{b2}, A_{b3}, A_{b4} represent the accelerations at different locations along the bushing. D_2, and D_3 (in inches) are the relative displacement values of the transformer model at the top and bottom, respectively.

Some of the response acceleration maps for the 1-D cases indicate the effect of isolation system at different levels of the transformer model. (Figure 64 through Figure

66). In these figures the x-axis shows the acceleration values normalized with respect to PGA. Absolute maximum total acceleration values at different levels of transformer model and bushing, is divided by absolute maximum acceleration of the earthquake record (PGA of shake table). The y-axis shows different locations along the height of the test specimen ranging from the top of the shake table to the top of the bushing. As one can see from these figures, the acceleration responses for fixed base cases increase as the height above the base of the transformer increases. However, when base isolation (FPS) is introduced, the acceleration is reduced significantly at different levels throughout the height above the base.

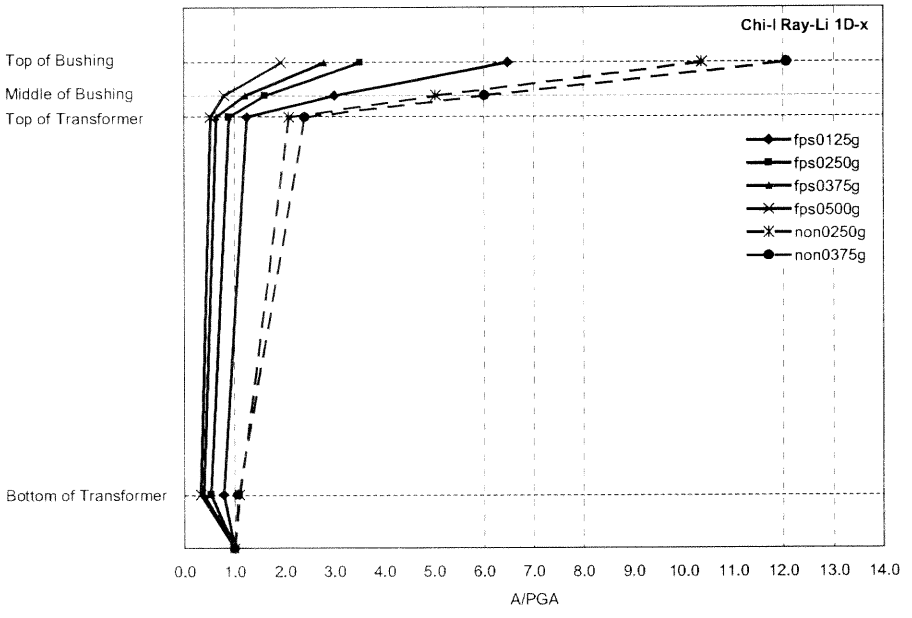

Figure 64 Acceleration Maps for Chi-I-Ray-Li Record for 1-D Case

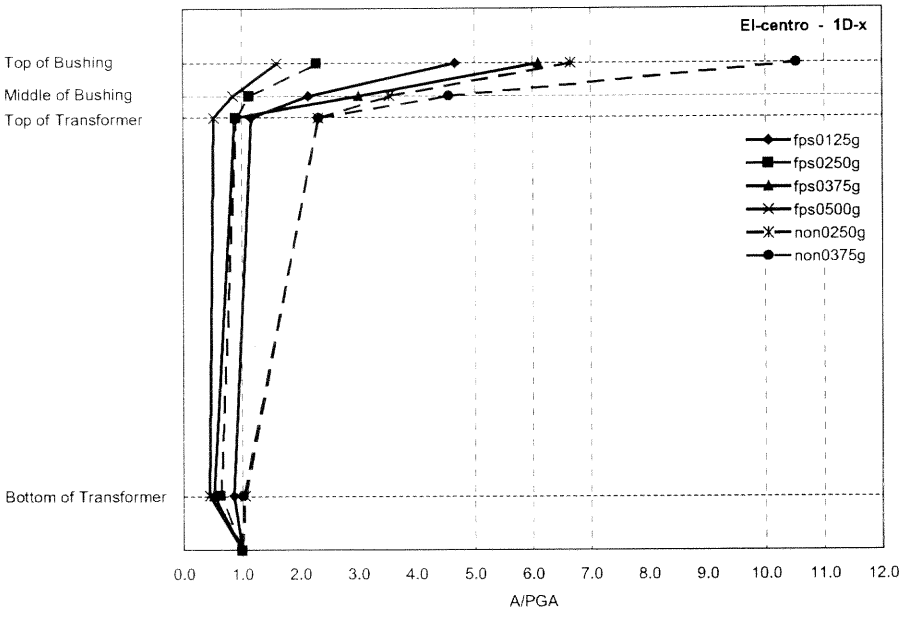

Figure 65 Acceleration Maps for El-Centro Record for 1-D Case

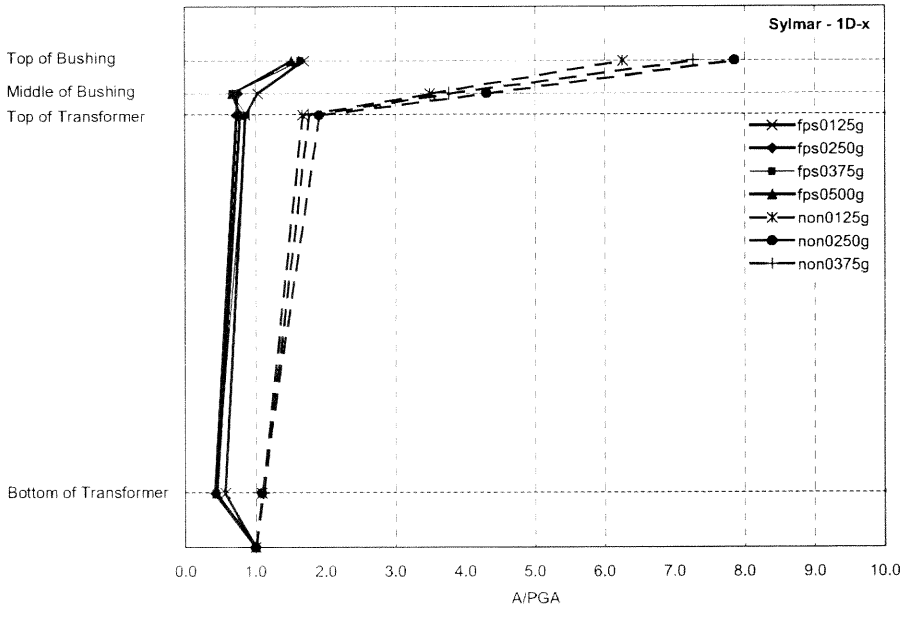

Figure 66 Acceleration Maps for Sylmar Record for 1-D Case

Typical response acceleration maps for 2-D cases indicating the effect of the isolation system for x and y directions at different levels of the transformer model are shown in Figure 67 and Figure 68 respectively. Response acceleration maps for 3-D

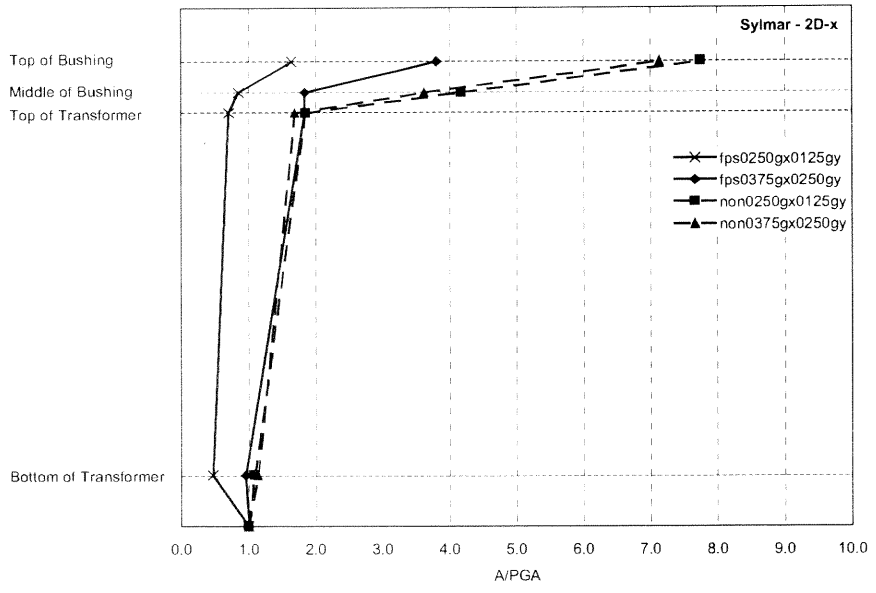

Figure 67 Acceleration Maps for Sylmar Record for 2-D Case in X Direction

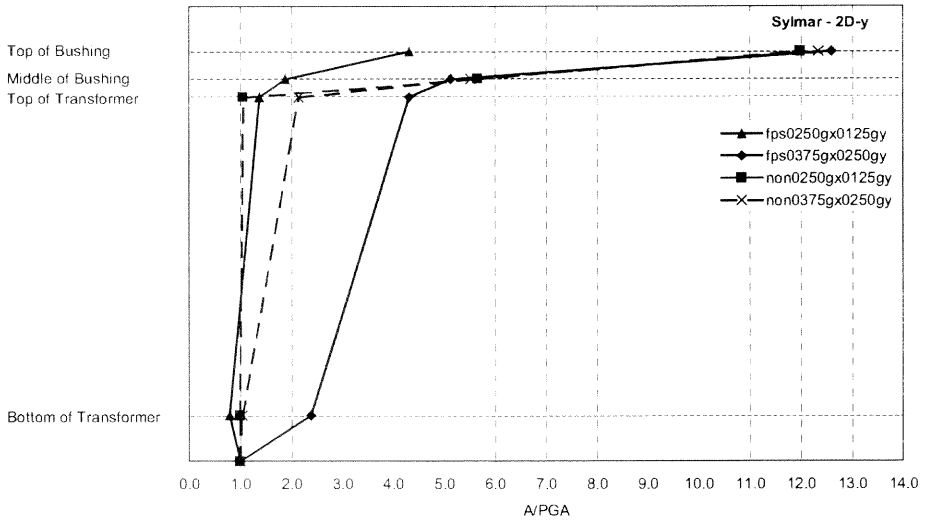

Figure 68 Acceleration Maps for Sylmar Record for 2-D Case in Y direction

results indicating the effect of isolation system for orthogonal horizontal and vertical directions at different levels of the transformer model are shown in Figure 69 through Figure 71.

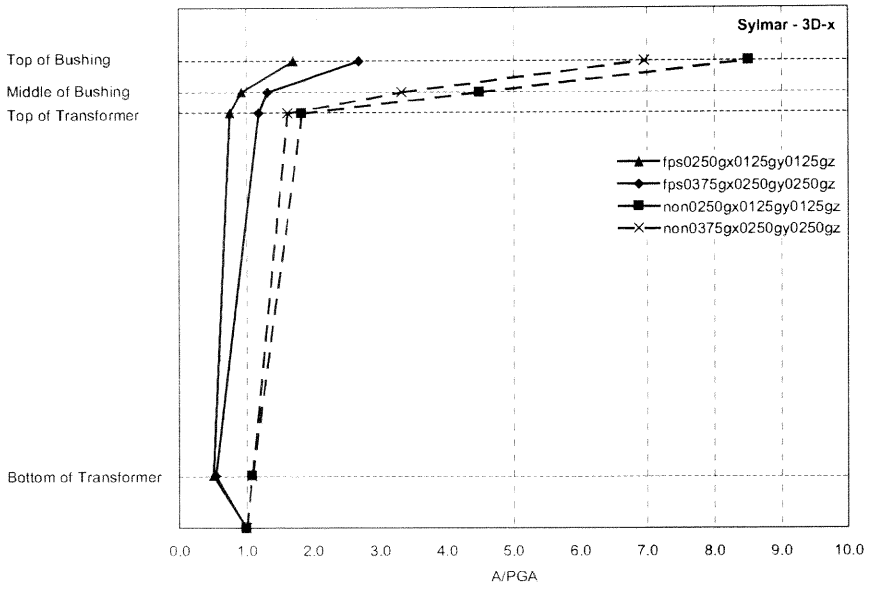

Figure 69 Acceleration Maps for Sylmar Record for 3-D Case in X-Direction

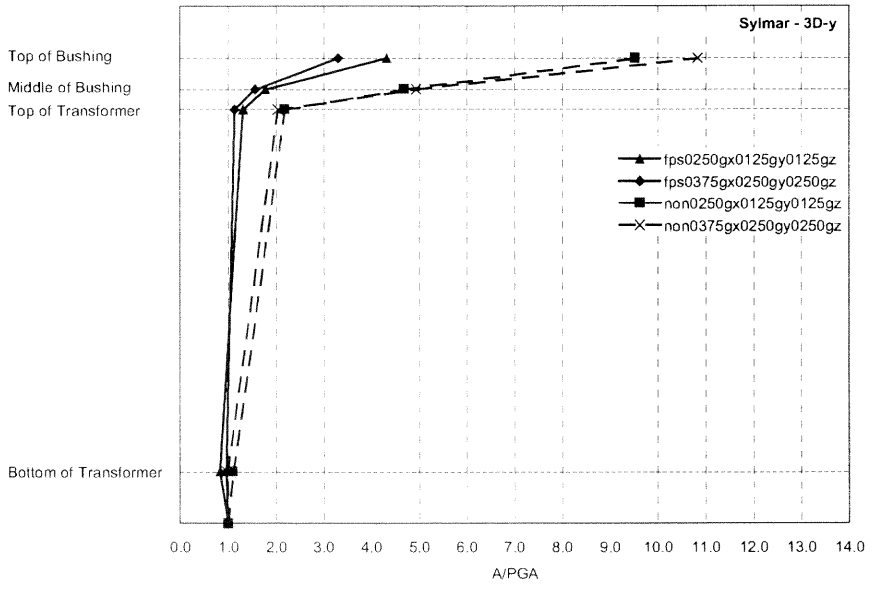

Figure 70 Acceleration Maps for Sylmar Record for 3-D Case in Y Direction

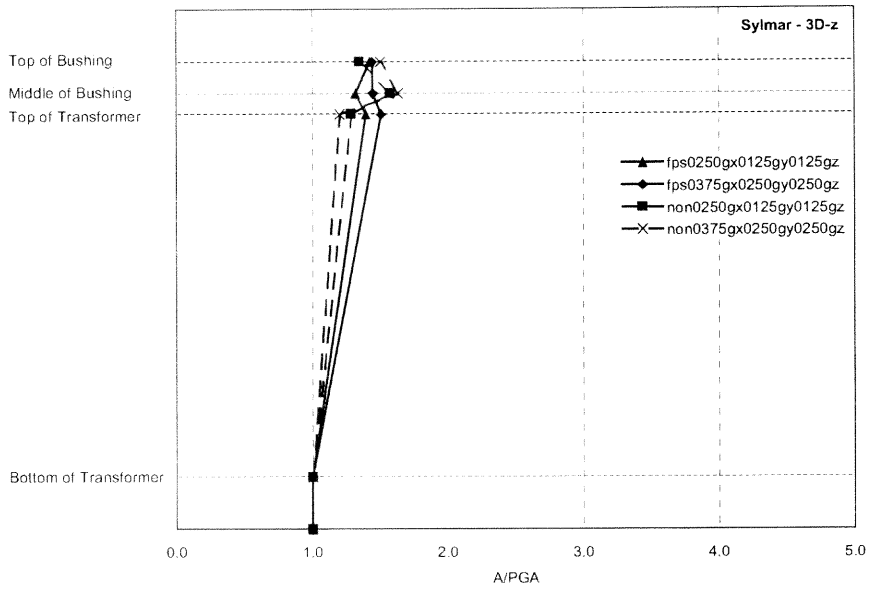

Figure 71 Acceleration Maps for Sylmar Record for 3-D Case in Z Direction

The level of acceleration reduction depends on the type of earthquake records used. That is, in addition to acceleration level and nature of the input (1-D vs. 2-D), the ground motion characteristics affect the level of acceleration reductions. Some of the observations from 1-D, 2-D and 3-D tests are discussed in the following paragraphs. Note that for flexible systems, accelerations are different at various levels (as seen in Figure 64 through Figure 71), and the effectiveness of the base-isolation is more apparent when one considers the entire system. For example, there is significantly more reduction in the bushing acceleration than that of the transformer. However, to simplify discussions and to be consistent with the discussions of the results based on SDOF idealization, in the following sections inertia reduction is used. Inertia reduction here is with respect to the isolation level (base of the transformer). That is, similar to the SDOF discussions, inertia reduction is the percentage difference between $-M_b(\ddot{U}_b + \ddot{U}_g)$ and $-M_b\ddot{U}_g$, where $\ddot{U}_b$ is the acceleration at the isolation level.

For 1-D experiment in the x-direction and employing the Chi-I Ray-Li record, 47% and 62% inertia reductions were attained with PGA of 0.25g and 0.375g, respectively. However, the El-Centro record produced 37% and 49% inertia reductions at the same location with PGAs of 0.25g and 0.375g, respectively. The Kobe-Takotori record with PGA of 0.25g shows a 7% reduction in system acceleration. For the target acceleration of 0.125g using the Kobe-Takotori record, the system acceleration has increased due to low level of acceleration and response. This could be due to errors in experimental readings. The significant difference in the maximum displacements between the two cases of 0.125g and 0.25g PGA supports the fact that there might be an error in the case with 0.125g acceleration. Thus, similar to the analytical results, it is apparent that PGA has an effect on the level of inertia reductions. Furthermore, records with dominant frequency in the vicinity of the effective period of the isolation system show less inertia reduction. The 2-D and 3-D results are discussed in the following paragraph. Note that in these discussions, including the discussions of 1-D results, the PGA referred to is the target PGA. The actual or real input acceleration may have been different due to difficulty in matching exactly the intended PGA. The inertia reductions are calculated with respect to actual acceleration not the target acceleration.

For a 2-D case with Northridge-Sylmar record and targeted PGA of 0.25g in the x-direction and PGA of 0.125g in the y-direction, the inertia reductions are 54% and 21% in x and y directions, respectively (case 4, Table 13). For the 3-D case using Northridge-Sylmar record with targeted 0.25g PGA in x-direction, 0.125g PGA in y-direction, and 0.125g in the vertical direction the inertia reduction in x-direction is 49% and it is 17% in the y-direction (case 6, Table 13).

Similar to analytical results in Chapter 3, the coupling effect is also observed experimentally. That is, there is a difference between the components of the 2-D responses compared to the 1-D ones. For example, consider the 1-D case versus the 2-D case for the Northridge-Sylmar record. For the 1-D case the target PGA is 0.25g in the x-direction (case 2, Table 12). For the 2-D case the target PGAs in the x-direction and y-direction are 0.25g and 0.125g, respectively (case 4, Table 13). The acceleration reduction for the 1-D case is 58%, which is to be compared to x-direction of 2-D case. The acceleration reduction in the x-direction for the 2-D case, as discussed before, is 54%. This can be further compared to the 3-D case (case 6, Table 13). For the 3-D case the target PGAs in x, y and vertical directions are 0.25g, 0.125g, and 0.125g, respectively. In this case the x-direction inertia reduction is equal to 49% and that for y-direction is 17%. Note that for the 2-D case the inertia reduction in the y-direction is equal to 21%. To summarize, in the x-direction the inertia reductions are 58%, 54% and 49% for 1-D, 2-D, and 3-D cases, respectively. In the y-direction they are 21%, and 17% for 2-D and 3-D cases, respectively.

To see the effect of higher PGAs, another three cases with Northridge-Sylmar record are compared. For the 1-D case the target PGA is 0.375g in x-direction (case 3, Table 12). For the 2-D case the target PGAs are 0.375g in x-direction, and 0.25g in y-direction (case 5, Table 13), and for the 3-D case the target PGAs are 0.375g in x-direction, 0.25g in y-direction, and 0.25g in the vertical direction (case 7, Table 13). The inertia reductions in the x-direction are 56%, 4%, and 45% for 1-D, 2-D and 3-D case, respectively. Inspection of the displacement results indicates that for the 2-D case the displacement capacity of the bearing has been reached, thus, resulting in higher system

acceleration (lower inertia reduction) due to impact. The displacement capacity of the bearing is about 4 inches. As it can be seen from the above discussion, the vertical motion also has an effect on the response of FPS isolated structure. Note that due to the low displacement capacity of the bearings, it was not possible to conduct further tests with higher PGAs. Some previous studies show that the response acceleration of the bushing in the base isolated system sometimes larger than that of the fixed base system [Murota, 2001]. This is believed due to the fact that the higher vertical accelerations change the pressure. This causes change in coefficient of friction, eventually in friction force, and high frequency vibration of bushing occurs. More test are required to draw more general conclusions.

Table 12 Responses for Northridge-Sylmar Record (Case 1 through Case 3)

Case No.	Input and Response	Fixed Base			Base Isolated		
		x	y	z	x	y	z
1	PGA_{Target}	0.125	-	-	0.125	-	-
	PGA_{Real}	0.147	-	-	0.138	-	-
	A_2	0.160	-	-	0.078	-	-
	A_3	0.246	-	-	0.117	-	-
	A_{B1}	0.272	-	-	0.166	-	-
	A_{B2}	0.251	-	-	0.128	-	-
	A_{B3}	0.513	-	-	0.142	-	-
	A_{B4}	0.919	-	-	0.232	-	-
	D_2	0.034	-	-	0.306	-	-
	D_3	0.050	-	-	0.310	-	-
2	PGA_{Target}	0.250	-	-	0.250	-	-
	PGA_{Real}	0.238	-	-	0.282	-	-
	A_2	0.259	-	-	0.119	-	-
	A_3	0.456	-	-	0.204	-	-
	A_{B1}	0.489	-	-	0.375	-	-
	A_{B2}	0.437	-	-	0.282	-	-
	A_{B3}	1.026	-	-	0.211	-	-
	A_{B4}	1.867	-	-	-	-	-
	D_2	0.067	-	-	1.032	-	-
	D_3	0.095	-	-	1.047	-	-
3	PGA_{Target}	0.375	-	-	0.375	-	-
	PGA_{Real}	0.378	-	-	0.379	-	-
	A_2	0.419	-	-	0.166	-	-
	A_3	0.666	-	-	0.332	-	-
	A_{B1}	0.826	-	-	0.572	-	-
	A_{B2}	0.602	-	-	0.420	-	-
	A_{B3}	1.424	-	-	0.256	-	-
	A_{B4}	2.749	-	-	0.623	-	-
	D_2	0.089	-	-	1.824	-	-
	D_3	0.120	-	-	1.840	-	-

Table 13 Responses for Northridge-Sylmar Record (Case 4 through Case 7)

Case No.	Input and Response	Fixed Base			Base Isolated		
		x	y	z	x	y	z
4	PGA_{Target}	0.250	0.125	-	0.250	0.125	-
	PGA_{Rcal}	0.231	0.109	-	0.264	0.146	-
	A_2	0.251	0.108	-	0.123	0.116	-
	A_3	0.428	0.116	-	0.188	0.201	-
	A_{B1}	0.482	0.481	-	0.398	0.448	-
	A_{B2}	0.427	0.284	-	0.272	0.373	-
	A_{B3}	0.966	0.618	-	0.226	0.274	-
	A_{B4}	1.793	1.310	-	0.433	0.631	-
	D_2	0.061	0.066	-	0.832	0.849	-
	D_3	0.114	0.130	-	0.886	0.856	-
5	PGA_{Target}	0.375	0.250	-	0.375	0.250	-
	PGA_{Rcal}	0.370	0.209	-	0.381	0.245	-
	A_2	0.421	0.217	-	0.364	0.583	-
	A_3	0.626	0.448	-	0.703	1.059	-
	A_{B1}	0.955	1.116	-	1.477	4.612	-
	A_{B2}	0.612	0.597	-	0.903	2.776	-
	A_{B3}	1.341	1.154	-	0.702	1.259	-
	A_{B4}	2.640	2.583	-	1.451	3.090	-
	D_2	0.105	0.132	-	2.559	3.117	-
	D_3	0.189	0.219	-	2.798	3.154	-
6	PGA_{Target}	0.250	0.125	0.125	0.250	0.125	0.125
	PGA_{Rcal}	0.236	0.116	0.119	0.268	0.153	0.124
	A_2	0.257	0.128	-	0.137	0.127	-
	A_3	0.432	0.254	0.154	0.202	0.201	0.173
	A_{B1}	0.521	0.416	0.161	0.408	0.423	0.175
	A_{B2}	0.413	0.267	0.178	0.305	0.344	0.173
	A_{B3}	1.061	0.543	0.188	0.248	0.271	0.163
	A_{B4}	2.010	1.105	0.161	0.453	0.659	0.176
	D_2	0.057	0.072	-	0.821	0.889	-
	D_3	0.115	0.131	-	0.875	0.880	-
7	PGA_{Target}	0.375	0.250	0.250	0.375	0.250	0.250
	PGA_{Rcal}	0.383	0.216	0.236	0.403	0.241	0.232
	A_2	0.415	0.212	-	0.221	0.233	-
	A_3	0.618	0.440	0.284	0.477	0.274	0.349
	A_{B1}	1.105	1.018	0.442	1.020	0.754	0.331
	A_{B2}	0.641	0.546	0.368	0.706	0.497	0.336
	A_{B3}	1.273	1.066	0.386	0.532	0.378	0.336
	A_{B4}	2.667	2.340	0.355	1.083	0.798	0.334
	D_2	0.102	0.147	-	2.380	2.979	-
	D_3	0.193	0.232	-	3.812	2.582	-

Some of the experimental cases are simulated by the computer code developed in Chapter 3. The results are in good agreement with the experimental cases. Simulated cases are tabulated in Table 14. Displacement and inertia reduction responses for the

Table 14 Simulated Experimental Cases

Case No.	PGA in x-direction	PGA in y-direction	PGA in z-direction
I	0.1376	-	-
II	0.2817	-	-
III	0.3793	-	-
IV	0.5164	-	-
V	0.2637	0.1462	-
VI	0.2676	0.1526	0.1526
VII	0.4031	0.2414	0.2316

cases shown in Table 14 are obtained through analytical study. Comparison of inertia reduction responses is shown in Figure 72. Displacement responses also follow the same pattern.

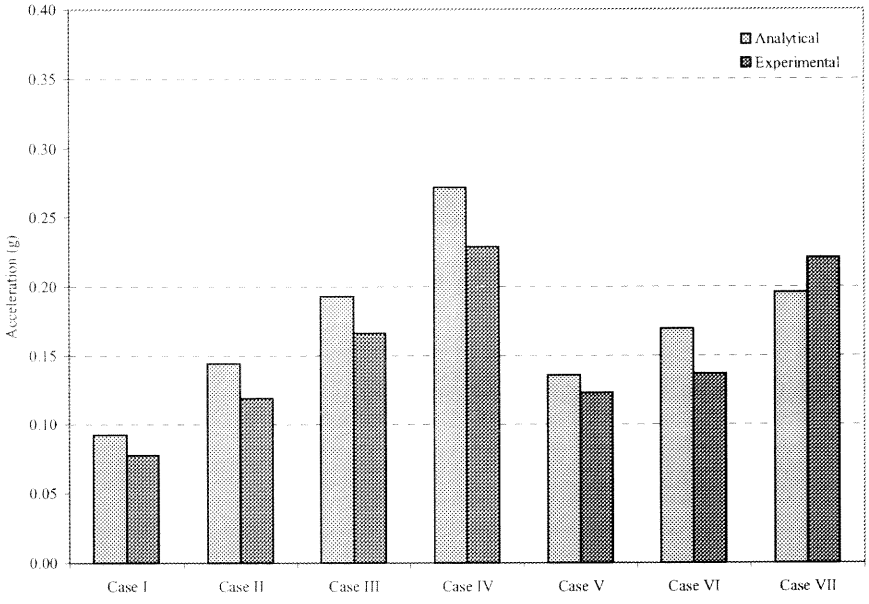

Figure 72 Comparison of Displacement Responses for Analytical and Experimental Studies

4.6 Force/Displacement Response of Transformer Model

The force/displacement responses of the transformer model are shown in the following figures. Figure 73 pertains to 1-D case for the Northridge-Sylmar record. It is seen that the since the displacement limits are not reached for these two cases, the shape of hysteresis loop is very close to a typical hysteresis loop (See Figure 58). In Figure 74, the force/displacement response of a 2-D case is shown. As can be seen from the figure, the displacement capacity of the bearing is reached since there is an abrupt increase in the force. Recalling that the radius of curvature of the bearings used for the tests was very small (i.e., R=18.64"), simultaneous application of orthogonal horizontal accelerations with a PGA of 0.375g and 0.25g caused displacements as large as the displacement limit and impact occurred. However, Figure 75 shows no impact although the same accelerations applied in horizontal orthogonal directions. Vertical ground motion reduces the displacements, which is consistent with the parametric study discussed earlier in that vertical motion can increase or reduce displacement responses.

Figure 73 Hysteresis Loop of Northridge-Sylmar Record for PGA of 0.25g in X-Direction

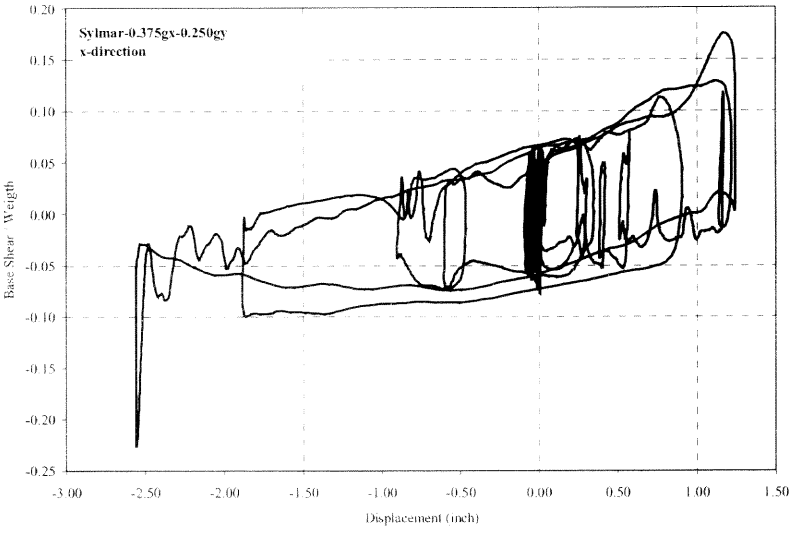

Figure 74 Hysteresis Loop of Northridge-Sylmar Record for PGA of 0.375g in X-Direction and 0.25g in Y-Direction

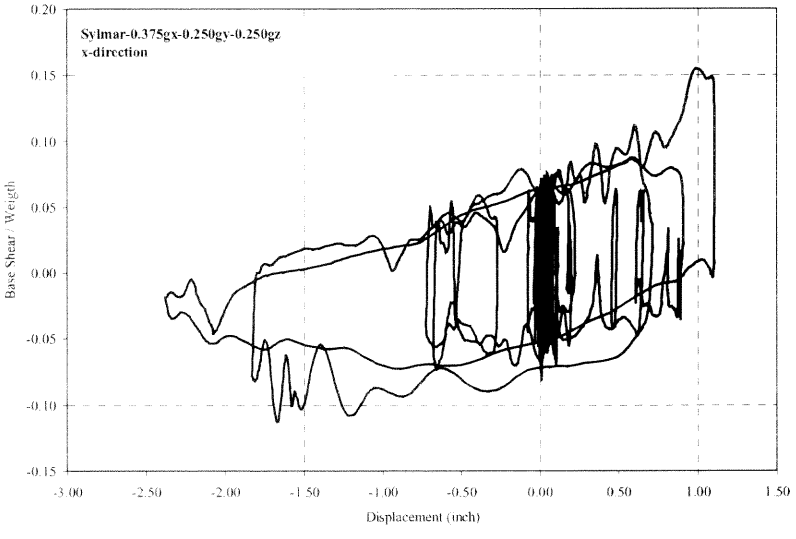

Figure 75 Hysteresis Loop of Northridge-Sylmar Record for PGA of 0.375g in X-Direction, 0.25g in Y-direction and 0.25g in Z-Direction

Bilinear idealization of the FPS isolator is used in Chapter 5 in a simplified model of the substation components and their interactions with each other. Such a study will better quantify the effectiveness of the bearings in reducing the input motion into the bushings supported by the transformer tank. Bushings are another key component in a substation and they have sustained significant damage during previous earthquakes.

CHAPTER 5
SIMPLIFIED MODEL APPROACH

Finite element study is performed to understand response of transformer bushing system in Chapter 2. Then, base isolation (FPS) is identified as a practical technology for their seismic rehabilitation in Chapter 3. Chapter 4 presents the results of the shake table experiments on transformer model and its bushing, with and without the base isolation. Both Chapter 3 and Chapter 4 support the effectiveness of FPS. However, an issue with the use of base isolation is the effect of possibly large displacements on the response of inter-connecting equipments, especially bushings. Therefore, a successful application of base isolation requires in-depth understanding of interaction of interconnecting system with transformer bushing system.

In this chapter, the interaction of the substation equipment is discussed through a parametric study of a simplified model. The interaction of the substation components with each other is one of most important causes of failure of bushings during earthquakes. Based on the finite element analysis presented in Chapter 2 and the previous post earthquake reports, bushing failure is one of the most common failure types. It is mostly caused by either failure of the gasket near the transformer top or interaction with other equipment components through cable conductors. A simple model is developed to investigate the effect of larger displacement for isolated case. A symbolic view of the modeled partial substation is given below in Figure 76. The transformer bushing system is usually connected to lighter and less stiff substation equipment by means of a flexible conductor or a rigid conductor.

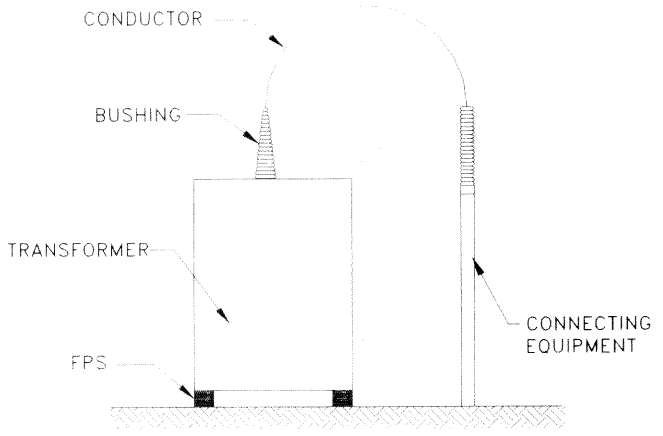

Figure 76 Typical Partial Substation

The proposed simplified model is shown in Figure 77. In this model, FPS is simulated using a nonlinear spring with kinematic bilinear material properties [Zayas, 1989]. This is also known as the simple bilinear model. There are two stiffness values considered in the model: the elastic and yielding stiffness, with unloading and load reversal stages the same as the elastic stage. Material properties are given based on the FPS model phenomena that are explained in Chapter 3 of this thesis. Transformer and bushing flexibility is introduced by a linear spring. The stiffness of the spring is determined based on the finite element analysis for the transformer mounted bushing model. The frequency of the transformer is taken as 14 Hz in the parametric study, and that of bushing is taken as 10 Hz. Typical interconnected substation electrical equipment components can be circuit switchers, insulator post of switches, bus supports and circuit breakers. Frequency values for these components are chosen as 1 Hz and 3 Hz for this study. The connection between transformer bushing systems and electrical equipment is simulated through a nonlinear link element having stiffness in tension only. Lumped mass elements are used for transformer and bushing.

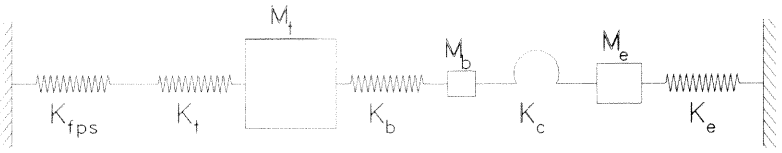

Figure 77 Simplified Model for Partial Substation

Rayleigh damping is introduced to the system, as in 3-D finite element cases, except that the damping values are slightly different from 3-D analysis. As noticed from Figure 78, the damping value is set to 2% for the frequencies of 2 Hz and 14 Hz. This frequency range gives a better approximation for 2% damping of the system. Two earthquake records are employed in this simple analysis. These two records (elcentro-s90w, taft-s69e) are selected as representative of soil and rock records based on the records used in FPS study, in which 10 soil and 10 rock records are used. The FPS results of these two records are closer to the average values of the rock and soil records. Two different stiffness values for the slack cable are chosen.

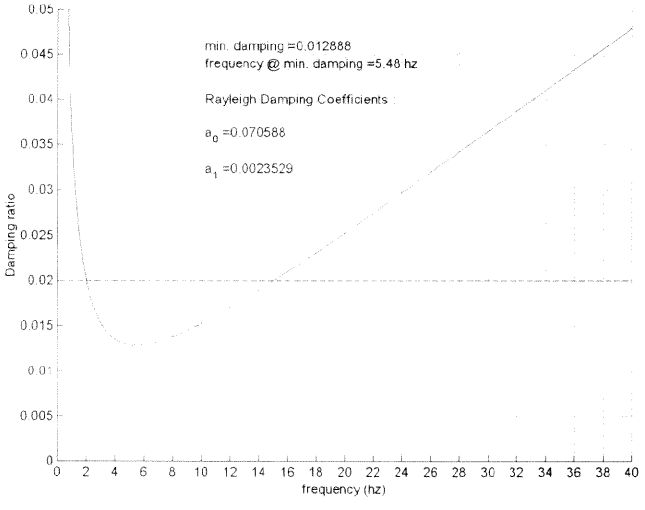

Figure 78 Rayleigh's Damping for Simple System

First, analysis is done on the 2-DOF system consisting of transformer mass, transformer stiffness, bushing mass, and bushing stiffness. Force in the bushing is an important parameter in bushing failure criteria so that bushing force in this simple model is matched to the force at the gasket level of bushing near the top of transformer in the FEA model. The force causing bushing failure at the gasket level (close to the transformer top) is about 2 kips.

In the first part of the parametric study, large slack is provided, i.e., no impact case. For all additional parametric studies, the slack configuration is based on the half circle assumption. For example, if straight line distance between the bushing and the connecting equipment item is x, then the total length of the slack cable is $\pi * x / 2$. And the amount of slack becomes $\frac{\pi - 2}{2} * x$. A simple model with base isolation and without impact is analyzed for two ground motions (one soil, and one rock record), two peak ground acceleration (0.5g, and 1.0g), and two radius of curvature (60", 120") of bearing. These results give the displacement response for the system in the case of no impact and they can be used with the FPS isolated system to eliminate the interaction of the transformer bushing system and the connecting equipment. Results from the base isolation chapter (Chapter 3) for SDOF systems (bushing has not been considered in that system), correlate well with this case.

In the second case, the effect of the interaction on the bushing and FPS is explored. From the first part of the parametric study the distances between the equipment are already obtained to prevent the interaction based on the half circle slack assumption. Two slack conditions are studied to assure the interaction; namely, no slack (cable is taut) and a slack equal to half of the maximum displacement of FPS. This part of the

parametric study is done for two ground motions, two PGAs, three cases of support conditions (fixed case, and two radii of curvature of FPS bearing), two-cable stiffnesses, two slack conditions as explained before, and two connecting equipment frequencies. Also some sensitivity studies have been performed to elaborate on the effect of the stiffness of connecting equipment

5.1 Simplified Model Analysis Results

The interaction between transformer bushing system and connecting equipment, depend on many parameters, like frequency of the transformer and the bushing, stiffness of the cable, the cable slack, stiffness of the connecting equipment, and base isolation parameters. This study is an attempt to incorporate all these variables into a viable, analytical model of the transformer and its attached components. When the amount of slack of the cable is greater than the total absolute displacement of the connected equipment, no interaction occurs. In case of insufficient slack, the interaction effect comes to bear and problem becomes nonlinear. The effect of interaction on the response of base isolation and bushing are the main concerns of this study.

The bushing spring force, transformer spring force, and effect of slack cable on the bushing and the isolation are monitored. The bushing spring force represents the shear at the base of the bushing near to the bushing flange. The transformer spring force shows the force at the base of a rigidly anchored transformer, while in the base isolated case, it shows the force at the isolation level. Displacement and inertia reduction responses for 3-DOF systems (FPS, transformer, and bushing) for different PGAs and two different

earthquake records (El-Centro S90W, and Taft S69E) are obtained. The maximum responses for FPS are shown in Table 15 and Table 16.

Table 15 FPS Response for El-Centro S90W Record

	Bearing Displacement (inch)		Inertia Reduction (%)	
Radius of Curvature of FPS (inch)	PGA = 0.5g	PGA = 1.0g	PGA = 0.5g	PGA = 1.0g
60	7.30	26.68	56.2	43.9
120	9.28	40.59	67.0	56.4

Table 16 FPS Response for Taft S69E Record

	Bearing Displacement (inch)		Inertia Reduction (%)	
Radius of Curvature of FPS (inch)	PGA = 0.5g	PGA = 1.0g	PGA = 0.5g	PGA = 1.0g
60	3.70	9.25	67.4	74.7
120	3.29	12.06	74.3	80.5

The parametric study cases are given in Table 17, Table 18, and Table 19. Case 1 through case 8, case 25 through case 32, case 49 through case 56, and case 73 through case 80 are for the fixed support cases. For these cases two different slack types are employed, namely no slack (taut condition), and very large slack. When the cable is taut, there is interaction between the transformer bushing system and the connecting equipment system. When very large slack is provided, there is no interaction between the systems (each system's response is independent from each other). In all the other cases FPS bearings are implemented as supports (with radii of curvature of 60 inch, and 120 inch). For FPS supported cases, two different slack conditions are provided: no slack (taut condition, slack type 1), and slack in the amount of half of the FPS displacement (slack type 2) shown in Table 15 and Table 16.

Table 17 Simple Model Case 1 through Case 32

Case No	Record Name	PGA	Bearing Type	Cable Area ($inch^{2}$)	Slack Type	fc (hz)
1	Elcentro-S90W	0.5g	Fixed	1	1	1
2	Elcentro-S90W	0.5g	Fixed	1	1	3
3	Elcentro-S90W	0.5g	Fixed	1	large	1
4	Elcentro-S90W	0.5g	Fixed	1	large	3
5	Elcentro-S90W	0.5g	Fixed	10	1	1
6	Elcentro-S90W	0.5g	Fixed	10	1	3
7	Elcentro-S90W	0.5g	Fixed	10	large	1
8	Elcentro-S90W	0.5g	Fixed	10	large	3
9	Elcentro-S90W	0.5g	FPS (R=60")	1	1	1
10	Elcentro-S90W	0.5g	FPS (R=60")	1	1	3
11	Elcentro-S90W	0.5g	FPS (R=60")	1	2	1
12	Elcentro-S90W	0.5g	FPS (R=60")	1	2	3
13	Elcentro-S90W	0.5g	FPS (R=60")	10	1	1
14	Elcentro-S90W	0.5g	FPS (R=60")	10	1	3
15	Elcentro-S90W	0.5g	FPS (R=60")	10	2	1
16	Elcentro-S90W	0.5g	FPS (R=60")	10	2	3
17	Elcentro-S90W	0.5g	FPS (R=120")	1	1	1
18	Elcentro-S90W	0.5g	FPS (R=120")	1	1	3
19	Elcentro-S90W	0.5g	FPS (R=120")	1	2	1
20	Elcentro-S90W	0.5g	FPS (R=120")	1	2	3
21	Elcentro-S90W	0.5g	FPS (R=120")	10	1	1
22	Elcentro-S90W	0.5g	FPS (R=120")	10	1	3
23	Elcentro-S90W	0.5g	FPS (R=120")	10	2	1
24	Elcentro-S90W	0.5g	FPS (R=120")	10	2	3
25	Elcentro-S90W	1.0g	Fixed	1	1	1
26	Elcentro-S90W	1.0g	Fixed	1	1	3
27	Elcentro-S90W	1.0g	Fixed	1	large	1
28	Elcentro-S90W	1.0g	Fixed	1	large	3
29	Elcentro-S90W	1.0g	Fixed	10	1	1
30	Elcentro-S90W	1.0g	Fixed	10	1	3
31	Elcentro-S90W	1.0g	Fixed	10	large	1
32	Elcentro-S90W	1.0g	Fixed	10	large	3

Table 18 Simple Model Case 33 through Case 64

Case No	Record Name	PGA	Bearing Type	Cable Area ($inch^{2)}$	Slack Type	fc (hz)
33	Elcentro-S90W	1.0g	FPS (R=60")	1	1	1
34	Elcentro-S90W	1.0g	FPS (R=60")	1	1	3
35	Elcentro-S90W	1.0g	FPS (R=60")	1	2	1
36	Elcentro-S90W	1.0g	FPS (R=60")	1	2	3
37	Elcentro-S90W	1.0g	FPS (R=60")	10	1	1
38	Elcentro-S90W	1.0g	FPS (R=60")	10	1	3
39	Elcentro-S90W	1.0g	FPS (R=60")	10	2	1
40	Elcentro-S90W	1.0g	FPS (R=60")	10	2	3
41	Elcentro-S90W	1.0g	FPS (R=120")	1	1	1
42	Elcentro-S90W	1.0g	FPS (R=120")	1	1	3
43	Elcentro-S90W	1.0g	FPS (R=120")	1	2	1
44	Elcentro-S90W	1.0g	FPS (R=120")	1	2	3
45	Elcentro-S90W	1.0g	FPS (R=120")	10	1	1
46	Elcentro-S90W	1.0g	FPS (R=120")	10	1	3
47	Elcentro-S90W	1.0g	FPS (R=120")	10	2	1
48	Elcentro-S90W	1.0g	FPS (R=120")	10	2	3
49	Taft-N69E	0.5g	Fixed	1	1	1
50	Taft-N69E	0.5g	Fixed	1	1	3
51	Taft-N69E	0.5g	Fixed	1	large	1
52	Taft-N69E	0.5g	Fixed	1	large	3
53	Taft-N69E	0.5g	Fixed	10	1	1
54	Taft-N69E	0.5g	Fixed	10	1	3
55	Taft-N69E	0.5g	Fixed	10	large	1
56	Taft-N69E	0.5g	Fixed	10	large	3
57	Taft-N69E	0.5g	FPS (R=60")	1	1	1
58	Taft-N69E	0.5g	FPS (R=60")	1	1	3
59	Taft-N69E	0.5g	FPS (R=60")	1	2	1
60	Taft-N69E	0.5g	FPS (R=60")	1	2	3
61	Taft-N69E	0.5g	FPS (R=60")	10	1	1
62	Taft-N69E	0.5g	FPS (R=60")	10	1	3
63	Taft-N69E	0.5g	FPS (R=60")	10	2	1
64	Taft-N69E	0.5g	FPS (R=60")	10	2	3

Table 19 Simple Model Case 65 through Case 96

Case No	Record Name	PGA	Bearing Type	Cable Area ($inch^{2)}$	Slack Type	fc (hz)
65	Taft-N69E	0.5g	FPS (R=120")	1	1	1
66	Taft-N69E	0.5g	FPS (R=120")	1	1	3
67	Taft-N69E	0.5g	FPS (R=120")	1	2	1
68	Taft-N69E	0.5g	FPS (R=120")	1	2	3
69	Taft-N69E	0.5g	FPS (R=120")	10	1	1
70	Taft-N69E	0.5g	FPS (R=120")	10	1	3
71	Taft-N69E	0.5g	FPS (R=120")	10	2	1
72	Taft-N69E	0.5g	FPS (R=120")	10	2	3
73	Taft-N69E	1.0g	Fixed	1	1	1
74	Taft-N69E	1.0g	Fixed	1	1	3
75	Taft-N69E	1.0g	Fixed	1	large	1
76	Taft-N69E	1.0g	Fixed	1	large	3
77	Taft-N69E	1.0g	Fixed	10	1	1
78	Taft-N69E	1.0g	Fixed	10	1	3
79	Taft-N69E	1.0g	Fixed	10	large	1
80	Taft-N69E	1.0g	Fixed	10	large	3
81	Taft-N69E	1.0g	FPS (R=60")	1	1	1
82	Taft-N69E	1.0g	FPS (R=60")	1	1	3
83	Taft-N69E	1.0g	FPS (R=60")	1	2	1
84	Taft-N69E	1.0g	FPS (R=60")	1	2	3
85	Taft-N69E	1.0g	FPS (R=60")	10	1	1
86	Taft-N69E	1.0g	FPS (R=60")	10	1	3
87	Taft-N69E	1.0g	FPS (R=60")	10	2	1
88	Taft-N69E	1.0g	FPS (R=60")	10	2	3
89	Taft-N69E	1.0g	FPS (R=120")	1	1	1
90	Taft-N69E	1.0g	FPS (R=120")	1	1	3
91	Taft-N69E	1.0g	FPS (R=120")	1	2	1
92	Taft-N69E	1.0g	FPS (R=120")	1	2	3
93	Taft-N69E	1.0g	FPS (R=120")	10	1	1
94	Taft-N69E	1.0g	FPS (R=120")	10	1	3
95	Taft-N69E	1.0g	FPS (R=120")	10	2	1
96	Taft-N69E	1.0g	FPS (R=120")	10	2	3

The most important observation for the simplified model approach is that the bushing forces are always larger than the capacity of the bushings for both records of PGA of 0.5g and 1.0g when there is impact. As one expected, the impact forces in the bushing for PGA of 0.5g cases are lower than the ones for PGA of 1.0g. Case 1 is one of the fixed cases with no slack condition (other parameters for this case are shown in Table 17). Figure 79 and Figure 80 show the displacement and forces for this case. As seen from Figure 79, the displacement value of the support is zero and the force in the bushing is 20 kips (Figure 80) which causes the bushing to fail. When the large slack is provided for the fixed base cases (case 3, case 4, case 7, case 8, case 27, case 28, case 31, case 32, case 51, case 52, case 55, case 56, case 75, case 76, case 79, case 80), the bushing forces are smaller and are safe. However, as was noted in Chapter 2, bushings could fail because of the interaction of transformer with bushing (amplification of ground motion due to transformer body). This depends on the characteristics of the ground motion used for the analysis.

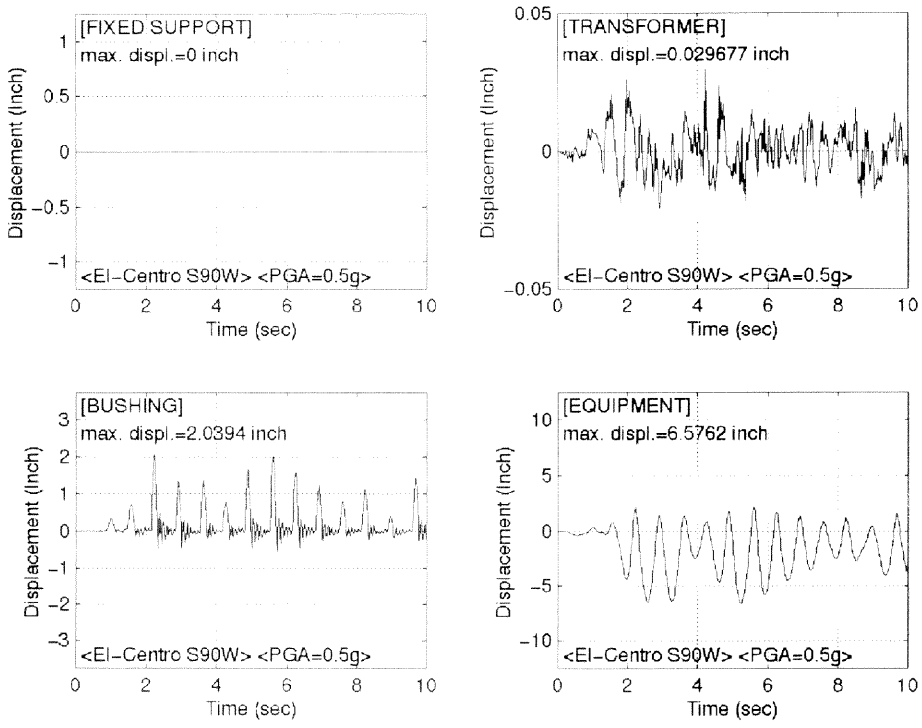

Figure 79 Displacement Responses of Case 1

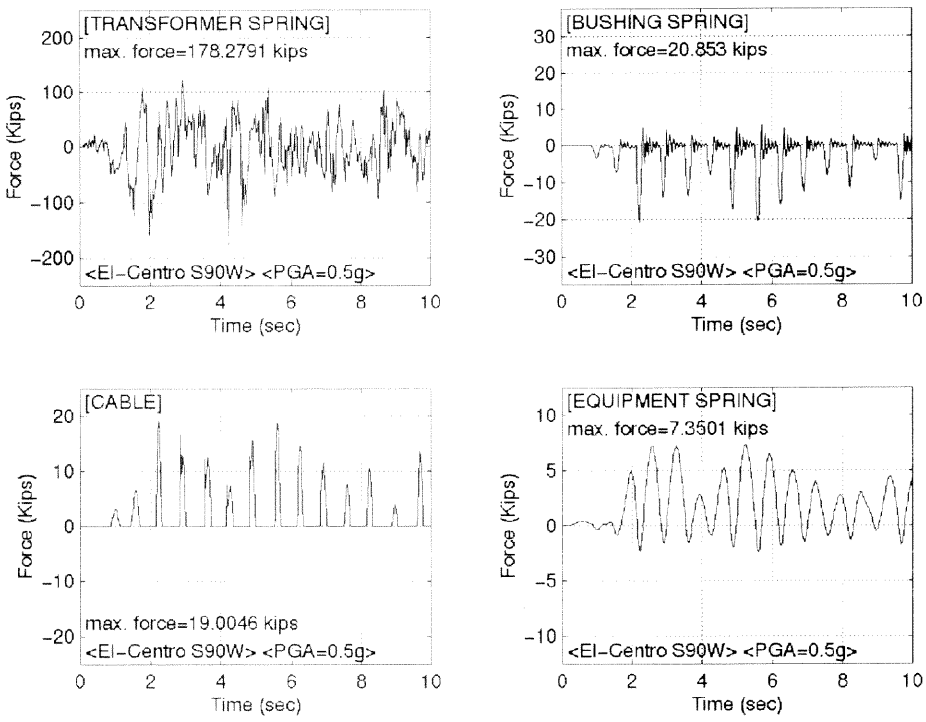

Figure 80 Force Responses for Case 1

The impact force of the bushing is larger for the base isolated cases of no slack than the fixed cases of no slack. Case 12 is one of the sample cases with FPS isolated support, shown in this section. Figure 81 and Figure 82 show the displacement and forces for this case. If there is no interaction the transformer bushing system displaces the same amount as the FPS support however when the interaction happens (cable is taut), impact occurs in the bushing. As noted from Figure 82, the bushing force becomes about 15 kips and causes failure of the bushing (force causing failure in the bushing is 2 kips). Similar charts have been developed for the all of the other cases, however for the sake of space they are not provided as figures. Instead, the maximum responses of the other cases are tabulated in Table 20 through Table 22.

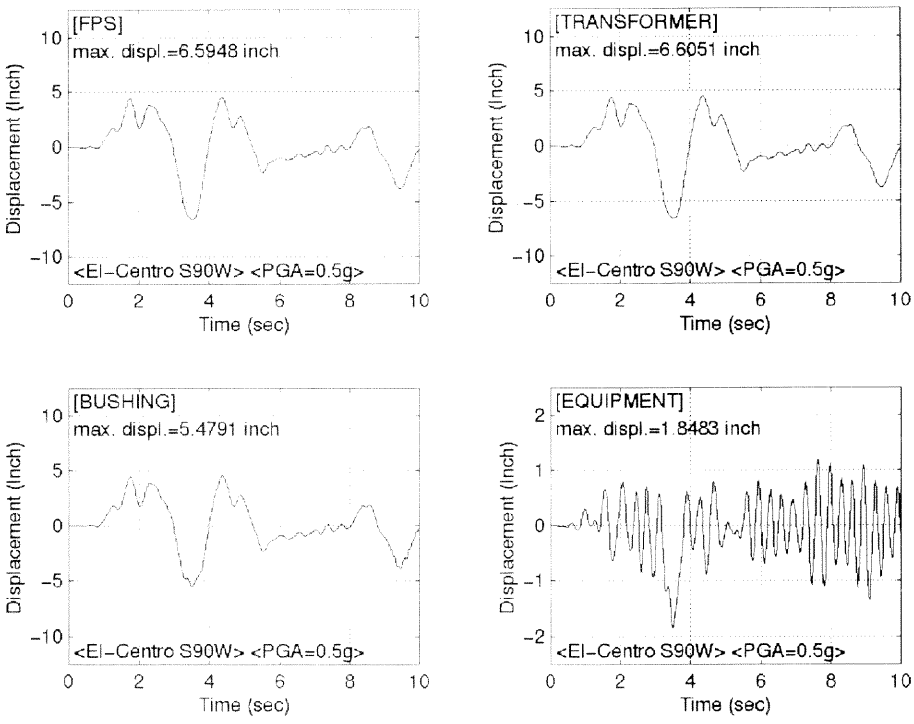

Figure 81 Displacement Responses of Case 12

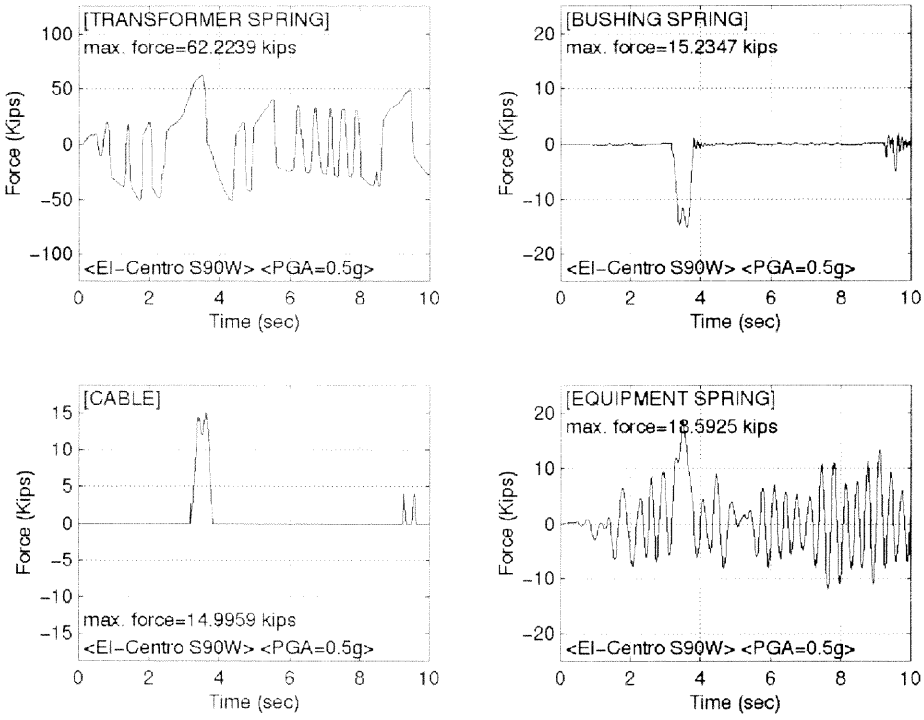

Figure 82 Force Responses of Case 12

The effect of interaction on the response of base isolation is one of the main concerns of this study. It is observed that the interaction does not have significant effect on base isolation response. Inertia reductions are affected by ± 15% compared to the first part of the parametric study (large slack is provided, no impact cases). The effect of the cable stiffness on the response for a practical range of cable area is compared (case 1 vs. case 5, case 2 vs. case 6, case 9 vs. case 13, case 10 vs. case 14, case 11 vs. case 15, case 12 vs. case 16, etc.). It is seen that effect of the cable stiffness on the bushing response force is insignificant for the practical range of cable stiffness used in this parametric study.

Table 20 Simplified Analysis Responses for Case 1 through Case 32

Case No	Displacements				Spring Forces			
	Support	Transformer	Bushing	Connecting Equipment	Transformer	Bushing	Cable	Connecting Equipment
1	0.00	0.03	2.04	6.58	178.28	20.85	19.00	7.35
2	0.00	0.03	0.73	0.94	172.39	7.26	6.05	9.45
3	0.00	0.03	0.12	5.28	171.37	1.14	0.00	5.90
4	0.00	0.03	0.12	1.48	171.37	1.14	0.00	14.87
5	0.00	0.03	2.05	6.47	177.50	20.96	29.59	7.23
6	0.00	0.03	0.75	0.93	172.52	7.44	6.19	9.40
7	0.00	0.03	0.12	5.28	171.37	1.14	0.00	5.90
8	0.00	0.03	0.12	1.48	171.37	1.14	0.00	14.87
9	6.47	6.48	6.63	8.26	61.58	19.15	17.94	9.24
10	5.13	5.14	4.43	3.23	54.92	30.18	29.32	32.47
11	6.72	6.73	6.93	7.37	62.81	17.99	17.57	8.23
12	6.59	6.61	5.48	1.85	62.22	15.23	15.00	18.59
13	6.47	6.48	6.63	8.25	61.58	19.31	42.31	9.22
14	5.11	5.12	4.43	3.26	54.79	30.75	29.85	32.77
15	6.71	6.72	6.95	7.35	62.79	18.27	45.72	8.22
16	6.59	6.60	5.45	1.87	62.18	15.47	15.22	18.78
17	8.21	8.22	8.21	9.25	50.15	23.19	21.82	10.34
18	6.14	6.15	5.55	3.66	44.97	34.89	34.15	36.83
19	8.53	8.54	8.74	8.43	50.93	23.20	21.37	9.42
20	8.30	8.31	6.31	2.36	50.38	25.77	25.15	23.72
21	8.21	8.22	8.20	9.23	50.14	23.29	21.87	10.32
22	6.09	6.10	5.55	3.69	44.82	35.42	34.66	37.08
23	8.53	8.54	8.74	8.41	50.92	23.48	21.56	9.40
24	8.29	8.30	6.28	2.38	50.34	26.20	25.55	23.95
25	0.00	0.06	4.08	13.15	356.56	41.71	38.01	14.70
26	0.00	0.06	1.47	1.88	344.78	14.53	12.10	18.90
27	0.00	0.06	0.25	10.56	342.74	2.28	0.00	11.81
28	0.00	0.06	0.25	2.96	342.74	2.28	0.00	29.73
29	0.00	0.06	4.10	12.94	354.99	41.92	59.18	14.47
30	0.00	0.06	1.50	1.87	345.03	14.89	12.38	18.80
31	0.00	0.06	0.25	10.56	342.74	2.28	0.00	11.81
32	0.00	0.06	0.25	2.96	342.74	2.28	0.00	29.73

Table 21 Simplified Analysis Responses for Case 33 through Case 64

Case No	Displacements				Spring Forces			
	Support	Transformer	Bushing	Connecting Equipment	Transformer	Bushing	Cable	Connecting Equipment
33	23.90	23.92	22.53	23.40	148.75	48.81	46.61	26.16
34	26.17	26.19	26.19	9.80	160.10	91.82	90.50	98.61
35	25.08	25.10	25.52	19.44	154.63	44.26	40.85	21.72
36	24.16	24.19	24.24	5.46	150.05	49.18	49.36	54.88
37	23.89	23.91	22.80	23.35	148.69	49.31	46.96	26.10
38	26.18	26.21	26.21	9.90	160.17	93.03	91.58	99.62
39	25.07	25.10	25.54	19.41	154.60	44.69	116.89	21.69
40	24.20	24.23	24.28	5.51	150.20	49.76	49.98	55.48
41	35.47	35.49	35.50	35.52	118.30	71.03	67.77	89.70
42	34.16	34.18	34.21	13.53	115.02	137.12	135.29	136.06
43	38.36	38.38	38.61	24.67	125.52	62.82	58.67	27.57
44	36.70	36.72	29.56	9.14	121.38	95.84	93.53	81.94
45	35.43	35.45	35.60	35.66	118.19	70.87	67.50	89.86
46	34.24	34.26	34.29	13.65	115.22	139.09	137.11	137.36
47	38.35	38.38	38.60	24.64	125.51	63.65	59.32	27.54
48	36.66	36.68	29.45	9.24	121.26	96.89	94.54	82.95
49	0.00	0.03	1.44	5.23	156.15	14.70	13.38	5.85
50	0.00	0.03	0.79	1.15	156.14	8.01	8.66	11.55
51	0.00	0.03	0.09	5.45	156.61	0.70	0.00	6.10
52	0.00	0.03	0.09	2.38	156.61	0.70	0.00	23.90
53	0.00	0.03	1.48	5.30	156.00	15.02	19.21	5.93
54	0.00	0.03	0.80	1.15	156.16	8.07	27.04	11.52
55	0.00	0.03	0.09	5.45	156.61	0.70	0.00	6.10
56	0.00	0.03	0.09	2.38	156.61	0.70	0.00	23.90
57	4.36	4.37	4.42	4.88	51.07	13.77	12.67	5.45
58	4.39	4.40	4.45	1.54	51.12	15.39	14.01	15.53
59	4.03	4.04	4.09	5.51	49.41	14.35	13.04	6.16
60	3.80	3.81	3.82	2.04	48.24	7.69	6.87	20.51
61	4.36	4.37	4.35	4.88	51.04	13.95	12.80	5.45
62	4.40	4.40	4.45	1.55	51.16	15.74	14.28	15.57
63	4.01	4.02	4.06	5.48	49.32	14.60	13.20	6.12
64	3.80	3.81	3.82	2.03	48.25	7.93	7.05	20.46

Table 22 Simplified Analysis Responses for Case 65 through Case 96

Case No	Displacements				Spring Forces			
	Support	Transformer	Bushing	Connecting Equipment	Transformer	Bushing	Cable	Connecting Equipment
65	4.24	4.24	4.28	4.94	40.20	15.10	13.88	5.53
66	4.49	4.50	4.51	1.22	40.85	12.50	11.76	12.31
67	3.94	3.94	3.98	5.67	39.46	14.57	13.21	6.34
68	3.61	3.62	3.65	1.79	38.64	8.76	8.02	18.04
69	4.24	4.25	4.30	4.97	40.21	15.29	14.01	5.96
70	4.51	4.52	4.53	1.23	40.91	12.82	17.87	12.40
71	3.92	3.92	3.95	5.65	39.41	14.83	13.39	6.32
72	3.62	3.62	3.65	1.79	38.65	8.97	11.26	18.00
73	0.00	0.05	2.88	10.46	312.30	29.41	26.77	11.69
74	0.00	0.05	1.58	2.30	312.27	16.02	17.33	23.11
75	0.00	0.05	0.18	10.91	313.23	1.39	0.00	12.19
76	0.00	0.05	0.18	4.75	313.23	1.39	0.00	47.79
77	0.00	0.05	2.96	10.61	312.00	30.03	38.42	11.86
78	0.00	0.05	1.59	2.29	312.31	16.14	54.08	23.04
79	0.00	0.05	0.18	10.91	313.23	1.39	0.00	12.19
80	0.00	0.05	0.18	4.75	313.23	1.39	0.00	47.79
81	9.74	9.75	9.85	12.41	77.94	33.27	30.93	13.87
82	11.13	11.15	11.21	4.60	84.92	46.68	45.46	46.32
83	9.54	9.56	9.73	13.52	76.96	36.72	33.49	15.11
84	9.25	9.26	9.29	3.28	75.49	26.13	24.30	32.97
85	9.80	9.82	9.92	12.44	78.27	33.92	55.27	13.90
86	11.20	11.21	11.27	4.67	85.24	47.81	46.53	46.97
87	9.52	9.54	9.71	13.37	76.87	36.87	49.79	14.95
88	9.25	9.26	9.29	3.31	75.49	26.61	24.72	33.25
89	11.21	11.22	11.23	10.00	57.64	28.20	25.91	11.18
90	11.53	11.53	11.50	2.68	58.44	25.55	23.86	26.91
91	11.85	11.86	11.92	16.12	59.26	33.07	32.26	18.01
92	12.06	12.07	12.09	3.77	59.78	17.23	16.75	37.90
93	11.16	11.17	11.18	10.04	57.53	28.55	26.17	11.22
94	11.52	11.53	11.49	2.69	58.42	26.10	44.31	27.04
95	11.83	11.84	11.89	16.08	59.21	33.39	30.06	17.97
96	12.06	12.07	12.09	3.76	59.78	17.53	16.17	37.81

Figure 83 shows the displacement response of the bushing and the connecting equipment of a representative fixed case (case 25). Figure 84 shows the displacement response of the bushing and the connecting equipment of a representative base isolated case (case 41). The amount of slack for both of these cases is zero. The support displacements for case 25 and case 41 are 0" and 35", respectively. It is noticed in Figure 83 that the vibrations of the bushing and the interconnecting equipment are mostly out of phase. Other fixed base cases support this observation. However, for the base isolated case (case 41), the bushing and the interconnecting equipment moves mostly in the same direction. Time histories of gap opening, (displacement difference of the connecting equipment and bushing) of these two cases (case 25, case 41) are shown in Figure 85. When the relative displacement value becomes positive, the interaction occurs between the bushing and the connecting equipment. It should be pointed out that even for the fixed transformer case there is a need to provide a good amount of slack because of the out of phase vibrations of the bushing and the interconnecting equipment. The maximum absolute relative displacements are 13 inch and 27 inch for fixed base case and base isolated case, respectively. On the other hand, support displacements are 0" and 41" for fixed base case and base isolated case, respectively. The feasibility of the base isolation is more obvious when the relative displacement between the bushing and the connecting equipment is compared to the support displacements of the two cases.

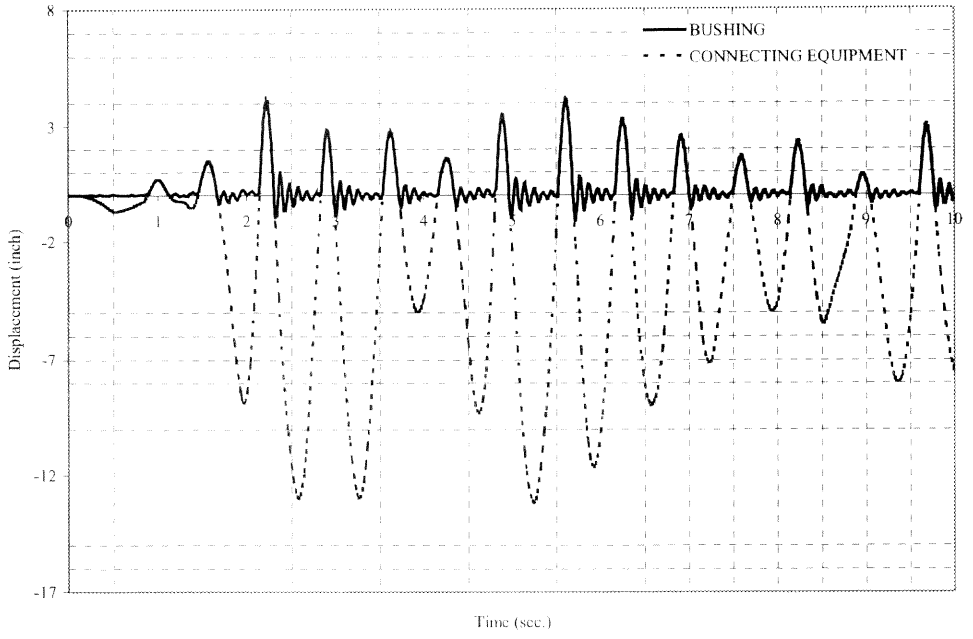

Figure 83 Displacement Response of Bushing and Connecting Equipment for Case 25

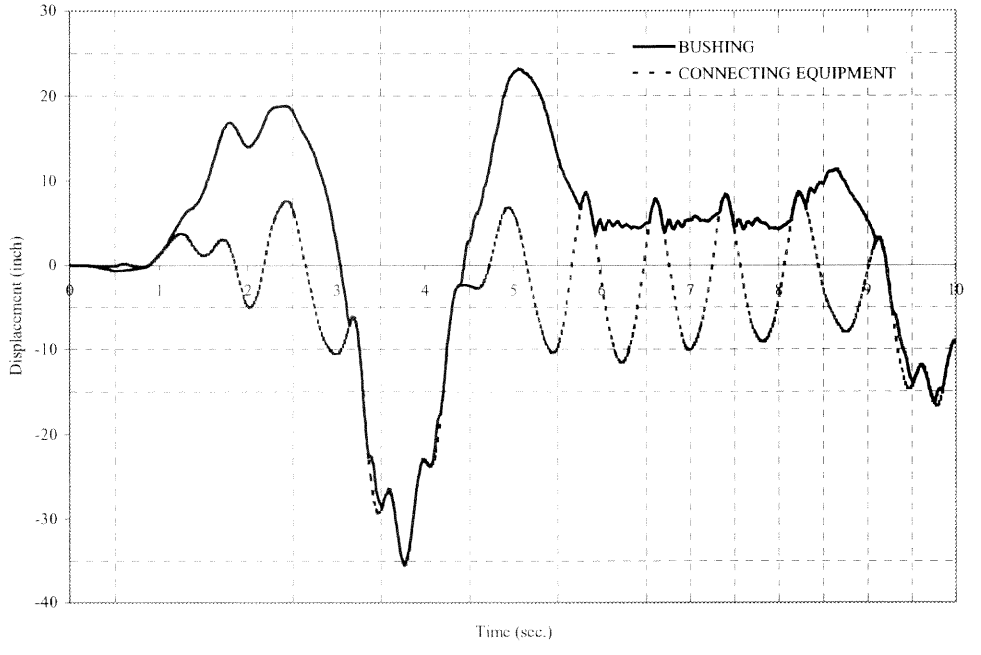

Figure 84 Displacement Response of Bushing and Connecting Equipment for Case 41

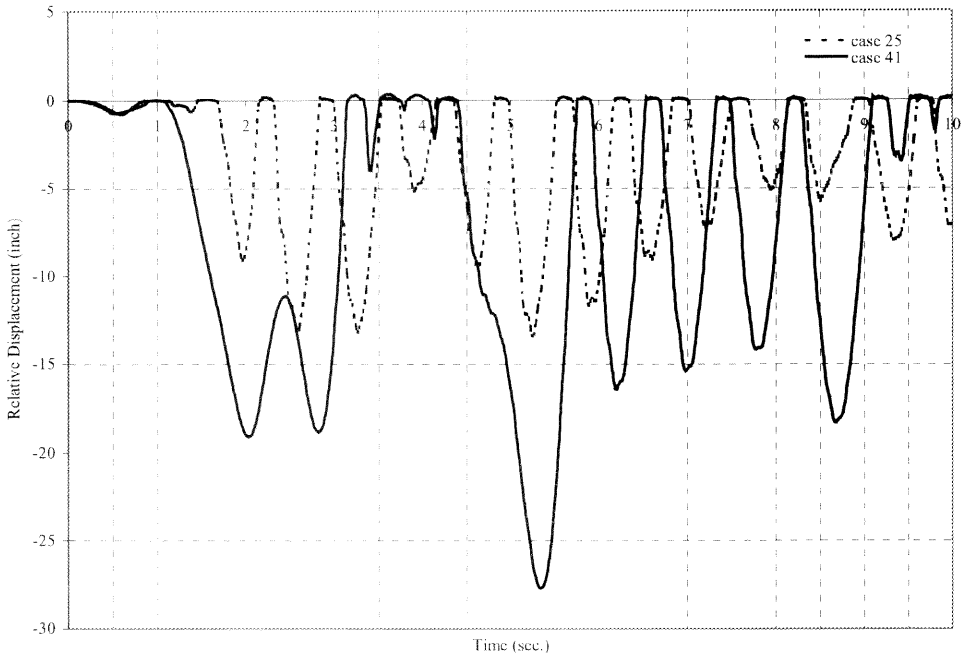

Figure 85 Relative Displacement of Bushing and Connecting Equipment for Case 25 and Case 41

For the cases studied, mass and stiffness parameters of the connecting equipment are taken from one of the sample equipment. Frequencies of the connecting equipment taken in these analyses are 1 Hz and 3 Hz. However mass and stiffness parameters of the connecting equipment can vary from equipment to equipment. The response effect of equipment items with different stiffness and mass properties having the same frequency are different. For example, consider two connecting equipment items with 1 Hz frequency. Assume one of them has stiffness, k and mass m and the other one has stiffness 1000 k and mass 1000 m. Even though they have the same frequency their displacement response will be same but force response will be different.

To study this effect, eight more cases are included. Two new cases are developed for each cases of 11, 12, 19, and 20. For the first one connecting equipment stiffness and mass are taken as 1/1000 k and 1/1000 m. For the other newly developed case, stiffness

and mass are taken as 1000 k and 1000 m. Figure 86 and Figure 87 show this effect for case 12 with stiffness and mass of 1000 k and 1000 m and with stiffness and mass of 1/1000 k and 1/1000 m. Recalling that the force response with stiffness (k) and mass (m) values of this case (case 12) is given in Figure 82, comparison can be made between case 12 and derivatives of case 12 (1000 k and 1000 m, 1/1000 k and 1/1000 m). Figure 86 and Figure 87 show that the stiffness of the connecting equipment has a significant effect on the bushing response. Stiffer connecting equipment develops significantly more forces on the bushing.

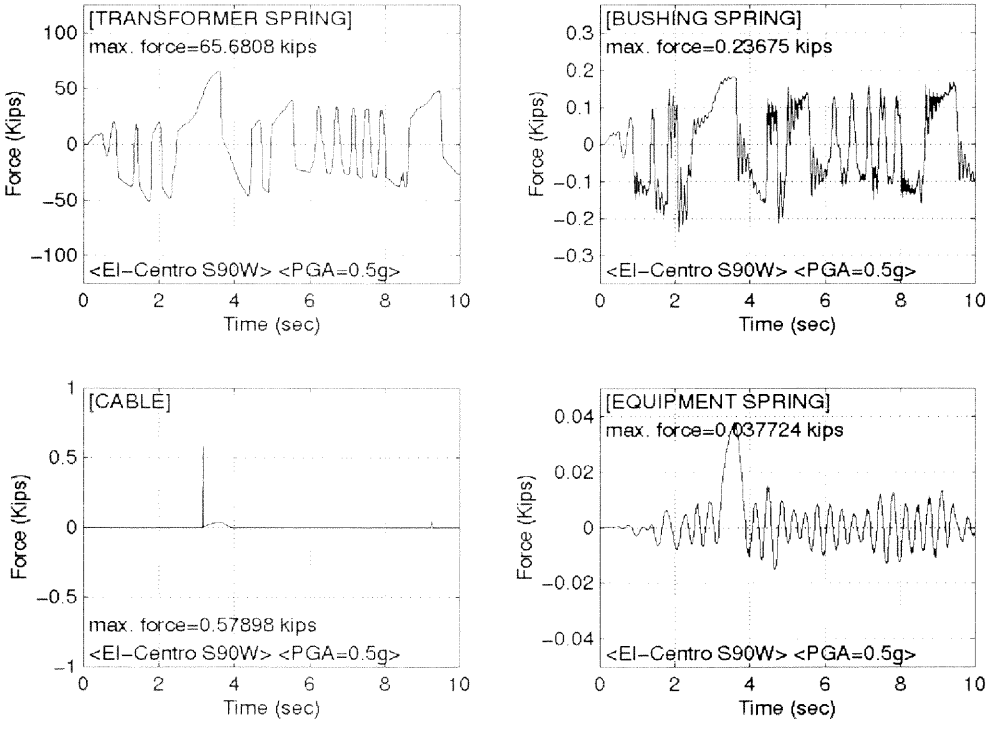

Figure 86 Force Response of Case 12 with 1/1000 k and 1/1000 m

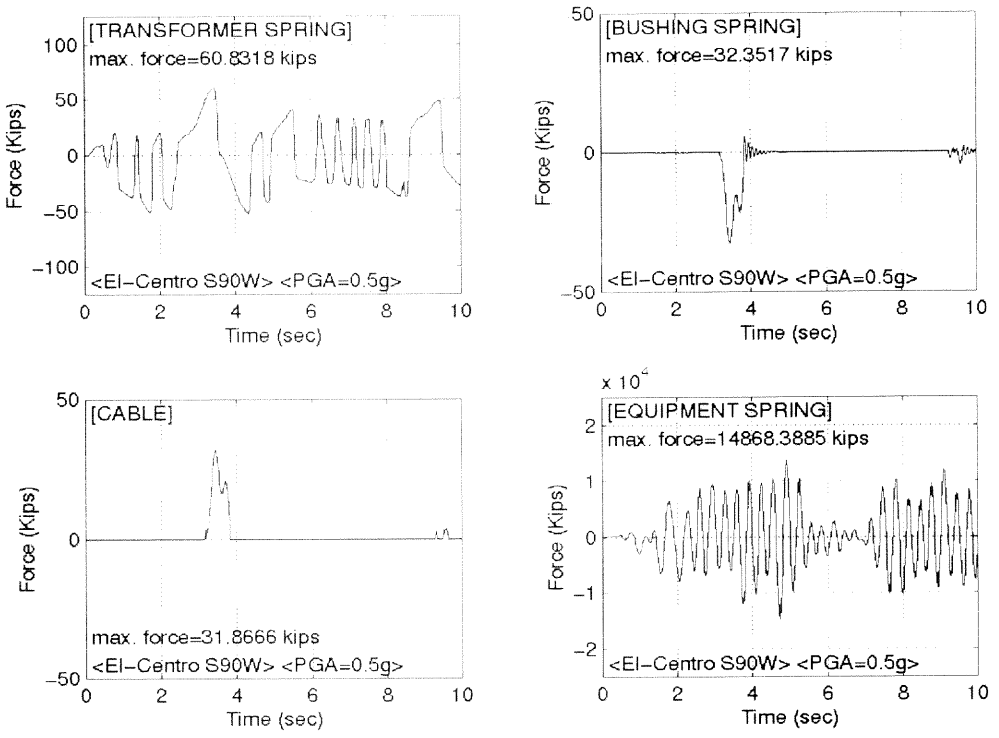

Figure 87 Force Response of Case 12 with 1000 k and 1000 m

5.2 Practical Aspects and Design Recommendations

Unanchored transformers should be avoided in earthquake prone regions. Tilting of an unanchored transformer is very likely in moderate and high seismic prone regions. As an example, consider TT3 in Chapter 2 of this thesis. The weight of the transformer is 512 kips and the dimensions of the transformer are B=100 inch, L=280 inch, H=180 inch (see Figure 88).

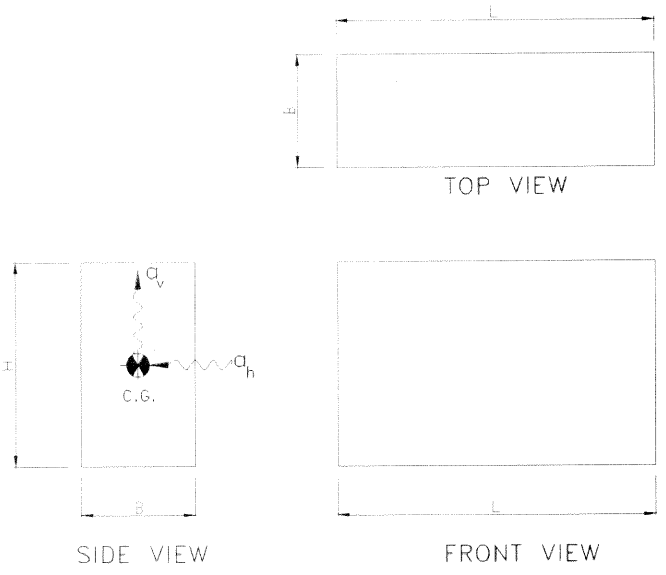

Figure 88 Outline View of TT3

Based on the IEEE requirement, 0.5g of horizontal acceleration and 0.4g of vertical acceleration are applied to the transformer center of gravity. Assuming the center of gravity of the transformer is located H/2 above the bottom of transformer, the overturning moment at the heel of transformer in critical direction (narrow side), M_o becomes,

$$M_o = \frac{W}{g} * a_h * \frac{H}{2} = \frac{512}{g} * 0.5g * \frac{180}{2} * \frac{1}{12} = 1920 \text{ kips-ft}$$

And the resisting moment, M_R becomes,

$$M_R = \frac{W}{g} * (1g - a_v) * \frac{B}{2} = \frac{512}{g} * (1g - 0.4g) * \frac{100}{2} * \frac{1}{12} = 1280 \text{ kips-ft}$$

Since resisting moment is less than overturning moment, tipping of the transformer is possible. Therefore anchorage of the transformer is required. Vertical tipping reaction, V, can be calculated as

$$V = \frac{M_O - M_R}{B} = \frac{1920 - 1280}{100/12} = 76.8 \text{ kips}$$

Assuming the transformer top is in contact with the concrete foundation and the coefficient of friction of concrete metal interface is 0.25. The lateral force at the bottom of transformer, F_h, becomes

$$F_h = \frac{W}{g} * a_{gh} - \mu_s W = W(0.5 - 0.25) = 128 \text{ kips}$$

And the resultant force at the base of the transformer is,

$$F_R = \sqrt{F_h^2 + V^2} = \sqrt{128^2 + 76.8^2} = 149 \text{ kips}$$

If welding with ½" leg is preferred for anchorage, and the allowable stress of the weld is assumed as 30 ksi, total length of the weld, W_L, along the narrow sides (both sides) of the transformer becomes,

$$W_L = \frac{F_R}{30 * \frac{(1/2)"}{\sqrt{2}}} = 21.07 \text{ inch}$$

Therefore, providing a 21-inch long weld is enough for fixing this transformer.

The same calculations are performed for high seismic performance level (1.0 g in horizontal, and 0.8g in vertical direction). The resultant force at the base of the transformer, F_R, and the required weld, W_L, become 561.5 kips and 73 inch respectively. It is clear that anchorage forces required increase dramatically for high seismic performance level. The maximum dynamic amplification factor at the midlevel of this transformer is found to be 1.624 in Chapter 2 of this thesis. Then, the required weld for this transformer type for high performance level becomes total of 153-inch long for two of the critical sides. Welding can be done in many ways, for example: some structural shape (angel, channel, etc.) with horizontal and vertical shear studs welded on it is

embedded inside the concrete foundation pad parallel to shorter sides of the transformer and transformer bottom plates welded to these plates (fillet weld, etc.).

Proper anchorage should be implemented for existing transformers in the moderate or high earthquake prone regions by use of welds and anchor bolts. Embedment of structural shapes in the concrete foundation for anchorage purposes is challenging so that some structural shapes could be anchored to the foundation through some anchor bolts. This structural shape can be welded to the transformer tank. New transformer tank designs should consider the anchorage of the transformer tank to the concrete pad below.

Advantages of using FPS for transformers have been mentioned before in previous chapters. It should also be mentioned that application of FPS has advantages in functionality and maintenance needs of transformers, compared to anchorage. They can be used when enough clearances are insured to provide slack for the connections. The minimum required clearances with the assumption of half circle connection between equipment item and the bushing, based on the average results of FPS study are given for moderate and high seismic performance level regions in Table 23 and Table 24 respectively. The use of base isolation reduces the lateral force, foundation forces at the base of the transformer and even the bushing forces are reduced. However, simplified analysis results show that base isolated systems without proper amount of slack cause high impact forces on the bushing. Therefore, FPS should not be used without providing proper amount of slack.

Table 23 Required Slack for FPS Displacements (Moderate Seismic Performance Level)

Radius of Curvature of FPS (inch)	Bearing Displacement (inch)	Minimum Required Distance Between Equipment Items (inch)
30	4.4	7.7
60	5.0	8.8
90	5.0	8.8
120	5.1	8.9
150	5.2	9.1

Table 24 Required Slack for FPS Displacements (High Seismic Performance Level)

Radius of Curvature of FPS (inch)	Bearing Displacement (inch)	Minimum Required Distance Between Equipment Items (inch)
30	14.9	26.1
60	17.9	31.4
90	20.6	36.1
120	21.1	37.0
150	21.3	37.3

The values given in Table 23 and Table 24 depend on the average values of the FPS displacements. It should be kept in mind that the displacement of the connecting equipment should also be taken into account. Average FPS displacement based on PGA and radius of curvature is discussed in Chapter 3 of this thesis. Displacement of connecting equipment (circuit breaker, disconnect switches, etc.) is obtained either through finite element modeling or from the IEEE response spectra. Absolute sum of these displacements provide the required slack amount.

CHAPTER 6
CONCLUSIONS

Based on the results of the finite element analysis performed on different types of transformers, the parametric and experimental studies of the friction pendulum system, and the study of the simplified model, the following general conclusions are obtained:

1. The flexibility of the transformer body has an effect on the bushing response. Translational modes of the transformers have the highest effect on the response of the bushing.
2. The dynamic amplification factor specified in IEEE code is not always conservative.
3. Qualification tests on bushings with twice the response spectra as specified in IEEE should be preceded by a finite element analysis of the transformer model. Qualification tests for bushings should be performed on a semi-rigid stand with a frequency equal to that of the translational mode of the transformer.
4. The frictional pendulum system can be utilized for seismic rehabilitation of transformers where enough slack between bushings and connecting electrical equipment item is provided.
5. The frictional pendulum system provides considerable inertia reductions depending on the peak ground acceleration (PGA) and the bearing radius of curvature. The FPS system is more effective in reducing inertia forces for higher PGAs. Furthermore, both inertia reductions and maximum displacements are affected by the earthquake record used. Records with dominant periods in the vicinity of the isolator period reduce the isolator effectiveness. On the average, FPS bearings can provide 60%

inertia reductions within their displacement limits. The amount of inertia reduction is significantly higher compared to the fixed based situation.

6. The coupling of responses in two horizontal directions does exist due to dependency of frictional characteristics on total velocity. However, this effect tends to diminish for higher PGAs since at higher velocities frictional constants are less sensitive to the magnitude of the velocity.
7. The CQC method is recommended for estimating the total resultant displacement for PGAs less than 0.5g. For higher PGAs the average of SRSS and CQC methods could be used for displacements in order to reduce the conservatism of CQC method at higher PGA values. For inertia reductions the average of the two methods is recommended for all PGAs.
8. Use of FPS bearings must be avoided where enough slack between bushings and connecting electrical equipment items is not provided. In this case transformers should be anchored to their foundation by use of welds or anchor bolts.

Some of the further study recommendations can be made as follow:

1. Finite element model of other substation equipment as well as shake table testing should be performed.
2. It was observed that the effect of vertical motion on the response of FPS is more pronounced on inertia reductions than on displacements. The effect of vertical is only significant for records of higher PGAs and of lower frequency contents, based on Chapter 2 of this thesis. However, higher vertical accelerations can change the friction force and high frequency vibration of bushing can occur. Further study should be performed to study this effect.

APPENDIX A

STATIC CALCULATIONS FOR TRANSFORMERS

The following are static calculations for transformer tanks (TT1, TT2, TT3).

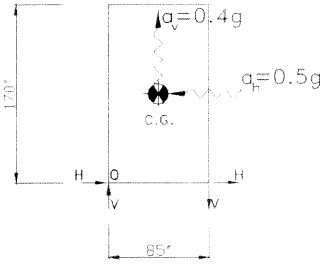

TT1

$$M_o = 0.5g * \frac{179 \text{ kips}}{g} * \frac{170"}{2} + 0.4g * \frac{179 \text{ kips}}{g} * \frac{85"}{2} = 10650 \text{ kips-in}$$

$$V = \frac{1}{2} * \frac{M_o}{85"} = 63 \text{ kips}, \quad H = \frac{1}{4} * 0.5g * \frac{179 \text{ kips}}{g} = 22 \text{ kips}$$

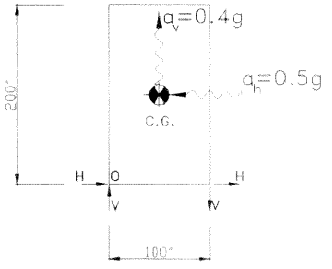

TT2

$$M_o = 0.5g * \frac{300 \text{ kips}}{g} * \frac{200"}{2} + 0.4g * \frac{300 \text{ kips}}{g} * \frac{100"}{2} = 21000 \text{ kips-in}$$

$$V = \frac{1}{2} * \frac{M_o}{100"} = 105 \text{ kips}, \quad H = \frac{1}{4} * 0.5g * \frac{300 \text{ kips}}{g} = 38 \text{ kips}$$

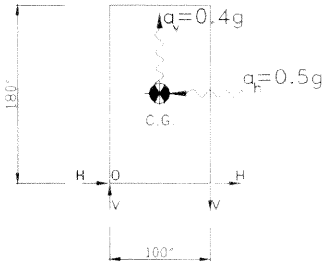

TT3

$$M_o = 0.5g * \frac{512 \text{ kips}}{g} * \frac{180"}{2} + 0.4g * \frac{512 \text{ kips}}{g} * \frac{100"}{2} = 33280 \text{ kips-in}$$

$$V = \frac{1}{2} * \frac{M_o}{100"} = 166 \text{ kips}, \quad H = \frac{1}{4} * 0.5g * \frac{512 \text{ kips}}{g} = 64 \text{ kips}$$

APPENDIX B

FORTRAN CODE FOR FPS

The following is the FORTRAN code for the analysis of FPS with small displacement assumption.

```
      INTEGER  NEQ, NPARAM,CCC,GGG,MMM,LLL,NOD,NOTS
      CHARACTER *15, FN1,FN2,FN3
      PARAMETER (NEQ=6, NPARAM=50)
      INTEGER IDO,IMETH, INORM, NOUT, IATYPE, MTYPE,MITER
      REAL A(1,1), FCN, FCNJ, HINIT,HMAX, PARAM(NPARAM),TOL, X
      REAL XEND, Y(NEQ), MXSTEP,XDISPMAX,XDISPMIN,YDISPMAX
      REAL MAXRESDISP,MAXTOTALACCX,INREDX,INREDY
      REAL MAXTOTALACCY, MAXTOTALACCXY,INREDXY
      REAL YDISPMIN,TOTALACCX(100000),TOTALACCY(100000)
      ,RESACC(100000)
      REAL TOTALACCXY(100000),GROUNDXY(100000),RESDISP(100000)
      REAL BASESHX(100000),BASESHY(100000),RESBASESH(100000)
      REAL MAXGROUNDX, MAXGROUNDY, MAXGROUNDZ, MAXGROUNDXY
      REAL UGX(10000),UGY(10000),UGUP(10000),DT
      COMMON UGXN(100000),UGYN(100000),UGUPN(100000)
      COMMON C10,C9,C12,C13,C14
      COMMON IEND,ACCX,ACCY
      EXTERNAL FCN,IVPAG,SSET,FCNJ
      OPEN (1,FILE='input.txt',STATUS='old')
      READ (1,100) FN1,FN2,FN3,DT,C10,C9,C12,C13,C14
100      FORMAT (/,A15,//,A15,//,A15,//,F6.3,//,F6.3,//,F6.3
      ,//,F7.4,//,F7.4,//,F7.4)
      PRINT '(A22,A15)', 'INPUT FILE NAME IN X: ',FN1
      PRINT '(A22,A15)', 'INPUT FILE NAME IN Y: ',FN2
      PRINT '(A22,A15)', 'INPUT FILE NAME IN Z: ',FN3
      PRINT '(A17,F6.3,A8)','TIME STEP      : ', DT, ' SECONDS'
      PRINT '(A17,F6.3,A4)','FRICTION       : ', C10
      PRINT '(A17,F7.3,A5)','RADIUS         : ', C9,' INCH'
      PRINT '(A17,F6.3)','X-SCALE FACTOR : ', C12
      PRINT '(A17,F6.3)','Y-SCALE FACTOR : ', C13
      PRINT '(A17,F6.3)','Z-SCALE FACTOR : ', C14
C     OPEN OUTPUT FILE
      OPEN (2,FILE='output.dat ',STATUS='REPLACE')
C     FIND THE MAXIMUMS OF THE GROUND INPUTS
      OPEN (22,FILE=FN1,STATUS='OLD')
      CCC=0
      DO WHILE (.NOT. EOF(22))
      CCC = CCC + 1
      READ(22,*) UGX(CCC)
      IF (CCC.EQ.1) MAXGROUNDX=0.0
      IF (ABS(UGX(CCC)).GT.MAXGROUNDX) MAXGROUNDX=ABS(UGX(CCC))
      END DO
      CLOSE (22)
      OPEN (33,FILE=FN2,STATUS='OLD')
      CCC=0
      DO WHILE (.NOT. EOF(33))
      CCC = CCC + 1
      READ(33,*) UGY(CCC)
      IF (CCC.EQ.1) MAXGROUNDY=0.0
      IF (ABS(UGY(CCC)).GT.MAXGROUNDY) MAXGROUNDY=ABS(UGY(CCC))
      END DO
```

```
      CLOSE (33)
      OPEN (44,FILE=FN3,STATUS='OLD')
      CCC=0
      DO WHILE (.NOT. EOF(44))
      CCC = CCC + 1
      READ(44,*) UGUP(CCC)
      IF (CCC.EQ.1) MAXGROUNDZ=0.0
      IF (ABS(UGUP(CCC)).GE.MAXGROUNDZ) MAXGROUNDZ=ABS(UGUP(CCC))
      END DO
      CLOSE (44)
C     SCALE PGA of GROUND INPUTS TO 1.0g
      DO 55 MMM=1,CCC
      UGX(MMM)=(UGX(MMM))/MAXGROUNDX*386.4
      UGY(MMM)=(UGY(MMM))/MAXGROUNDY*386.4
      UGUP(MMM)=(UGUP(MMM))/MAXGROUNDZ*386.4
   55 CONTINUE
      NOD=10
      DO 505 LLL=1,CCC-1
      UGXN(NOD*(LLL-1)+1)=UGX(LLL)
      UGXN(NOD*LLL+1)=UGX(LLL+1)
      UGYN(NOD*(LLL-1)+1)=UGY(LLL)
      UGYN(NOD*LLL+1)=UGY(LLL+1)
      UGUPN(NOD*(LLL-1)+1)=UGUP(LLL)
      UGUPN(NOD*LLL+1)=UGUP(LLL+1)
      DO 606 GGG=1,NOD-1
      UGXN(NOD*(LLL-1)+1+GGG)=UGX(LLL)+GGG*(UGX(LLL+1)-UGX(LLL))/NOD
      UGYN(NOD*(LLL-1)+1+GGG)=UGY(LLL)+GGG*(UGY(LLL+1)-UGY(LLL))/NOD
      UGUPN(NOD*(LLL-1)+1+GGG)=UGUP(LLL)+GGG*(UGUP(LLL+1)-
      UGUP(LLL))/NOD
  606    CONTINUE
  505    CONTINUE
      NOTS=20
      HINIT=1.0E-05
      HMAX=DT/(NOTS*NOD)
      INORM=0
      IMETH=2
      IATYPE=0
      MTYPE=0
      MITER=0
      MXSTEP=100000000
C     SET PARAMETERS FOR SOLVING DIFFERENTIAL EQUATIONS
      CALL SSET (NPARAM,0.0,PARAM,1)
      PARAM(1)=HINIT
      PARAM(4)=MXSTEP
      PARAM(10)=INORM
      PARAM(12)=IMETH
      PARAM(13)=MITER
      PARAM(14)=MTYPE
      PARAM(19)=IATYPE
      IDO=1
      X=0.0
      Y(1)=0.0
      Y(2)=0.0
      Y(3)=0.0
      Y(4)=0.0
      Y(5)=0.0
      Y(6)=0.0
      TOL=1.0E-07
      XDISPMAX=0.0
      XDISPMIN=0.0
      YDISPMAX=0.0
      YDISPMIN=0.0
      MAXRESDISP=0.0
      MAXTOTALACCX=0.0
```

```
      MAXTOTALACCY=0.0
      MAXTOTALACCXY=0.0
      WRITE (2,99998)
      CCC=NOD*(CCC-1)+1
      DO 10 IEND=1,CCC
      XEND=(IEND)*DT/NOD
      CALL IVPAG(IDO,NEQ,FCN,FCNJ,A,X,XEND,TOL,PARAM,Y)
      IF ((Y(1)).GT.XDISPMAX) XDISPMAX=Y(1)
      IF ((Y(1)).LT.XDISPMIN) XDISPMIN=Y(1)
      IF ((Y(3)).GT.YDISPMAX) YDISPMAX=Y(3)
      IF ((Y(3)).LT.YDISPMIN) YDISPMIN=Y(3)
      RESDISP(IEND)=SQRT((Y(1))**2+((Y(3))**2))
      IF (RESDISP(IEND).GT.MAXRESDISP) MAXRESDISP=RESDISP(IEND)
      GROUNDXY(IEND)=SQRT((C12*UGXN(IEND))**2+(C13*UGYN(IEND))**2)
      TOTALACCX(IEND)=ACCX+C12*UGXN(IEND)
      TOTALACCY(IEND)=ACCY+C13*UGYN(IEND)
      WRITE (2,99999) X,(Y(II), II=1, 6),TOTALACCX(IEND),
      TOTALACCY(IEND)
      TOTALACCXY(IEND)=SQRT((TOTALACCX(IEND))**2+
      (TOTALACCY(IEND))**2)
      IF (MAXGROUNDXY.LT.ABS(GROUNDXY(IEND)))
      MAXGROUNDXY=ABS(GROUNDXY(IEND))
      (MAXTOTALACCX.LT.ABS(TOTALACCX(IEND)))
      MAXTOTALACCX=ABS(TOTALACCX(IEND))
      (MAXTOTALACCY.LT.ABS(TOTALACCY(IEND)))
      MAXTOTALACCY=ABS(TOTALACCY(IEND))
      IF (MAXTOTALACCXY.LT.ABS(TOTALACCXY(IEND)))
      MAXTOTALACCXY=ABS(TOTALACCXY(IEND))
      IF (IEND.EQ.CCC) THEN
      INREDX=(MAXTOTALACCX-C12*386.4)/(C12*386.4)*100
      INREDY=(MAXTOTALACCY-C13*386.4)/(C13*386.4)*100
      INREDXY=(MAXTOTALACCXY-MAXGROUNDXY)/MAXGROUNDXY*100
      END IF
      IF (IEND.EQ.CCC) THEN
      PRINT '(A27, F6.2,A11)','MAXIMUM RESULTANT GROUND :',
      MAXGROUNDXY/386.4,'g'
      PRINT '(A27, F6.2,A5)','MAXIMUM X-DISPLACEMENT   : ', XDISPMAX,
      ' INCH'
      PRINT '(A27, F6.2,A5)','MINIMUM X-DISPLACEMENT   : ', XDISPMIN,
      ' INCH'
      PRINT '(A27, F6.2,A5)','MAXIMUM Y-DISPLACEMENT   : ', YDISPMAX,
      ' INCH'
      PRINT '(A27, F6.2,A5)','MINIMUM Y-DISPLACEMENT   : ', YDISPMIN,
      ' INCH'
      PRINT '(A37, F6.3,A2)','MAXIMUM TOTAL ACCELERATION IN X    : ',
      MAXTOTALACCX/386.4,' g'
      PRINT '(A37, F6.3,A2)','MAXIMUM TOTAL ACCELERATION IN Y    : ',
      MAXTOTALACCY/386.4,' g'
      PRINT '(A37, F6.2,A5)','MAXIMUM RESULTANT DISPLACEMENT     : ',
      MAXRESDISP, ' INCH'
      PRINT '(A37, F6.1,A2)','INERTIA REDUCTION IN X DIRECTION   : ',
      INREDX,' %'
      PRINT '(A37, F6.1,A2)','INERTIA REDUCTION IN Y DIRECTION   : ',
      INREDY,' %'
      PRINT '(A37, F6.1,A2)','INERTIA REDUCTION IN X-Y DIRECTION : ',
      INREDXY,' %'
      END IF
10    CONTINUE
      IDO=3
      CALL IVPAG(IDO,NEQ,FCN,FCNJ,A,X,XEND,TOL,PARAM,Y)
99998 FORMAT 11X,'X',14X,'Y(1)',11X,'Y(2)',11X,'Y(3)',11X,'Y(4)',11X,
      'Y(5)',11X,'Y(6)',11X,'TOTALACCX',11X,'TOTALACCY')
99999 FORMAT (9F15.5)
      CLOSE (1)
```

```
CLOSE (2)
END
SUBROUTINE FCN (NEQ,X,Y,YPRIME)
INTEGER NEQ
REAL X, Y(NEQ), YPRIME(NEQ), C1,C2,C3,C4
REAL C8(100000)
COMMON UGXN(100000),UGYN(100000),UGUPN(100000)
COMMON C10,C9,C12,C13,C14
COMMON IEND,ACCX,ACCY
C1=0.005
C2=0.9
C3=0.1
C4=1.0
C8(IEND)=386.4+C14*UGUPN(IEND)
YPRIME(1)=Y(2)
YPRIME(2)=-((C8(IEND))/C9)*Y(1)-(C10*C8(IEND))*Y(5)-
12*UGXN(IEND)
YPRIME(3)=Y(4)
YPRIME(4)=-((C8(IEND))/C9)*Y(3)-(C10*C8(IEND))*Y(6)-
C13*UGYN(IEND)
YPRIME(5)=(C4/C1)*Y(2)-(C3/C1)*(Y(4))*(Y(5))*(Y(6))-(C2/C1)*
(ABS((Y(4))*(Y(6))))*Y(5)-C3/C1*(Y(2))*(Y(5))**2-(C2/C1)
*(ABS((Y(2))*(Y(5))))*Y(5)
YPRIME(6)=(C4/C1)*Y(4)-(C3/C1)*(Y(2))*(Y(5))*(Y(6))-(C2/C1)*
(ABS((Y(2))*(Y(5))))*Y(6)-C3/C1*(Y(4))*(Y(6))**2-(C2/C1)
*(ABS((Y(4))*(Y(6))))*Y(6)
ACCX=YPRIME(2)
ACCY=YPRIME(4)
RETURN
END
SUBROUTINE FCNJ(NEQ, X,Y,DYPDY)
INTEGER NEQ
REAL  X,Y(NEQ),DYPDY(*)
RETURN
END
```

REFERENCES

ANSYS, "Engineering Analysis System," ANSYS Inc., Rev 5.5, Canonsburg, Pennsylvania 15301

ASCE, "Guide to Post Earthquake Investigation of Lifelines," ASCE Technical Council on Lifeline Earthquake Engineering, 1998

ASCE, "Guide to Improved Earthquake Performance of Electric Power Systems," ASCE Manuals and Reports on Engineering Practice No. 96, 1999

Al-Hussaini, T., Zayas, V., and Constantinou, M. C., "Seismic Isolation of Multi-Storey Frame Structures Using Spherical Sliding Isolation System," Report NCEER-94-0007, 1994

Almazan, J. L., De La Llera, J. C., and Inaudi, J., "Modeling Aspects of Structures Isolated with the Frictional Pendulum System," Earthquake Engineering and Structural Dynamics, Vol. 27, pp 845-867, 1998

Bellorini, S., Salvetti, M., Bettinali, F., Zafferani, G., "Seismic Qualification of Transformer High Voltage Bushings," IEEE Transactions on Power Delivery, Vol. 13, No. 4, pp 1208-1213, 1998

Chopra, A. K., Dynamics of Structures, Theory and Applications to Earthquake Engineering, Prentice Hall, New Jersey, 1995

Constantinou, M. C., Mokha, A. S., and Reinhorn, A. M., "Teflon Bearings in Base Isolation: Modeling," Journal of Structural Engineering, Vol. 116, pp 455-473, 1990

Constantinou, M. C., Tsopelas, P., Kim, and Y-S., Okamoto, S., "NCEER-Taisei Corporation Research Program on Sliding Isolation Systems for Bridges: Experimental and Analytical Study of a Friction Pendulum System (FPS)," Report NCEER-93-0020, 1993

Constantinou, M., Whittaker, A. S., and Velivasakis, E., "Seismic Evaluation and Retrofit of the Ataturk International Airport Terminal Building," Proceedings of the 2001 Structures Congress and Exposition, ASCE, 2001

EERI Newsletter, "The Izmit (Kocaeli), Turkey Earthquake of August 17, 1999," Vol. 33, No. 10, 1999

Earthquake Protection Systems (EPS), "Friction Pendulum Seismic Isolation for Bridges," EPS Inc., Richmond, California 94806

Ersoy, S., Saadeghvaziri, M. Ala, Liu, K., and Mau, S.T., "Analytical and Experimental Evaluation of Friction Pendulum System for Seismic Isolation of Transformers", Earthquake Spectra, Vol. 17, No. 4, 2001

Gilani, A. S., Chavez, J. V., Fenves, G. L. and Whittaker, A. S., "Seismic Evaluation of 196 kV Porcelain Transformer Bushings," Report No. PEER-98/02, 1998

Gilani, A. S., Whittaker, A. S., and Fenves, G. L., "Seismic Evaluation and Retrofit of 230 kV Porcelain Transformer Bushings," Report No. PEER 1999/14, 1999

Gilani, A. S., Whittaker, A. S., and Fenves, G. L., "Seismic Evaluation of 550 kV Porcelain Transformer Bushings," Report No. PEER 1999/05, 1999

IEEE, IEEE Std. 693-1997, Recommended Practices for Seismic Design of Substations, Piscataway, New Jersey, 1998

Kiureghian, A., Sackman, J. L., and Hong, K., "Interaction in Interconnected Electrical Substation Equipment Subjected to Ground Motions," Report No. PEER 1999/01, 1999

Naeim, F., Kelly, J. M., Design of Seismic Isolation Structures, John Wiley & Sons Inc., Canada, 1999

Newmark, N. M., Rosenblueth, E., Fundamentals of Earthquake Engineering, Prentice Hall, Englewood Cliffs, New Jersey, 1971

MCEER, "The Marmara, Turkey Earthquake of August 17, 1999: Reconnaissance Report", Technical Report, 2000

Mokha, A. S., Constantinou, M. C., and Reinhorn, A. M., "Teflon Bearings in Base Isolation: Testing," Journal of Structural Engineering, Vol. 116, No. 2, 1990

Mokha, A. S., Constantinou, M. C., Reinhorn, A. M., Zayas, V. A., "Experimental Study of Friction-Pendulum Isolation System," Journal of Structural Engineering, Vol. 117, No. 4, 1991

Mokha, A., Amin, N., Constantinou, M., and Zayas, V., "Seismic Isolation Retrofit of Large Historic Buildings," Journal of Structural Engineering, Vol. 122, 298-308, 1996

Murota, N., Feng, M. Q., "Hybrid Base-Isolation of Bushing-Transformer Systems," *Proceedings of the 2001 Structures Congress and Exposition*, ASCE, 2001.

Pansini, A. J., Electrical Transformer and Power Equipment, Fairmont Press, Georgia, 1999

Saadeghvaziri, M. A., Ersoy, S., Mau, S. T., "Friction Pendulum System for Seismic Isolation for Transformers," PVP-Vol. 402-1, pp 123-134, 2000

Villaverde, R., Pardoen, Gerald C., and Carnalla, S., "Ground Motion Amplification at Base of Bushing Mounted on Electric Substation Transformer," Technical Report PGE-09566, 1999

Zayas, V., Low, S., Bozzo, L., Mahin, S., "Feasibility and Performance Studies on Improving the Resistance of New and Existing Buildings Using the Friction Pendulum System." Technical Report UCB-EERC-89/09, 1989

Zayas, V., Low, S., and Mahin, S., "A Simple Pendulum Technique for Achieving Seismic Isolation," Earthquake Spectra, Vol. 6, pp 317-334, 1990